

Agonist Binding Studies at Two Subtypes of the  
Nicotinic Acetylcholine Receptor Involved in  
Parkinson's Disease and Addiction

Thesis by  
Michael Robert Post

In Partial Fulfillment of the Requirements for  
the degree of  
Doctor of Philosophy

The logo for the California Institute of Technology (Caltech), featuring the word "Caltech" in a bold, orange, sans-serif font.

CALIFORNIA INSTITUTE OF TECHNOLOGY

Pasadena, California

2016

(Defended 27 May, 2016)

© 2016

Michael R. Post

ORCID: 0000-0002-3214-7619

## Acknowledgements

While the scientific work presented in this dissertation filled the bulk of the last five years, it is the following people who have infused them with value and meaning. There are countless individuals who have made my time at Caltech exceptional, but several demand special thanks:

Dennis Dougherty for his unwavering support and mentorship. From the moment he became my advisor, Dennis has encouraged me to think critically and creatively about my work. He has been an ideal advisor – letting me explore both scientific and extracurricular passions while constantly maintaining an open door and a willingness to push me to reach my fullest potential. He has allowed and encouraged me to pursue the most far-fetched of ideas, from incorporating  $\delta$ -amino acids to chairing the GSC, and I cannot imagine having worked with anyone else. Dennis will serve as a paradigm as I begin to shape my own path in academia;

Henry Lester, for having such a meaningful impact on the direction of both my science and my career. His input at our monthly Unnaturals meetings has shaped the work in this thesis for the better. I thank him for thinking of me whenever an opportunity to collaborate arose and for providing me with thoughtful and honest advice while I was looking for post-doctoral opportunities;

The members of my thesis committee for giving focus and direction to my doctoral work. Jackie Barton and David Tirrell have given me thoughtful input at our annual meetings and exams, and I am grateful for Sarah Reisman's approachability as chair of the committee. I would also be remiss to not mention Linda Syme for keeping the lab in proper

functional order and Agnes Tong for always lending a supportive ear and making me feel welcome my first days at Caltech;

Carla Swick, William Shelley, Deni Ors, and the late Michael Stuart for kindling my love for science. They were the amazing teachers in middle and high school who encouraged me to go above and beyond the material they taught, giving me extra opportunities to learn and introducing me to scientific research;

Joshua Maurer, for giving me the opportunity to work in his lab during my time at Washington University in St Louis. His creative ideas and approaches showed me there are no limits in how to solve a complex problem, and his lab introduced me to chemical biology and its use in studying neuroscience;

The entire Dougherty lab, of which I'm certain there is no better environment to spend five years of graduate school in. This group is full of so many fun and talented people, and no matter what state my science was in, because of them I have always looked forward to heading into lab. Kay Limapichat showed me the ropes – everything from how to linearize DNA to the importance of green clips. She showed me by example how to thoughtfully and thoroughly approach a scientific problem. Ethan van Arnam also served as an example of the consummate scientist, tackling projects head on with innovative ideas and a positive if not sarcastic attitude. Noah Duffy, Kristina Daeffler, and Tim Miles formed the foundation of the North Bay Nation, and my interior years in grad school would not have been the same without them. Noah was always the one to get things done and I'm lucky he taught me some of his MacGyverish ways. Kristina was my biggest role model and one of my best friends in the lab – I knew I could always turn to her for help and expect real and honest advice. Tim is also a great source of inspiration and friendship – I will

always appreciate how well-read he is, whether it be in Nature, the New York Times, or Pitchfork. Clint Regan has shown me how to approach a scientific problem with rigor, Ximena da Silva showed me how to perform single channel analysis, and I will always cherish my conversations with Betty Wong about GSC politics. Oliver Shafaat is someone I always seem to find myself with in deep conversation, and I am always impressed with his dedication to doing something new and novel in this lab. Chris Marotta will forever be my co-Opus captain and Tryptoman coach. Chris was a year ahead of me and left footsteps I was eager to follow in. Whether in a clown mask or a business suit, Paul Walton knows exactly how to brighten my day. He is a brilliant scientist and I look forward to seeing all the great things he accomplishes. Annet Blom is a wonderful person who I am so glad to have gotten to know so well. We have such similar philosophies about Caltech and the world and share a similar penchant for creating Latin phrases. Catie is another lab member who shares a similar world-view, and I always enjoy our humanities-oriented conversations in a sea of scientific thought. Bryce Jarmin has always strove to do science beyond the limits of what we have traditionally done in the group, a trait I admire. He also shares my passion for overproduced music and enablement; I am glad the group will continue to have someone encouraging keynote games and rooftop Fridays. Richard, Steve, and Malaney are the future of the Dougherty lab and appear primed to continue the amazing environment that has come before them. I have also had the pleasure of mentoring Gabby Tender for the last two years. From the start, when she was just a freshman, I knew Gabby was an exceptional undergraduate. She knows exactly what questions to ask and works incredibly hard. I am grateful for the opportunity to have mentored her and all that she has contributed to our project together, and cannot wait to see what path she takes in the scientific world;

Matt Rienzo and Matt Davis, for embodying the epitome of what it means to be both a colleague and a friend. Matt Rienzo joined the lab weeks before I did, and has taught me so much and helped me grow in both lab and life. More than any other grad student, he has helped me become more confident as a scientist and a person. Whether exasperatingly ranting about the downs together, or excitedly celebrating the ups, I am lucky to have joined the lab with someone like him. Not only has Matt Davis been one of my best friends in grad school, he has also been one of my closest collaborators. Our project together was a long and interesting one, and I am grateful for how easy it was to share ideas and get things done. Matt and his other half, Rachel Sparr, have become my California family, and from baseball games to Shabbas dinners, our time spent together is always awesome;

The graduate student council and all of its members for giving me an outlet to do what I love outside of the lab. I have been very fortunate to have had leadership roles in such a great organization, and even luckier to have stumbled across Joel Schmidt, Sunita Darbe, and Max Lloyd in the process. I always valued working with them in the GSC and becoming such great friends outside of it was even better. I was also fortunate to have been advised by Joe Shephard and Anneila Sargent while serving as chair. I could always count on their sagacious advice, and I thank them for providing an example of how to be leaders on a campus while part of the professoriate. Felicia Hunt also served as a mentor throughout my time in the GSC and words cannot describe how much of an impact she has had on my time here. I am forever thankful of how much support and care she graciously gave me throughout my time here;

Alli Akagi, Tania Darnton, Brandon Carroll, and Julian Edwards, for being such amazing friends. I will always remember sitting in NMR class and awkwardly asking if I could hang out with Tania and Alli when overhearing their plans. From there a beautiful friendship blossomed with each of them. Tania is the ultimate stitcher-in-arms and I am never afraid to confide in her about even the most important or trivial of matters. I will miss being able to walk down the hall to talk to Alli about whatever is on my mind and whether we are at the Red Door or a pool table, we always have the best time together. Julian was gracious enough to include me in his annual pilgrimage to Telluride our first year, and from then on I knew I had found a life-long friend. Our hyperintellectual rants about the most mundane of things are typically the best part of my day and I look forward to whatever epicness the future holds for him;

Carl Blumenfeld, Brett McGuire, Adam Boynton, and Larry Dooling for fostering the perfect home-life. These gentleman have been my roommates at various times throughout grad school, and as much as I looked forward to getting into lab, I have always looked forward more to heading back home at the end of the day because of them. Carl was one of my first friends at Caltech and is the best at adventuring and making you feel like you have known him forever. Brett introduced me to so many things, from Game of Thrones to fitness, and my life is much fuller because of him. Boyntz has a knack for sending me a fresh new track right when I need it, and his down-for-whatever attitude has made for two solid years of living at the Orange Grove estate;

Anna Henkel, Jeremy Carlson, David Ingber, and Ricky Steiner for having remained so close after college, even when I moved so far away. That I can still dial any of them to help make important life decisions or to just catch up, no matter how much time

has elapsed since the last call, means the world to me. I feel like our friendships have only grown stronger since our days at Wash U, and I am lucky to still have you all a part of my life;

Jordan Forman, for making the last year of graduate school so unexpectedly special. Jordan has caused me to live G5 to the fullest, instead of crammed in a lab or an office, and I really value the time we have spent together so far;

My brother and sister, though it could easily go unsaid, for being such a massively important part of my entire life. Jennie has been my idol growing up; I always wanted to be just like her whether it was in band, BBYO, school, or camp, and I specifically remember sitting in the SHS auditorium at her senior research symposium thinking I wanted to do that one day. Now that I have gotten a taste of science and research, I realize how grateful I am for having such a powerful role model throughout my life. Not only that, she has been so supportive throughout grad school and I do not know what I would do without her and Ben. My brother Daniel has been my twenties spirit guide, serving as a never-ending source of wisdom for how to live my life. I'm so appreciative of all of the advice he's given me throughout the years, of how close we have gotten as I've grown older, and of his yearly summer trips to the west coast. I cannot wait to be just a short subway ride away from him in the coming years and the adventures that I am sure will ensue;

And finally my parents, because for all of the passion-kindling those mentioned already have done, it was my mom and dad who set off the initial spark. Though not scientists themselves, they always encouraged me to learn more, ask questions, and explore my environment. From giving me and my siblings free range of the local creek and cages

to keep salamanders in, to Magic School Bus toys and books about space, to underwater slide shows and trips to the aquarium or science center, my parents from early on provided me the foundation for a career in science. As I grew older, their support never waned, as toothpick bridges turned into science fair boards into research posters and talks. Their simultaneous phone calls on their way home from work have kept me going throughout grad school, although I will be happy when the frog egg dad-jokes cease. I am who I am today because of them, and for that I am forever grateful.

## Abstract

Neuronal nicotinic acetylcholine receptors (nAChR) consist of pentameric ligand gated ion channels that typically regulate the release of neurotransmitter. This group of receptors is made of many subunits that combine into pentamers to form different subtypes, with each subtype having a unique pharmacology, function, and localization in the nervous system. The  $\alpha 6\beta 2$  subtype is found predominantly in the dopaminergic pathways in the brain, and is therefore a promising target for addiction and Parkinson's disease. A major goal in treating these disorders is to develop subtype-selective agonists, and advanced knowledge of the binding site which sits at the  $\alpha 6$ - $\beta 2$  subunit interface is critical. This thesis dissertation describes high precision, chemical scale structure-function studies designed to probe specific interactions between a variety of agonists and the amino acids which make up the  $\alpha 6\beta 2$  binding site.

Before these studies, which utilize nonsense suppression-based non-canonical amino acid mutagenesis, could be conducted, a heterologous expression system for  $\alpha 6\beta 2$  had to be developed. Chapter 2 details four reporter mutations that allow high expression levels of  $\alpha 6\beta 2$  in *Xenopus* oocytes. Further work presented in this chapter characterizes a variety of compounds at this subtype including acetylcholine, the endogenous agonist, nicotine, and TC299423, a promising drug candidate designed to be  $\alpha 6$ -selective.

Chapters 3 and 4 discuss the structure-function studies used to probe for binding interactions of acetylcholine, nicotine, and TC299423 with the  $\alpha 6$ - $\beta 2$  interface. Fluorination series were executed to probe for cation- $\pi$  interactions with TrpB, TyrA, and TyrC2, all sites of the  $\alpha 6$  face. Of the nine possible agonist-side chain interactions, the

only functionally important cation- $\pi$  interaction was found between acetylcholine and TrpB, suggesting the subtype has a unique pharmacology. Studies utilizing  $\alpha$ -hydroxy acids were then performed to determine whether these agonists make a functional hydrogen bond between their amine NH and the backbone carbonyl associated with TrpB. Here, nicotine was found to make a strong hydrogen bond, whose energy was quantified via double-mutant cycle analysis, but TC299423 was not.

Chapter 5 further explores TC299423 at the  $\alpha 4\beta 2$  subtype. Experiments here showed that TC299423 makes a dual cation- $\pi$  interaction with both TrpB and TyrC2. Further studies revealed this dual cation- $\pi$  effect to be true for several secondary amines, and a structure-function study with nornicotine established this as a general feature for secondary amines.

Chapter 6 describes work done to probe for a hydrogen bond between the indole NH of  $\alpha 4$  TrpB and a backbone carbonyl associated with L119 on the  $\beta 2$  subunit. This study required development of a new strategy to probe for hydrogen bonds as the amino acid sequence does not allow for  $\alpha$ -hydroxy substitution. Instead, a fluorinated side chain strategy was used to inductively attenuate the hydrogen bond accepting ability of the carbonyl, and it proved the  $\alpha 4$ - $\beta 2$  interfacial hydrogen prediction false.

Finally two appendices suggest possible avenues to explore with the new  $\alpha 6\beta 2$  expression system. Appendix A describes work done to determine whether there is cross-talk between  $\alpha 6\beta 2$  and P2X receptors. Appendix B details initial investigations on the effects of ethanol and other alcohols on the function of  $\alpha 6\beta 2$ .

## Published Content and Contributions

Post, M. R., Limapichat, W., Lester, H. A. & Dougherty, D. A. Heterologous expression and nonsense suppression provide insights into agonist behavior at  $\alpha 6\beta 2$  nicotinic acetylcholine receptors. *Neuropharmacology* **97**, 376-382 (2015).

doi:10.1016/j.neuropharm.2015.04.009

Wieskopf, J.S. et. al. The nicotinic  $\alpha 6$  subunit gene determines variability in chronic pain sensitivity via cross-inhibition of P2X2/3 receptors. *Science Translational Medicine*

**7:287** 287ra72 (2015). doi:10.1126/scitranslmed.3009986

## Table of Contents

Acknowledgements.....	iii
Abstract.....	x
Published Content and Contributions .....	xii
Table of Contents.....	xiii
Chapter 1: Introduction.....	1
1.1 nAChR overview	3
1.2 The Structure-Function Study as a Means of Probing Noncovalent Interactions	7
1.3 Non-canonical Amino Acid Mutagenesis	10
1.4 Thesis Summary	13
1.5 References	15
Chapter 2: Heterologous Expression of $\alpha 6\beta 2$ nAChRs .....	19
2.1 Abstract	19
2.2 Introduction	20
2.2 Reporter Mutations Resulting in Functional Expression of $\alpha 6\beta 2$	22
2.3 Characterization of $\alpha 6\beta 2^{\ddagger}$	25
2.3.1 Stoichiometry Control of $\alpha 6\beta 2^{\ddagger}$	25
2.3.2 Pharmacology of $\alpha 6\beta 2^{\ddagger}$	27
2.4 Conclusions	29
2.5 Materials and Methods	30
2.6 References	32
Chapter 3: Probing for Agonist Cation- $\pi$ Interactions in $\alpha 6\beta 2$ nAChRs.....	34
3.1 Abstract	34
3.2 Introduction	35
3.3 Cation- $\pi$ Binding Studies at TrpB	40
3.3.1 Acetylcholine binding at TrpB	40
3.3.2 Nicotine and TC299423 binding at TrpB	43
3.4 Cation- $\pi$ Binding Studies at Tyrosines	45
3.4.1 Cation- $\pi$ Binding Studies at TyrC2	45
3.4.2 Cation- $\pi$ binding studies at TyrA	47

3.4 Conclusion	49
3.6 Materials and Methods	49
3.7 References	52
Chapter 4: Probing for Agonist Hydrogen Bonds in $\alpha 6\beta 2$ .....	54
4.1 Abstract	54
4.2 Introduction	55
4.3 Probing for Hydrogen Bonds in $\alpha 6\beta 2$ at the TrpB Carbonyl	56
4.3.1 The $\alpha$ -hydroxy acid Strategy	56
4.3.2 $\alpha$ -hydroxy acid Substitution at T150	58
4.4 Quantifying the $\alpha 6\beta 2$ -nicotine Hydrogen Bond	59
4.4.1 The Double-Mutant Cycle Analysis	59
4.4.2 Proof of Concept in $\alpha 4\beta 2$	61
4.4.3 Quantifying the Nicotine Hydrogen Bond in $\alpha 6\beta 2^{\ddagger}$	62
4.5 Conclusion	62
4.6 Materials and Methods	63
4.7 References	66
Chapter 5: Investigating a Dual Cation- $\pi$ Interaction Trend with Secondary Amines at $\alpha 4\beta 2$ .....	68
5.1 Abstract	68
5.2 Introduction	69
5.3 Binding Studies of TC299423 at $\alpha 4\beta 2$	71
5.3 Binding Studies of Metanictine at $\alpha 4\beta 2$	74
5.4 Establishing a Binding Trend for Secondary Amines	77
5.5 Conclusions	81
5.6 Materials and Methods	84
5.7 References	86
Chapter 6: Evaluating a Predicted Interfacial Hydrogen Bond Interaction Across the $\alpha 4$ - $\beta 2$ Interface .....	88
6.1 Abstract	88
6.2 Introduction	89
6.3 Strategies to Probe for Hydrogen Bonding at Loop E Leu-Pro-Pro	94

6.3.1 The $\delta$ -amino acid Strategy	95
6.3.2 The Gly-Gah Strategy	96
6.3.3 The Fluorination Strategy	99
6.4 Computational and Experimental Support for the Fluorination Strategy	102
6.4.1 Electrostatic Potential Maps to Predict Hydrogen Bonding Attenuation	102
6.4.2 Evaluating F <sub>3</sub> Ala with <sup>19</sup> F-NMR	105
6.5 Double-Mutant Cycle Results	108
6.6 Studies with 3-Benzothiophene	110
6.7 Conclusions	112
6.8 Materials and Methods	113
6.9 References	116
Appendix A: Investigations of Possible $\alpha 6\beta 2$ -P2X Cross-talk.....	118
A.1 Introduction	118
A.2 $\alpha 6\beta 2$ -P2X2 Cross-talk Experiments	120
A.3 $\alpha 6\beta 2$ -P2X3 Cross-talk Experiments	121
A.4 Materials and Methods	122
A.5 References	123
Appendix B: Initial Studies of Alcohol- $\alpha 6\beta 2$ Interactions .....	124
B.1 Introduction	124
B.2 Determining the Allosteric Effects of EtOH at $\alpha 6\beta 2$	126
B.3 Materials and Methods	129
B.4 References	130

## Chapter 1: Introduction

Nicotine addiction and Parkinson's disease remain major public health issues in the United States. According to the Centers for Disease control, twenty percent of Americans smoke.<sup>1</sup> Of those smokers, eighty percent smoke every day, and three quarters smoke one half to one whole pack of cigarettes per day.<sup>2</sup> Another recent survey showed that in the previous thirty days, nearly three million middle school and high school students reported using an e-cigarette.<sup>3</sup> While the long term effects of e-cigarettes are largely unknown, health issues related to smoking generate 96 billion dollars in costs per year, and smoking is the greatest cause of death in the U.S. – more than alcohol, drugs, homicide, car accidents, and AIDS combined.<sup>4</sup> As nicotine is a recreational drug, its negative impact on health is mostly preventable; however, while sixty percent of those smokers surveyed above expressed a desire to quit, only fifteen percent actually did.<sup>5</sup> This is because nicotine is highly addictive.

Parkinson's disease, on the other hand, is not preventable. This neurodegenerative disorder is characterized by severe motor issues including tremor, postural imbalance, slowness of movement, and rigidity. It affects nearly one million Americans with 60,000 new diagnoses every year, a number expected to double by 2030 as the baby boomer generation ages.<sup>6</sup> One of the many challenges Parkinson's disease presents is that by the time it is detectable, between sixty to eighty percent of neurons in the midbrain have died, a major reason why both an etiology and a cure remain elusive.<sup>7</sup>

Nicotine addiction and Parkinson's disease are linked to the mesocorticolimbic and nigrostriatal dopaminergic pathways, respectively (Figure 1). The mesocorticolimbic

pathway, the pathway central to addiction, starts in the ventral tegmental area and extends into both the nucleus accumbens, which is responsible for reward, and the cortex, an area responsible for decision making. The nigrostriatal pathway, which starts in the substantia nigra pars compacta and extends into the dorsal striatum, contains the neurons responsible for motion, which are the cells that die in the course of Parkinson's disease. Because both disorders revolve around the dopaminergic pathways, they are intricately linked. In fact, smoking cigarettes has shown a neuroprotective effect. This phenomenon has been documented in studies involving sets of identical twins in which one smokes and one does not, where the former is less likely to develop Parkinson's disease than the latter.<sup>8,9</sup> While the specific cause of this effect is unknown, it is likely due to the fact that dopamine release is regulated by the cholinergic system and its neurotransmitter, acetylcholine (ACh).

Nicotinic acetylcholine receptors (nAChRs), the primary target of ACh released by cholinergic neuron inputs, are found at synapses at both ends of a dopaminergic neuron

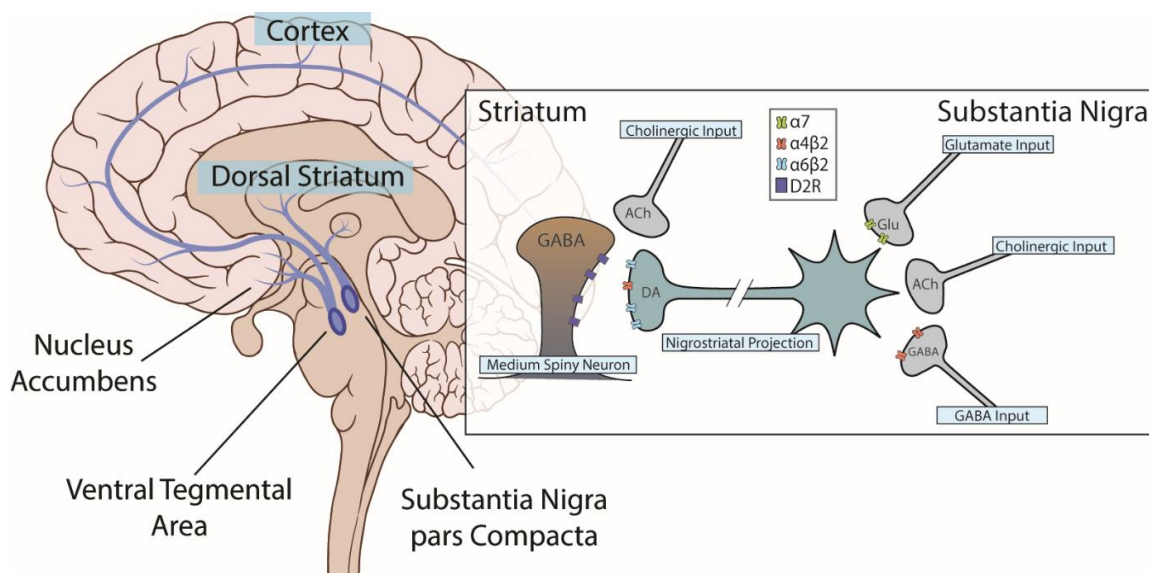


**Figure 1.** A schematic of the mesocorticolimbic and nigrostriatal dopaminergic pathways. The inset is a simplified cartoon of how dopamine release is regulated by acetylcholine receptors at both the dendritic end (such as in the substantia nigra) and the axonal end (such as in the striatum).

(Figure 1, inset).<sup>10</sup> On the dendritic end, they are on presynaptic neurons which release of excitatory glutamate (Glu) and inhibitory (GABA) and therefore govern the signals the dopaminergic system receives by these inputs. On the axonal end, nAChRs are found on the presynaptic terminals of the dopaminergic neurons, and control the release of dopamine into the synapse which then activates medium spiny neurons.<sup>11</sup> Thus, nAChRs are responsible for modulating the release of dopamine, and understanding how both acetylcholine and other nAChR agonists, such as nicotine, bind to the receptors is important to understanding how to better treat the diseases associated with these pathways.

### 1.1 nAChR overview

Nicotinic acetylcholine receptors are members of the pentameric ligand-gated ion channel (pLGIC) family, which also includes receptors for serotonin (5HT), glycine, and  $\gamma$ -aminobutyric acid (GABA).<sup>12</sup> All members of this family are transmembrane proteins and share a similar topology (Figure 2). As the name suggests, five subunits combine

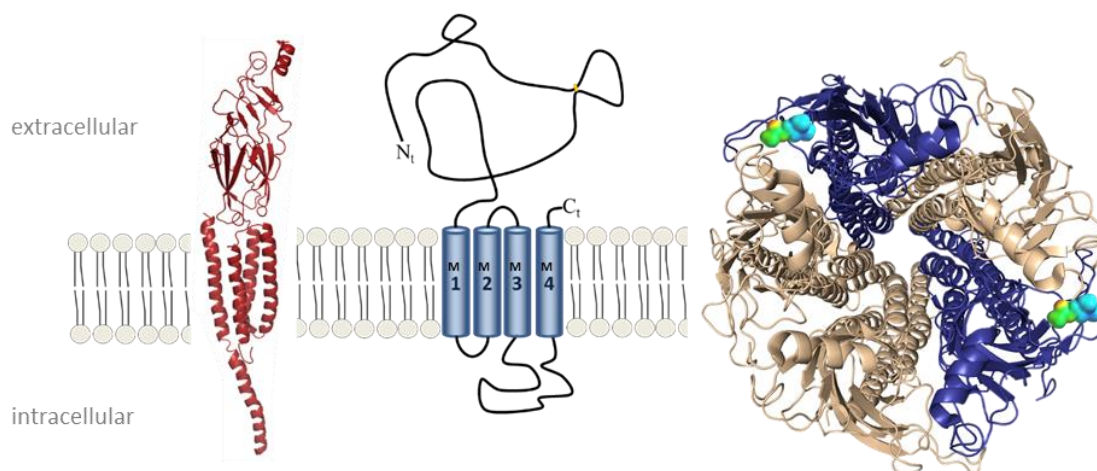


**Figure 2.** A look at the general topology of the nAChR subunit. The view on the left is from the side and is modeled by the cartoon in the center. The view on the right is looking top-down at the extracellular face. Structures are from a cryo-EM structure of the *Torpedo* ray nAChR, PDB 2BG9.

around a central ion-conducting pore that opens upon agonist binding, allowing ions to flow across the membrane. Each subunit has three major domains. The first is an N-terminal ligand-binding domain, with the agonist binding site forming at the interface of two subunits. Next is a transmembrane domain composed of four alpha helices, labeled M1-M4. The M2 helix lines the channel pore and serves as the channel gate, nearly 60 Å away from binding site.<sup>13</sup> Third, is an intracellular domain, consisting mostly of the M3-M4 loop; it is the most highly variable across subunits.<sup>14</sup> This region is thought to be involved in transport of the protein from the endoplasmic reticulum to the plasma membrane.<sup>15</sup>



**Figure 3.** The sixteen different nAChR subunits can combine to form many different subtypes, examples of which are shown here. Binding sites form at the interface of a primary (+) and complementary (-) face typically between  $\alpha$  and  $\beta$  subunits and are indicated by a gray box.

In humans, there are 16 different nAChR subunits expressed:  $\alpha 1$  through  $\alpha 7$ ,  $\alpha 9$ , and  $\alpha 10$ ,  $\beta 1$  through  $\beta 4$ ,  $\gamma$ ,  $\delta$ , and  $\epsilon$ .<sup>16,17</sup> These subunits form pentamers in different combinations, with each stoichiometry making up a unique subtype (Figure 3).<sup>18</sup> Each subtype has a unique pharmacology, function, and localization.<sup>19</sup> The  $\alpha 1\beta 1\gamma\delta$

and  $\alpha 1\beta 1\gamma\epsilon$  subtypes are muscle-type, and are found at the neuromuscular junction, while the remaining subtypes are found at synapses in both the central and peripheral nervous systems. Among the neuronal subunits,  $\alpha 4\beta 2$  and  $\alpha 7$  are the most expressed in the brain, found in almost every region.<sup>20</sup> Other neuronal subtypes are more localized, such as those containing  $\alpha 6\beta 2$ , which are found mainly on presynaptic terminals of dopaminergic neurons.<sup>21</sup>

Because  $\alpha 6\beta 2$ -containing subtypes are localized to the areas responsible for addiction and Parkinson's disease, they are an important target for therapeutics.<sup>22</sup> However, a major challenge in neuropharmacology is to design agonists that can selectively target just one nAChR subtype.<sup>23</sup> By creating a compound that activates  $\alpha 6\beta 2$  subtypes while avoiding  $\alpha 4\beta 2$  and  $\alpha 7$ , the effect of that candidate can be contained within a specific neuronal pathway; thus, avoiding side effects which may make it ultimately untenable as a drug. One strategy to overcome this challenge is to develop detailed binding maps of each subtype that highlight differences across the subtypes. Such pictures have been developed for the  $\alpha 4\beta 2$ ,  $\alpha 4\beta 4$ ,  $\alpha 7$ , and muscle subtypes. Chapters 2, 3, and 4 of this thesis describe progress toward creating a binding model for the  $\alpha 6\beta 2$  subtype with the goal of distinguishing differences in the  $\alpha 4$ - $\beta 2$  and  $\alpha 6$ - $\beta 2$  binding interfaces.

In  $\alpha 4\beta 2$ , and most of the other nAChRs studied to date, the binding site is at the interface of the primary  $\alpha$  face and complementary  $\beta$  face. This site is made of six loops – A, B, and C, from the primary face, and D, E, and F from the complementary face – that

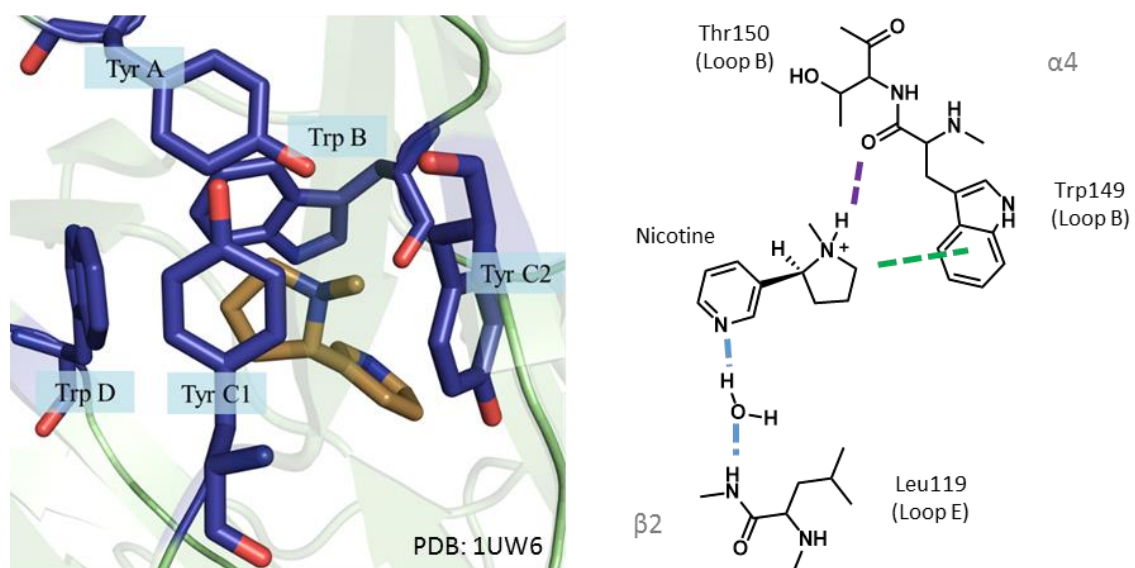


**Figure 4.** Left: a view of nicotine in the aromatic box binding site of AChBP. Right: a summary of the three noncovalent binding interactions between nicotine and  $\alpha 4\beta 2$  previously found to be functionally important. These are hydrogen bonds in purple and blue, and a cation- $\pi$  interaction with TrpB in green.

contribute a cluster of aromatic residues, deemed the aromatic box.<sup>24,25</sup> These aromatic residues are highly conserved across all PLGICs and consist of a tyrosine residue on loop A, a tryptophan residue on both loops B and D, and two tyrosine residues on loop C.<sup>26</sup> Loop C is thought to be particularly mobile, and likely moves toward the cluster during agonist binding, causing a conformational shift in the protein which eventually leads to gating.<sup>27</sup> In the  $\alpha 4\beta 2$  binding pocket, three specific noncovalent interactions have been found functionally important for agonist binding.<sup>28</sup>

The first is a cation- $\pi$  interaction between the agonist – the typical nAChR agonist is a cation – and the tryptophan on loop B, often designated TrpB or Trp149. The cation- $\pi$  interaction is an electrostatic interaction between the positive electrostatic potential of the agonist, and the negative electrostatic potential concentrated in the center of the aromatic side chain.<sup>29,30</sup> Not only has a cation- $\pi$  interaction at TrpB been found to be critical in every agonist tested in  $\alpha 4\beta 2$ ,<sup>31,32</sup> the same is true with  $\alpha 4\beta 4$  nAChR subtypes,<sup>33</sup> the serotonin type A receptor with several agonists and antagonists,<sup>34,35</sup> with agonists at a tyrosine in the same site in the  $\rho$  subtype of GABA<sub>A</sub> receptor,<sup>36</sup> and a phenylalanine in the glycine and ELIC receptors.<sup>37–39</sup>

The other important noncovalent binding interactions in  $\alpha 4\beta 2$  are hydrogen bonds between the agonist and the protein backbone. The first hydrogen bond only applies to agonists with non-quaternary amine group, such as nicotine, where the NH group binds with the backbone carbonyl associated with TrpB. In  $\alpha 4\beta 2$  this interaction was shown for nicotine, varenicline, and cytosine, but as expected not acetylcholine.<sup>31,32</sup> This hydrogen bond was also seen with nicotine in the  $\alpha 4\beta 4$  subtype.<sup>40</sup> The other hydrogen bond occurs between the other end of the agonist and a backbone NH associated with Leu119 on  $\beta 2$

loop E.<sup>40,41</sup> In  $\alpha 4\beta 2$ , the carbonyl group of acetylcholine and cytosine, and the pyridine nitrogen of nicotine were shown to make this functionally important hydrogen bond. It was also demonstrated with cytosine in  $\alpha 4\beta 4$ , as well as with acetylcholine and nicotine in muscle-type.<sup>34</sup>

Together, as summarized in Figure 4, these three interactions make up the three most important binding interactions between an agonist and the  $\alpha 4\beta 2$  nAChR binding pocket. Much of the work described in this thesis seeks to either add more detail to the  $\alpha 4\beta 2$  binding model as in Chapters 5 and 6 or to describe and distinguish the  $\alpha 6\beta 2$  model compared to the one outlined above as in Chapters 2 through 4.

## **1.2 The Structure-Function Study as a Means of Probing Noncovalent Interactions**

Historically, there has been a dearth of structural data for the pLGIC family. Most of the detail about agonist binding at these receptors described in the previous section has instead come from biochemical experiments and structure-function studies. Results from these experiments were later confirmed by a cryo-electron microscopy structure of the *Torpedo* electric ray muscle-derived nAChR<sup>13</sup> at 4 Å, solved in 2003, and crystal structures of the acetylcholine binding protein (AChBP), a soluble protein homologous to the extracellular binding region of the nAChR, that have been solved with many different ligands. In recent years, there has been a rapid increase in published pLGIC structures. Discoveries of prokaryotic homologues ELIC<sup>42</sup> and GLIC,<sup>43,44</sup> and their corresponding structures in 2008 and 2009, were followed with successful structural studies of an invertebrate glutamate channel<sup>45</sup> in 2011, mouse serotonin receptor<sup>46</sup> in 2015, and human GABA<sup>47</sup> and glycine<sup>48</sup> receptors in 2014 and 2015.

Even with this new wealth of structures, it is important to recognize their limitations. Importantly, the only published nAChR structures are of homologous non-neuronal invertebrate subtypes. Furthermore, cryo-EM and crystal structure solutions merely present a snapshot of the receptors in a single conformational state, and not necessarily one that is biologically relevant. They fail to take into account the dynamic nature of an allosteric protein such as those which make up the pLGIC family. Therefore, while they are able to predict noncovalent interactions, the functional importance of these predictions must be verified by experimentation in a living cell system. The classical experiment to probe for noncovalent interactions is the structure-function study. For the nAChR binding site, this means making a small perturbation to protein structure through site-specific mutagenesis, and monitoring any corresponding shift in binding. Such changes are measured with  $EC_{50}$ , the effective concentration of agonist required to elicit a half-maximal response from all expressed receptors.

Structure-function studies with nAChRs are performed in oocytes derived from *Xenopus laevis*, an African clawed frog. This type of expression system is ideal because the cells are large enough to inject with a solution containing RNA and to impale with electrodes, characteristics which are utilized in the determination of an  $EC_{50}$  (Figure 5).<sup>49</sup> First, mRNA coding for each of the subunits in a specific nAChR subtype, prepared *in vitro*, is injected into the oocyte. Then, during an incubation period, the cell machinery translates that mRNA into proteins, folds and assembles them into pentamers, and traffics them to the plasma membrane.<sup>50</sup> Once a sufficient level of nAChRs has been expressed and trafficked to the surface, channel function is monitored using two-electrode voltage clamp (TEVC) electrophysiology.<sup>51</sup> In this type of experiment, a voltage electrode and a

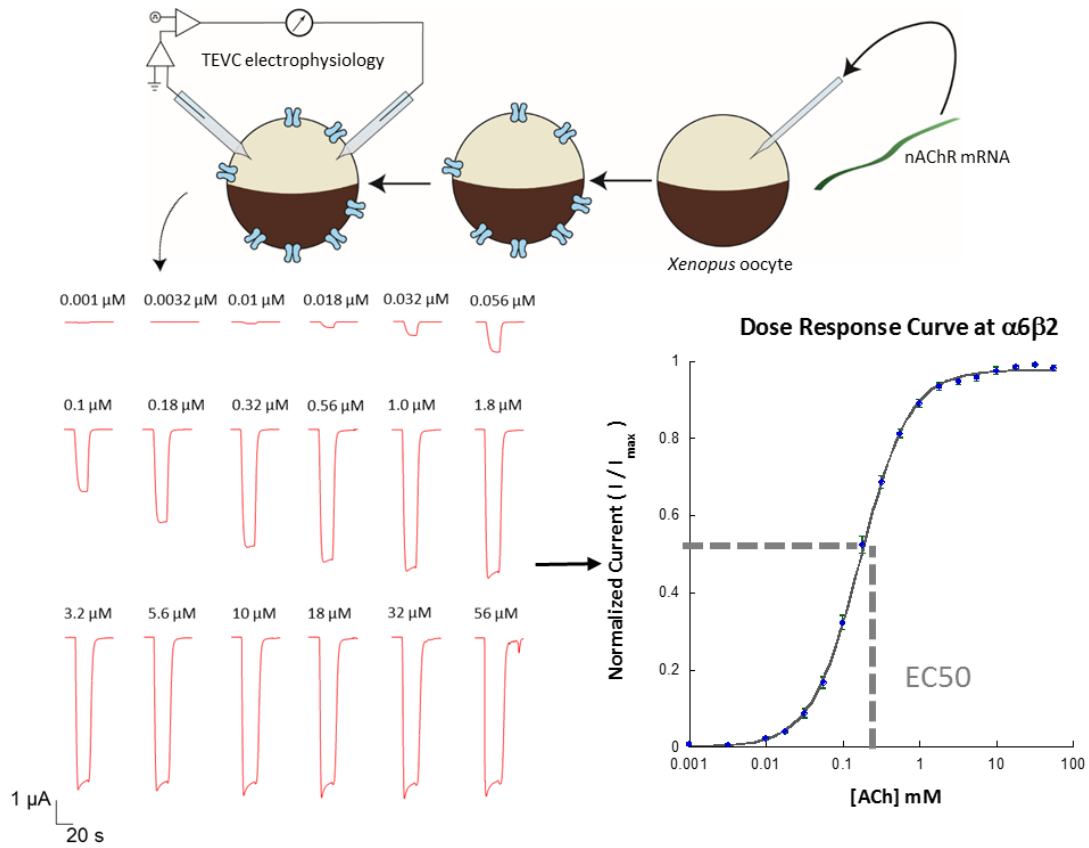


**Figure 5.** A schematic detailing the process for determining an  $EC_{50}$ . Starting at the top right, mRNA of the desired nAChR subunits is injected into *Xenopus* oocytes. After incubation, the channels are expressed and can be studied using TEVC electrophysiology. The bottom left shows ACh-induced currents in  $\alpha 6\beta 2$  at increasing concentrations, the results of which have been normalized and plotted on the bottom right and fit to the Hill equation.

current electrode are both impaled into one oocyte. The former monitors the voltage across the membrane, while the latter is able to inject a variable current in order to hold the voltage across the membrane to a set value. Thus, when the cell is clamped at a specific voltage, and agonist is applied, the total amount of current flowing into the whole cell can be measured.

$EC_{50}$  measurements are determined from a dose response experiment. In a dose response experiment, agonist is applied in increasing concentrations until a saturated response is achieved. The current measured at each dose is normalized against the maximum current achieved and then plotted against concentration to form a dose response

curve. These data get fit to the Hill equation where  $I_{\text{norm}} = 1/(1 + (EC_{50}/[\text{agonist}])^{n_H})$ , and  $n_H$  is the Hill coefficient. To determine changes in binding, a dose response experiment is performed for both the wild-type and mutant nAChRs and a quantitative fold-shift in  $EC_{50}$  is calculated by dividing the mutant  $EC_{50}$  by the wild-type  $EC_{50}$ . An increase in  $EC_{50}$ , shown by a fold shift greater than one, means more agonist is required to activate the same number of receptors and that the mutation has caused a loss of function. A decrease in  $EC_{50}$ , shown by a fold shift less than one, means less agonist is required to activate the same number of receptors and therefore indicates a gain of function mutation. A fold-shift of one describes a case where a change in function has no effect on function. Thus, mutating specific residues predicted by structure or homology to be involved in noncovalent interactions and comparing their  $EC_{50}$  to wild-type can determine whether those interactions are indeed functionally important.

### **1.3 Non-canonical Amino Acid Mutagenesis**

Traditionally in a structure-function study, the mutation is made to the protein using conventional mutagenesis, wherein a single amino acid is site specifically substituted with another one of the twenty naturally occurring amino acids. This type of substitution can be used to, for example, entirely remove side chain functionality of an amino acid by switching it to an alanine. The process is fairly straightforward in a nAChR. The codon of the residue of interest is simply changed to the desired amino acid in the cDNA of the subunit, and the process described in the previous section resumes as usual, with the injected mRNA transcribed from the mutated cDNA.

Conventional mutagenesis, albeit useful, is also quite limited. If the targeted binding interaction was a cation- $\pi$  interaction with TrpB, the perturbation made from

substituting a tryptophan to an alanine is a large one, and though a resulting loss of function from this mutation might suggest a cation- $\pi$  interaction, it would be impossible to rule out the effect that shift in steric bulk has on the binding pocket. Furthermore, because conventional mutagenesis can only affect the side chain, it does not provide any means for probing hydrogen bonds with the protein backbone. Nonsense suppression-based, non-canonical amino acid mutagenesis, however, offers a solution to these problems.<sup>52</sup> In this method, the residue of interest is replaced with an amino acid outside the canonical twenty. In theory, the method is only limited by what can be synthesized in the chemistry lab. In practice, this technique has been used to incorporate over 100 non-canonical amino acids in over 20 different ion channels.<sup>53</sup>

Non-canonical amino acid mutagenesis utilizes nonsense suppression, where the codon of the amino acid of interest is mutated to stop codon, and a suppressor tRNA inserts the amino acid during translation (Figure 6).<sup>54</sup> The cDNA of the gene is mutated to a stop codon at the residue of interest and the gene is then transcribed *in vitro* and injected into *Xenopus* oocytes alongside a suppressor tRNA preloaded with the desired non-canonical amino acid. This tRNA, also prepared *in vitro*, has an anticodon which recognizes the stop codon mutation and has been engineered to be bioorthogonal to the oocyte's endogenous tRNA synthetases.<sup>55</sup> The non-canonical amino acid is synthesized with a dinucleotide (dCA) appendage, which is then enzymatically ligated to a shortened version, or 74-mer, of the bioorthogonal tRNA. With this design, the tRNA will recognize the stop codon during translation, the ribosome will then insert the non-canonical amino acid into the nascent strand, and the used tRNA will be unable to get recharged by a canonical amino acid, thereby ensuring the only amino acid in the site of interest is the non-canonical one.

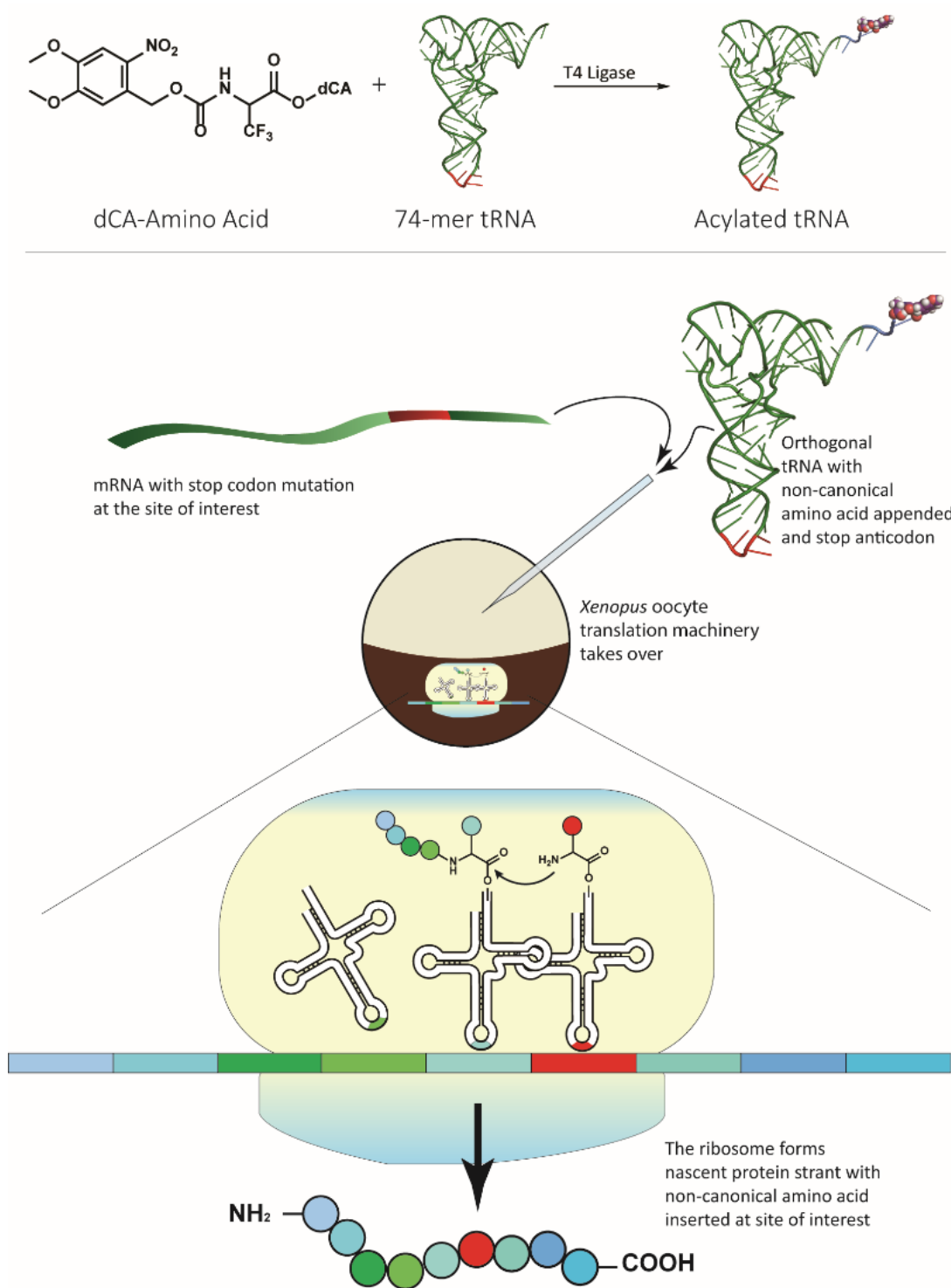


**Figure 6.** Top: T4 ligase is used to enzymatically append NVOC-protected dCA-amino acid to a 74-mer suppressor tRNA. Bottom: this tRNA-AA is injected alongside stop codon mutated mRNA into oocytes, wherein the ribosome takes over and inserts the amino acid into the nascent strand of the gene.

To ensure the final protein has the non-canonical amino acid incorporated, several controls are necessary. As a negative control, just the 74-mer tRNA is injected with the mRNA containing the stop codon mutation. In this case, translation would likely end at the stop codon, and running a dose response experiment ensures that this truncated protein is not viable. In an additional negative control, non-acylated but full length 76-mer tRNA is injected with the mRNA to check for reaminoacylation. If this control works, and there is no reaminoacylation of the 76-mer, then there should be no agonist-evoked current.

As previously mentioned, once the tRNA has been used in the ribosome, it becomes inert. Because of this, the tRNA behaves as a stoichiometric reagent in the translation process, and the amount of protein produced takes a large hit compared to conventional mutagenesis. Thus, experiments utilizing this chemical acylation method of nonsense suppression must be able to amplify the eventual read out. Although some nAChR subtypes are harder to express than others in their wild-type form and require mutations to be made that will increase expression levels and current without affecting binding,<sup>56</sup> TEVC electrophysiology is typically a sensitive enough technique to detect small amounts of protein made.

## 1.4 Thesis Summary

The primary focus of the work presented in this thesis is focused on developing a binding map for  $\alpha 6\beta 2$  in an effort to both advance our knowledge of nAChR function and to establish differences in binding between  $\alpha 6\beta 2$  and  $\alpha 4\beta 2$ . The first step toward this goal was to develop a heterologous  $\alpha 6\beta 2$  expression system in *Xenopus* oocytes, described in Chapter 2. With a set of mutations that allowed consistently high expression levels, the next step was to determine whether the binding interactions found to be important in  $\alpha 4\beta 2$

are functionally relevant in  $\alpha 6\beta 2$ . Chapter 3 details structure-function studies aimed at probing cation- $\pi$  interactions with three aromatic residues while Chapter 4 investigates hydrogen bonding between agonists and the carbonyl associated with TrpB.

In the process of pursuing these goals, some interesting characteristics about  $\alpha 4\beta 2$  became apparent that warranted further investigation. Chapter 5 probes several agonists that have been found to make a cation- $\pi$  interaction with both TrpB and TyrC2 in  $\alpha 4\beta 2$ . It seems likely that this is a general feature of secondary amines, as tertiary and quaternary amines only make a cation- $\pi$  interaction with TrpB. Finally, while most of this thesis has involved agonist-protein interactions, Chapter 6 details work done to probe for a functionally important hydrogen bond across the  $\alpha 4$  and  $\beta 2$  subunits, between the NH of the Trp B indole ring, and a backbone carbonyl on loop E. No such hydrogen bond was observed, but a new hydrogen bond structure-function study approach was developed.

The structure-function studies outlined above and discussed fully in this thesis reveal intricate details about how agonists bind, and how this binding differs at each subtype. The nAChR family plays an important role in cognitive function, and the  $\alpha 6\beta 2$  subtypes are important targets in both addiction and Parkinson's disease research; however, there are many subtypes, each with a different role. To truly tap into the potential of the nicotinic acetylcholine receptors as a drug target, each subtype must be distinguishable. With the work presented in the remaining chapters, we have come closer toward achieving that goal.

## 1.5 References

1. Nguyen, K., Marshall, L., Hu, S., Neff, L. & Centers for Disease Control and Prevention (CDC). State-specific prevalence of current cigarette smoking and smokeless tobacco use among adults aged  $\geq 18$  years - United States, 2011-2013. *MMWR Morb. Mortal. Wkly. Rep.* **64**, 532–536 (2015).
2. Centers for Disease Control and Prevention (CDC). Vital signs: current cigarette smoking among adults aged  $\geq 18$  years with mental illness - United States, 2009-2011. *MMWR Morb. Mortal. Wkly. Rep.* **62**, 81–87 (2013).
3. Singh, T. *et al.* Tobacco Use Among Middle and High School Students — United States, 2011–2015. *MMWR Morb. Mortal. Wkly. Rep.* **65**, 361–367 (2016).
4. Centers for Disease Control and Prevention (CDC). Smoking-attributable mortality, years of potential life lost, and productivity losses--United States, 2000-2004. *MMWR Morb. Mortal. Wkly. Rep.* **57**, 1226–1228 (2008).
5. Lavinghouze, S. R. *et al.* Trends in Quit Attempts Among Adult Cigarette Smokers — United States, 2001–2013. *MMWR Morb. Mortal. Wkly. Rep.* **64**, 1129–1135 (2015).
6. Dorsey, E. R. *et al.* Projected number of people with Parkinson disease in the most populous nations, 2005 through 2030. *Neurology* **68**, 384–386 (2007).
7. de Lau, L. M. & Breteler, M. M. Epidemiology of Parkinson's disease. *Lancet Neurol.* **5**, 525–535 (2006).
8. Tanner, C. M. *et al.* Smoking and Parkinson's disease in twins. *Neurology* **58**, 581–588 (2002).
9. Wirdefeldt, K., Gatz, M., Pawitan, Y. & Pedersen, N. L. Risk and protective factors for Parkinson's disease: a study in Swedish twins. *Ann. Neurol.* **57**, 27–33 (2005).
10. Quik, M. & Wonnacott, S.  $\alpha 6\beta 2^*$  and  $\alpha 4\beta 2^*$  Nicotinic Acetylcholine Receptors As Drug Targets for Parkinson's Disease. *Pharmacol. Rev.* **63**, 938–966 (2011).
11. Wonnacott, S. Presynaptic nicotinic ACh receptors. *Trends Neurosci.* **20**, 92–98 (1997).
12. Smart, T. G. & Paoletti, P. Synaptic Neurotransmitter-Gated Receptors. *Cold Spring Harb. Perspect. Biol.* **4**, a009662 (2012).
13. Miyazawa, A., Fujiyoshi, Y. & Unwin, N. Structure and gating mechanism of the acetylcholine receptor pore. *Nature* **423**, 949–955 (2003).
14. Kracun, S., Harkness, P. C., Gibb, A. J. & Millar, N. S. Influence of the M3–M4 intracellular domain upon nicotinic acetylcholine receptor assembly, targeting and function. *Br. J. Pharmacol.* **153**, 1474–1484 (2008).

15. Srinivasan, R. *et al.* Nicotine up-regulates  $\alpha 4\beta 2$  nicotinic receptors and ER exit sites via stoichiometry-dependent chaperoning. *J. Gen. Physiol.* **137**, 59–79 (2011).
16. Le Novère, N., Corringer, P.-J. & Changeux, J.-P. The diversity of subunit composition in nAChRs: Evolutionary origins, physiologic and pharmacologic consequences. *J. Neurobiol.* **53**, 447–456 (2002).
17. Millar, N. S. Assembly and subunit diversity of nicotinic acetylcholine receptors. *Biochem. Soc. Trans.* **31**, 869–874 (2003).
18. Millar, N. S. & Harkness, P. C. Assembly and trafficking of nicotinic acetylcholine receptors (Review). *Mol. Membr. Biol.* **25**, 279–292 (2008).
19. Gotti, C., Zoli, M. & Clementi, F. Brain nicotinic acetylcholine receptors: native subtypes and their relevance. *Trends Pharmacol. Sci.* **27**, 482–491 (2006).
20. Zoli, M., Pistillo, F. & Gotti, C. Diversity of native nicotinic receptor subtypes in mammalian brain. *Neuropharmacology* doi:10.1016/j.neuropharm.2014.11.003
21. Yang, K., Jin, G. & Wu, J. Mysterious  $\alpha 6$ -containing nAChRs: function, pharmacology, and pathophysiology. *Acta Pharmacol. Sin.* **30**, 740–751 (2009).
22. Quik, M. & McIntosh, J. M. Striatal  $\alpha 6^*$  Nicotinic Acetylcholine Receptors: Potential Targets for Parkinson's Disease Therapy. *J. Pharmacol. Exp. Ther.* **316**, 481–489 (2006).
23. Rucktooa, P., Smit, A. B. & Sixma, T. K. Insight in nAChR subtype selectivity from AChBP crystal structures. *Biochem. Pharmacol.* **78**, 777–787 (2009).
24. Brejc, K., *et al.* Crystal structure of an ACh-binding protein reveals the ligand-binding domain of nicotinic receptors. *Nature* **411**, 269–276 (2001).
25. Lester, H. A., Dibas, M. I., Dahan, D. S., Leite, J. F. & Dougherty, D. A. Cys-loop receptors: new twists and turns. *Trends Neurosci.* **27**, 329–336 (2004).
26. Corringer, P.-J., Novère, N. L. & Changeux, J.-P. Nicotinic Receptors at the Amino Acid Level. *Annu. Rev. Pharmacol. Toxicol.* **40**, 431–458 (2000).
27. Purohit, P. & Auerbach, A. Loop C and the mechanism of acetylcholine receptor–channel gating. *J. Gen. Physiol.* **141**, 467–478 (2013).
28. Van Arnam, E. B. & Dougherty, D. A. Functional Probes of Drug–Receptor Interactions Implicated by Structural Studies: Cys-Loop Receptors Provide a Fertile Testing Ground. *J. Med. Chem.* **57**, 6289–6300 (2014).
29. Dougherty, D. A. Cation- $\pi$  Interactions in Chemistry and Biology: A New View of Benzene, Phe, Tyr, and Trp. *Science* **271**, 163–168 (1996).
30. Dougherty, D. A. The Cation- $\pi$  Interaction. *Acc. Chem. Res.* **46**, 885–893 (2013).

31. Xiu, X., Puskar, N. L., Shanata, J. A. P., Lester, H. A. & Dougherty, D. A. Nicotine binding to brain receptors requires a strong cation- $\pi$  interaction. *Nature* **458**, 534–537 (2009).
32. Tavares, X. D. S. *et al.* Variations in Binding Among Several Agonists at Two Stoichiometries of the Neuronal,  $\alpha 4\beta 2$  Nicotinic Receptor. *J. Am. Chem. Soc.* **134**, 11474–11480 (2012).
33. Puskar, N. L., Xiu, X., Lester, H. A. & Dougherty, D. A. Two Neuronal Nicotinic Acetylcholine Receptors,  $\alpha 4\beta 4$  and  $\alpha 7$ , Show Differential Agonist Binding Modes. *J. Biol. Chem.* **286**, 14618–14627 (2011).
34. Cashin, A. L., Petersson, E. J., Lester, H. A. & Dougherty, D. A. Using Physical Chemistry To Differentiate Nicotinic from Cholinergic Agonists at the Nicotinic Acetylcholine Receptor. *J. Am. Chem. Soc.* **127**, 350–356 (2005).
35. Duffy, N. H., Lester, H. A. & Dougherty, D. A. Ondansetron and Granisetron Binding Orientation in the 5-HT<sub>3</sub> Receptor Determined by Unnatural Amino Acid Mutagenesis. *ACS Chem. Biol.* **7**, 1738–1745 (2012).
36. Lummis, S. C. R., L. Beene, D., Harrison, N. J., Lester, H. A. & Dougherty, D. A. A Cation- $\pi$  Binding Interaction with a Tyrosine in the Binding Site of the GABAC Receptor. *Chem. Biol.* **12**, 993–997 (2005).
37. Pless, S. A. *et al.* A cation- $\pi$  interaction in the binding site of the glycine receptor is mediated by a phenylalanine residue. *J. Neurosci. Off. J. Soc. Neurosci.* **28**, 10937–10942 (2008).
38. Pless, S. A. *et al.* A cation- $\pi$  interaction at a phenylalanine residue in the glycine receptor binding site is conserved for different agonists. *Mol. Pharmacol.* **79**, 742–748 (2011).
39. Spurny, R. *et al.* Pentameric ligand-gated ion channel ELIC is activated by GABA and modulated by benzodiazepines. *Proc. Natl. Acad. Sci. U. S. A.* **109**, E3028–3034 (2012).
40. Blum, A. P., Arnam, E. B. V., German, L. A., Lester, H. A. & Dougherty, D. A. Binding Interactions with the Complementary Subunit of Nicotinic Receptors. *J. Biol. Chem.* **288**, 6991–6997 (2013).
41. Blum, A. P., Lester, H. A. & Dougherty, D. A. Nicotinic pharmacophore: The pyridine N of nicotine and carbonyl of acetylcholine hydrogen bond across a subunit interface to a backbone NH. *Proc. Natl. Acad. Sci.* **107**, 13206–13211 (2010).
42. Hilf, R. J. C. & Dutzler, R. X-ray structure of a prokaryotic pentameric ligand-gated ion channel. *Nature* **452**, 375–379 (2008).
43. Bocquet, N. *et al.* X-ray structure of a pentameric ligand-gated ion channel in an apparently open conformation. *Nature* **457**, 111–114 (2009).
44. Hilf, R. J. C. & Dutzler, R. Structure of a potentially open state of a proton-activated pentameric ligand-gated ion channel. *Nature* **457**, 115–118 (2009).

45. Hibbs, R. E. & Gouaux, E. Principles of activation and permeation in an anion-selective Cys-loop receptor. *Nature* **474**, 54–60 (2011).
46. Hassaine, G. *et al.* X-ray structure of the mouse serotonin 5-HT<sub>3</sub> receptor. *Nature* **512**, 276–281 (2014).
47. Miller, P. S. & Aricescu, A. R. Crystal structure of a human GABA<sub>A</sub> receptor. *Nature* **512**, 270–275 (2014).
48. Huang, X., Chen, H., Michelsen, K., Schneider, S. & Shaffer, P. L. Crystal structure of human glycine receptor- $\alpha$ 3 bound to antagonist strychnine. *Nature* **526**, 277–280 (2015).
49. Peng, H. B. *Xenopus laevis*: Practical uses in cell and molecular biology. Solutions and protocols. *Methods Cell Biol.* **36**, 657–662 (1991).
50. Wagner, C. A., Friedrich, B., Setiawan, I., Lang, F. & Bröer, S. The use of *Xenopus laevis* oocytes for the functional characterization of heterologously expressed membrane proteins. *Cell. Physiol. Biochem. Int. J. Exp. Cell. Physiol. Biochem. Pharmacol.* **10**, 1–12 (2000).
51. Dascal, N. in *Current Protocols in Neuroscience* (eds. Crawley, J. N. *et al.*) (John Wiley & Sons, Inc., 2001).
52. Beene, D. L., Dougherty, D. A. & Lester, H. A. Unnatural amino acid mutagenesis in mapping ion channel function. *Curr. Opin. Neurobiol.* **13**, 264–270 (2003).
53. Dougherty, D. A. & Van Arnem, E. B. In Vivo Incorporation of Non-canonical Amino Acids by Using the Chemical Aminoacylation Strategy: A Broadly Applicable Mechanistic Tool. *ChemBioChem* **15**, 1710–1720 (2014).
54. Dougherty, D. A. Unnatural amino acids as probes of protein structure and function. *Curr. Opin. Chem. Biol.* **4**, 645–652 (2000).
55. Saks, M. E. *et al.* An engineered *Tetrahymena* tRNA<sup>Gln</sup> for in vivo incorporation of unnatural amino acids into proteins by nonsense suppression. *J. Biol. Chem.* **271**, 23169–23175 (1996).
56. Post, M. R., Limapichat, W., Lester, H. A. & Dougherty, D. A. Heterologous expression and nonsense suppression provide insights into agonist behavior at  $\alpha$ 6 $\beta$ 2 nicotinic acetylcholine receptors. *Neuropharmacology* **97**, 376–382 (2015).

## Chapter 2: Heterologous Expression of $\alpha 6\beta 2$ nAChRs\*

### 2.1 Abstract

In order to perform structure-function studies at the  $\alpha 6\text{-}\beta 2$  nAChR binding interface using the chemical acylation nonsense suppression method, a heterologous expression system must be used where cells produce consistently large agonist-induced current waveforms with an ideally square shape. Historically,  $\alpha 6\beta 2$  has presented several challenges, as the wild-type subunits produce no functional receptors when expressed *Xenopus* oocytes. This chapter discusses four reporter mutations to the wild-type receptor – one in the  $\alpha 6$  M2 helix, one in the  $\beta 2$  M2 helix, and two in the  $\beta 2$  M3-M4 loop – to create the construct deemed  $\alpha 6\beta 2^{\ddagger}$ . This results in a receptor population that produces large agonist-induced currents and monophasic dose response curves. Once developed,  $\alpha 6\beta 2^{\ddagger}$  was optimized and characterized. Experiments were performed that varied the injected mRNA ratio of  $\alpha 6$  to  $\beta 2$ , demonstrating there are likely two possible stoichiometries able to be expressed in oocytes. However, only the  $\alpha 6$ -biased injection yields a dose response curve with a high Hill coefficient and a monophasic curve, suggesting the  $\beta 2$ -biased responses are from a mixed population of subtype stoichiometries. A broad panel of agonists that typically activate other nAChR subtypes was then surveyed against  $\alpha 6\beta 2^{\ddagger}$ , and all of the compounds studied proved to be efficacious, with little attenuating effects on a post-agonist acetylcholine dose. With  $\alpha 6\beta 2^{\ddagger}$  characterized and fully optimized, it has the potential to be an invaluable tool for studying pharmacology of the  $\alpha 6\beta 2$  subtype, and the

---

\* A portion of the work presented in this chapter is adapted, with permission, from: Post, M. R., Limapichat, W., Lester, H. A. & Dougherty, D. A. Heterologous expression and nonsense suppression provide insights into agonist behavior at  $\alpha 6\beta 2$  nicotinic acetylcholine receptors. *Neuropharmacology* **97**, 376-382 (2015). doi:10.1016/j.neuropharm.2015.04.009

construct will be used in future chapters to perform structure-function studies via nonsense suppression-based non-canonical amino acid mutagenesis.

## 2.2 Introduction

The  $\alpha 6$  nAChR subunit is primarily localized to the ventral tegmental area and substantia nigra pars compacta areas of the brain.<sup>1-3</sup> Specifically,  $\alpha 6\beta 2$ -containing subtypes are expressed at the presynaptic terminals of dopaminergic neurons found in the mesocorticolimbic and nigrostriatal pathways.<sup>4-6</sup> Because they influence the release of dopamine from these neurons,  $\alpha 6\beta 2$ -containing subtypes have been of recent interest, and finding agonists that bind specifically to the  $\alpha 6$ - $\beta 2$  interface, while avoiding other subtypes, is a priority for both addiction and Parkinson's disease research.<sup>7-9</sup> Thus, developing detailed maps of the binding site at this interface and how it differs from  $\alpha 4\beta 2$  would aid in that endeavor. As Chapter 1 has outlined, structure-function studies using nonsense suppression-based non-canonical amino acid mutagenesis is a powerful tool used toward this aim. However, because tRNA is essentially a stoichiometric reagent in the chemical acylation technique used in nAChR structure-function studies, protein expression can be quite low. A robust heterologous expression system in *Xenopus* oocytes is needed for the non-suppressed, wild-type nAChR in order to compensate for such a hit once the suppression technique is incorporated.

A heterologous expression system which isolates the  $\alpha 6$ - $\beta 2$  binding interface has not previously been reported, mainly because  $\alpha 6\beta 2$  presents several challenges.<sup>10</sup> In the brain, the  $\alpha 6$  subunit is thought to form  $\alpha 6\beta 2$  pentamers, as well as complex subtypes with three or more different subunits, such as  $\alpha 6\alpha 4\beta 2$ ,  $\alpha 6\beta 2\beta 3$ , and  $\alpha 6\alpha 4\beta 2\beta 3$ .<sup>1</sup> This makes studying the pharmacology of  $\alpha 6$ -containing nAChRs quite challenging *in vivo* as it is

difficult to resolve the roles each subtype contributes. Furthermore, though  $\alpha 6$  and  $\beta 2$  have been shown to be translated in *Xenopus* oocytes, they are unable to form functional pentamers, instead forming oligomers that have functional agonist-binding sites but no ability to conduct ions.<sup>11</sup> In fact, when  $\alpha 6$  was first discovered, it was deemed the “orphan subunit,” because it could not be functionally expressed in oocytes no matter which other subunits were coinjected. Recent studies have relied on chimeras with an  $\alpha 6$  extracellular binding domain and an  $\alpha 3$  transmembrane domain.<sup>12,13</sup> While this strategy yields functional expression, it remains unclear what effect the different transmembrane domain might have on assembly, and therefore the  $\alpha 6$ - $\beta 2$  binding interface. Others have reported developing complex concatemers that have linked as many as five subunits into one gene.<sup>14,15</sup> While this solution effectively produces pentamers with the desired stoichiometry, nonsense suppression in these large single protein chains is likely difficult.

Rather, the ideal expression system to tolerate nonsense suppression-based non-canonical amino acid mutagenesis is one that utilizes one or more reporter mutations – conventional amino acid substitutions designed to increase translation, transport, or ion conductivity without affecting the binding site. Such a construct must result in a receptor that produces large and consistent agonist-induced current traces as well as dose-response curves that are monophasic, indicating only a single population of receptors has been expressed. In the work detailed in this chapter, four such reporter mutations were introduced into  $\alpha 6\beta 2$ , and when injected into oocytes produce functional receptors meeting all of those requirements.

## 2.2 Reporter Mutations Resulting in Functional Expression of $\alpha 6\beta 2$

In order to perform structure-function studies that probe noncovalent interactions between agonists and the  $\alpha 6\text{-}\beta 2$  interface, a pure population of  $\alpha 6\beta 2$  receptors must be heterologously expressed in *Xenopus* oocytes. However, merely injecting oocytes with wild-type  $\alpha 6\beta 2$  mRNA does not result in the formation of functional ion channels, as applications of high doses of acetylcholine (ACh) do not result in any current (Figure 1). In other

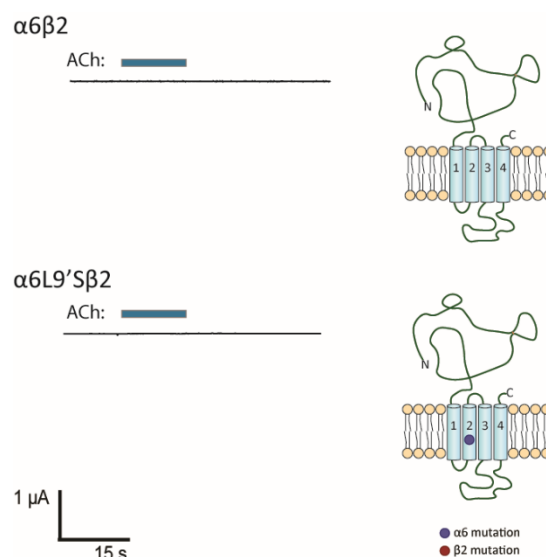


**Figure 1.** The cartoon depicts a schematic of the nAChR subunit with circles representing any reporter mutations made. Neither wild-type  $\alpha 6\beta 2$  nor  $\alpha 6\text{L}9'\text{S}\beta 2$  produce agonist-induced current.

challenging receptors such as  $\alpha 4\beta 2$ , a mutation made to the ninth residue in the M2 helix, which lines the channel pore and whose residues are numbered by a prime notation starting from the intracellular end, has resulted in both increased expression and conductance without affecting the pharmacological properties of the receptor.<sup>16-18</sup> Yet, unlike  $\alpha 4\text{L}9'\text{A}\beta 2$ , when the analogous  $\alpha 6\text{L}9'\text{S}\beta 2$  construct is injected into oocytes, no increase in current is seen (Figure 1). Rather, the same result as wild-type  $\alpha 6\beta 2$  is achieved in that no agonist-induced current is observed at all.

Interestingly,  $\alpha 6\text{L}9'\text{S}\beta 4$  does show some agonist-induced currents.<sup>19</sup> The lack of expression observed with  $\alpha 6\text{L}9'\text{S}\beta 2$  is therefore likely due to some interesting characteristics of the  $\beta 2$  M3-M4 loop, the domain thought to be responsible for trafficking from the endoplasmic reticulum (ER) to the cell membrane. Unlike other beta-like

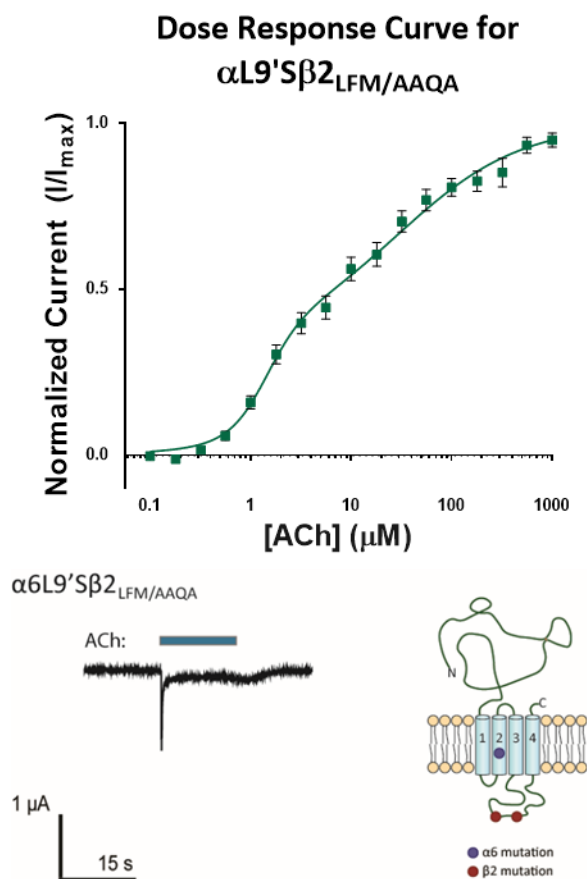


**Figure 2.** Shown is an example of the agonist-induced current trace at  $\alpha$ 6L9'S $\beta$ 2<sub>LFM/AAQA</sub> demonstrating an initial current spike and residual steady-state until wash out. The mutations made are shown in the cartoon schematic, and results of dose response experiments ( $N = 27$ ) are shown above, fit to the biphasic Hill equation:

$$I_{norm} = n * (1 / (1 + EC50_1)^{nH1}) + (1 - n) * (1 / (1 + EC50_2)^{nH2})$$

with each component having its own  $EC_{50}$  and Hill coefficient.

a smaller but sustained current until the agonist is washed out. The receptor is possibly entering into a desensitized state, but the sustained portion of the trace makes this conclusion slightly less certain. The highly biphasic dose response curve for this construct suggests that the unusual looking current trace (an ideal trace would show a square-ish wave form with a quick channel opening upon agonist application and sustained activation until agonist washout) is due to a mixed population of receptor stoichiometries. One

subunits, such as  $\beta$ 4, the M3-M4 loop of  $\beta$ 2 not only lacks an LXM ER exit motif, it also has an RRQR ER retention motif. Previous studies in mammalian cell line showed increased expression of fluorescent analogues of  $\alpha$ 4 $\beta$ 2 and  $\alpha$ 6 $\beta$ 2 by introducing an ER exit motif and eliminating the ER retention motif in  $\beta$ 2.<sup>20,21</sup> The mutations 347LFL/LFM349 and 365RRQR/AAQA368 were therefore incorporated into the  $\beta$ 2 subunit. When the  $\alpha$ 6L9'S $\beta$ 2<sub>LFM/AAQA</sub> construct was then injected into oocytes, ACh-induced currents were observed.

The current waveform observed with  $\alpha$ 6L9'S $\beta$ 2<sub>LFM/AAQA</sub> shows a quick spike of current upon ACh application followed by

stoichiometry perhaps experiences quick desensitization while another experiences a sustained activation until wash out, and the observed trace is a composite of both. However these possible stoichiometries were unable to be resolved by manipulating the mRNA injection ratio of  $\alpha 6$  to  $\beta 2$ . Furthermore, neither the traces nor the dose response curves showed much consistency from cell to cell, with large variances in  $EC_{50_1}$  and  $EC_{50_2}$  observed from curve to curve (as shown by the relatively large error bars and low Hill coefficients in Figure 2). Finally, the average maximum current from these dose response experiments was only  $0.25 \mu A$ , which along with other inconsistencies makes  $\alpha 6L9'S\beta 2_{LFM/AAQA}$  unconvincing for nonsense suppression.

An additional L9'S mutation was made in the  $\beta 2$  subunit in an attempt to further increase expression. The resulting  $\alpha 6L9'S\beta 2L9'S_{LFM/AAQA}$  (abbreviated as  $\alpha 6\beta 2^\ddagger$  throughout the rest of this thesis) showed currents consistently greater than  $1 \mu A$  in

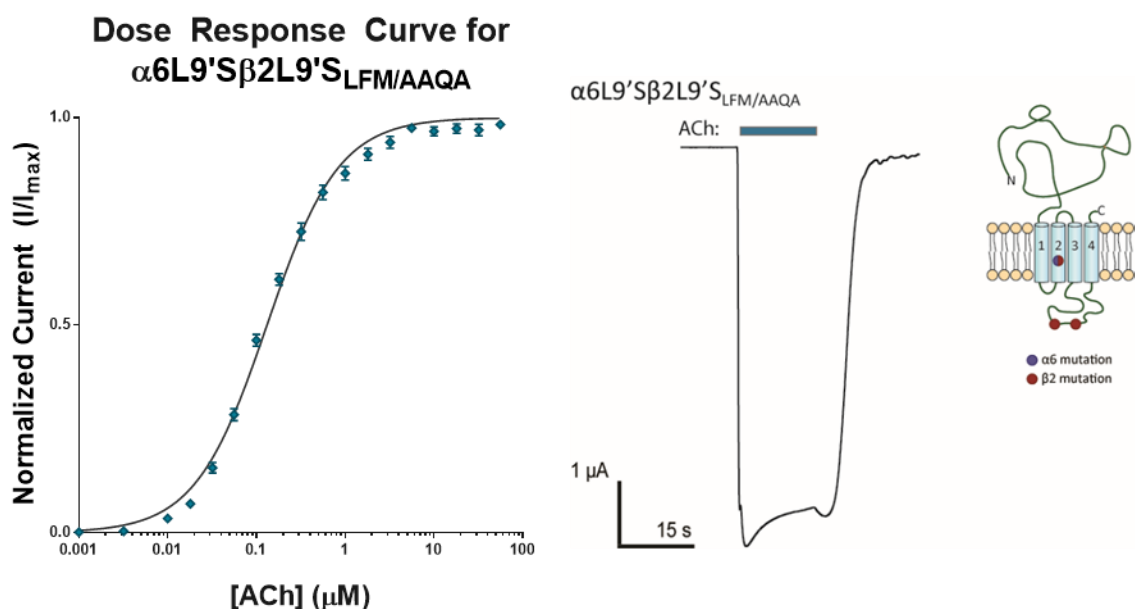


**Figure 3.** Shown is a representative current trace produced from application of ACh on cells injected with  $\alpha 6L9'S\beta 2L9'S_{LFM/AAQA}$  ( $\alpha 6\beta 2^\ddagger$ ) as well as a schematic picturing each mutation's location. The results of dose response experiments ( $N=16$ ) show a monophasic curve that suggests only one population of nAChRs is being expressed.

response to ACh. Additionally the waveforms had an ideal square shape that were typical from cell to cell (Figure 3). Dose response experiments produced a monophasic dose response curve with little variance in  $EC_{50}$  from cell to cell. Previous studies on the muscle-type receptor had shown baseline leak currents to be prohibitively high when all five subunits had an L9'S mutation, but the  $\alpha 6\beta 2^{\ddagger}$  construct typically produced baseline leak currents far less than agonist-induced current.

## 2.3 Characterization of $\alpha 6\beta 2^{\ddagger}$

### 2.3.1 Stoichiometry Control of $\alpha 6\beta 2^{\ddagger}$

Initial experiments with the  $\alpha 6\beta 2^{\ddagger}$  construct suggest the receptor can tolerate nonsense suppression, but before any structure-function studies are performed, the receptor must be fully optimized and characterized. As part of that process, the mRNA injection ratio of  $\alpha 6$  to  $\beta 2$  was varied from 50:1 to 1:20 while keeping the total amount of mRNA constant at 10 ng injected per cell. Two phenotypes were observed based on which subunit

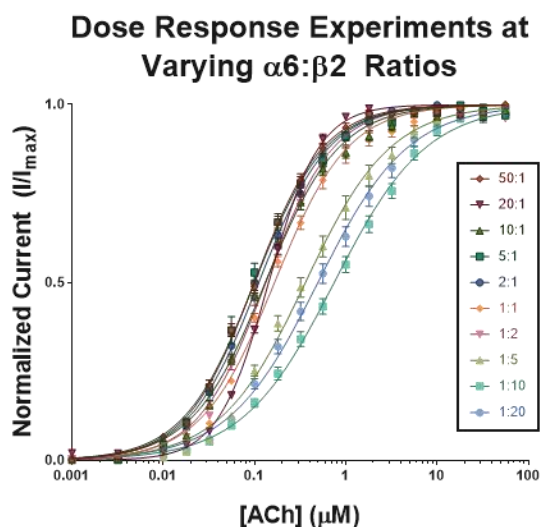


**Figure 4.** Results from dose response experiments performed at different mRNA  $\alpha 6:\beta 2$  ratio injections. Note that the  $\alpha 6$ -biased population's curves are concise with a steep Hill coefficient, whereas the more  $\beta 2$ -biased curves are spread out and have a low Hill coefficient.

was biased. An  $\alpha 6$ -biased population that included mRNA ratios from 50:1 to 1:2 ( $\alpha 6:\beta 2$ ) had an  $EC_{50}$  around 0.11  $\mu\text{M}$  and a Hill coefficient greater than 1. A second phenotype was observed in the three most  $\beta 2$ -biased injection ratios with an  $EC_{50}$  around 0.5  $\mu\text{M}$  and a Hill coefficient less than 1. A general attenuation in

**Table 1.** Varying mRNA  $\alpha 6:\beta 2$  Injection Ratios

Ratio	EC <sub>50</sub> (uM)	n <sub>H</sub>	I <sub>max</sub> (μA)	N
50:1	0.097 ± 0.002	1.17 ± 0.03	8.25 - 57.3	11
20:1	0.139 ± 0.003	1.64 ± 0.05	0.25 - 1.44	15
10:1	0.119 ± 0.004	1.17 ± 0.04	4.85 - 70.7	16
5:1	0.094 ± 0.003	1.17 ± 0.04	0.7 - 79.9	18
2:1	0.109 ± 0.002	1.14 ± 0.03	0.94 - 79.5	11
1:1	0.15 ± 0.01	1.15 ± 0.06	4.42 - 14.18	10
1:2	0.125 ± 0.003	1.23 ± 0.05	3.06 - 31.7	11
1:5	0.35 ± 0.02	0.095 ± 0.04	0.7 - 8.21	13
1:10	0.8 ± 0.04	0.83 ± 0.02	1.01 - 4.67	16
1:20	0.52 ± 0.03	0.86 ± 0.03	1.01 - 10.9	11

maximum currents was also observed in the  $\beta 2$ -biased population, though this trend is difficult to quantify because of oocyte variability.

The different phenotypes observed likely result from a difference in subunit stoichiometries correlated to the ratio of  $\alpha 6$  to  $\beta 2$  mRNA injected into cells. In cases where more  $\alpha 6$  mRNA is injected relative to  $\beta 2$ , more  $\alpha 6$  subunits will be translated and pentamers are more likely to have a majority  $\alpha 6$ . The reverse could be true for the  $\beta 2$  biased scenarios; however, while the tight distribution of EC<sub>50</sub> values and Hill coefficients suggest a single stoichiometry is activated in the  $\alpha 6$ -biased case, high variance in EC<sub>50</sub> values and low Hill coefficients suggest the  $\beta 2$ -biased ratios present a mixed population of stoichiometries at the cell surface. Previous studies of  $\alpha 4L9'$ A $\beta 2$  receptors have shown that they are able to adopt two different stoichiometries, confirmed to be  $(\alpha 4)_2(\beta 2)_3$  and  $(\alpha 4)_3(\beta 2)_2$ .<sup>22,23</sup> As with  $\alpha 6\beta 2^\ddagger$ , the  $\alpha 4L9'$ A $\beta 2$  stoichiometry expressed can be influenced by the mRNA injection ration, but more work is needed to confirm the exact make-up of the two populations observed in  $\alpha 6\beta 2^\ddagger$ . Because the  $\alpha 6$ -biased population is better behaved, a high  $\alpha 6$  to  $\beta 2$

**Table 2.** Results of Dose Response and Efficacy Experiments with a Panel of nAChR Agonists at  $\alpha 6\beta 2^{\ddagger}$ 

Agonist	EC <sub>50</sub> ( $\mu$ M)	n <sub>H</sub>	I <sub>max</sub> ( $\mu$ A)	N EC <sub>50</sub>	Eff	Attenuation	N Eff
ACh	0.17 ± 0.00	1.36 ± 0.03	0.28 - 14.87	12			
CCh	1.36 ± 0.05	1.12 ± 0.04	3.63 - 52.45	13	0.87 ± 0.04	0.98 ± 0.04	18
Ch	159 ± 7	1.32 ± 0.05	2.08 - 15.41	14	0.33 ± 0.02	1.06 ± 0.03	15
Var	0.031 ± 0.003	1.08 ± 0.08	0.51 - 12.07	15	0.33 ± 0.02	0.94 ± 0.02	19
TC299	0.071 ± 0.003	0.99 ± 0.04	1.73 - 21.86	12	0.59 ± 0.04	0.81 ± 0.05	16
Nic	0.057 ± 0.002	1.38 ± 0.05	9.48 - 54.42	10	0.49 ± 0.03	0.93 ± 0.02	22
MetaNic	0.74 ± 0.02	0.98 ± 0.03	0.43 - 40.38	13	0.64 ± 0.04	0.90 ± 0.03	15
NorNic	0.51 ± 0.01	1.32 ± 0.03	0.31 - 2.36	11	0.72 ± 0.02	0.84 ± 0.04	15
Cyt	0.027 ± 0.001	1.31 ± 0.05	0.57 - 31.91	11	0.28 ± 0.01	0.97 ± 0.02	20
Epi	0.00035 ± 0.00003	1.9 ± 0.2	0.47 - 2.81	12	0.54 ± 0.02	0.94 ± 0.04	19

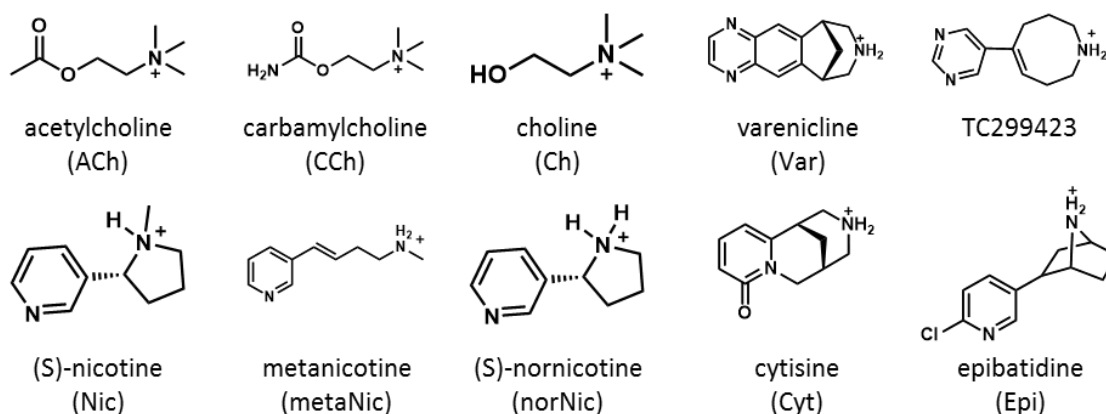
injection ratio will be used in the characterization studies in the following section as well as in the binding studies presented throughout this thesis.

### 2.3.2 Pharmacology of $\alpha 6\beta 2^{\ddagger}$

In order to better understand how this new construct behaves compared to other subtypes, and to get an idea of what compounds would be interesting to use in structure-function studies, a panel of agonists was screened at  $\alpha 6\beta 2^{\ddagger}$ . Several known nAChR agonists – ACh, nicotine, metanicotine, nornicotine, varenicline, cytisine, choline, carbamylcholine, and epibatidine – were evaluated in addition to TC299423, an emerging candidate for the treatment of nAChR-related disorders and thought to be potentially  $\alpha 6$ -selective.<sup>24</sup> Dose response experiments were performed for each agonist to determine the EC<sub>50</sub> and Hill coefficient. As shown in Table 2, metanicotine, nornicotine, choline, and carbamylcholine have higher EC<sub>50</sub> values – and are thus less potent – than ACh. Nicotine, varenicline, cytisine, and TC29423 are slightly more potent, while epibatidine has an observed EC<sub>50</sub> several orders of magnitude lower than ACh. These trends are consistent

with previously reported data using ( $\alpha 6/\alpha 3$ ) $\beta 2$  chimeric constructs where nicotine was found to be more potent than ACh.

Efficacy tests were also conducted at  $\alpha 6\beta 2^{\ddagger}$  with the same panel of agonists. In this experiment, ACh is applied to cells, followed by the agonist of interest and a second dose of ACh. The concentration used for each agonist corresponded to the one that achieves a maximum response on the dose response curve. The current elicited from the agonist dose was divided by the initial ACh current to determine efficacy, while the second ACh current



### Agonist Screen Results at $\alpha 6\beta 2^{\ddagger}$

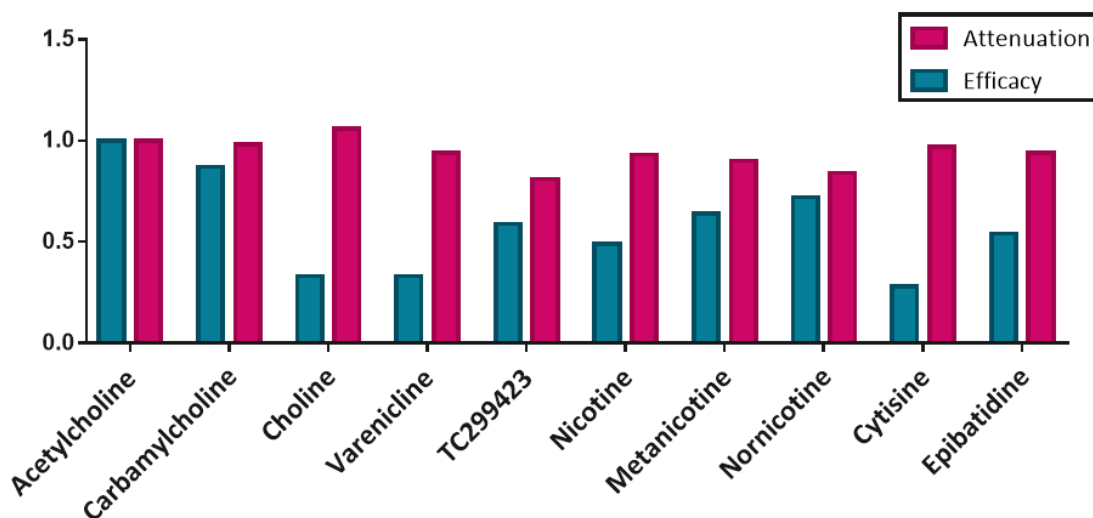


**Figure 5.** Top: chemical structures of all the agonists screened at  $\alpha 6\beta 2^{\ddagger}$  in this chapter. Bottom: a bar graph showing the relative efficacies of each agonist to acetylcholine (in blue), as well as the level of attenuation each agonist has on the second dose of acetylcholine (in red).

was divided to determine the attenuation level (results shown in Figure 6). The agonists screened were partial agonists, as they all induced a channel response but had efficacy values less than 1. Only TC299423 and nornicotine showed any meaningful levels of attenuation at 0.81 and 0.79 respectively.

## 2.4 Conclusions

All together, these results show that  $\alpha 6\beta 2$  nAChRs can be expressed as a controlled and pure population in the form of  $\alpha 6\beta 2^{\ddagger}$ , with consistently large agonist-induced currents elicited from ACh as well as a broad panel of compounds. The results presented in this chapter show that  $\alpha 6\beta 2^{\ddagger}$  is a good candidate for nonsense suppression-based non-canonical amino acid mutagenesis. The next two chapters will discuss structure-function studies using the  $\alpha 6\beta 2^{\ddagger}$  construct that probe functional binding interactions made by ACh, nicotine, and TC299423 at the  $\alpha 6$ - $\beta 2$  interface in order to distinguish this binding site from  $\alpha 4\beta 2$ . Still, more work can be done to further characterize  $\alpha 6\beta 2^{\ddagger}$ . Single-channel patch clamp recording and analysis of the receptor would be particularly informative and reveal information about the gating and kinetics of  $\alpha 6\beta 2$  in addition to binding. Experiments to determine the actual stoichiometry of the  $\alpha 6$ -biased injection ratio population would also be useful.

The  $\alpha 6\beta 2$  nAChR subtype has emerged as an important target in the study of addiction and Parkinson's disease, but research has been challenging because of the lack of a method for interrogating a pure population of  $\alpha 6\beta 2$  receptors. The  $\alpha 6\beta 2^{\ddagger}$  construct has been shown here to be an excellent heterologous expression system in *Xenopus* oocytes and a useful tool for comparing agonists amongst each other. Furthermore, it has opened

avenues for more complex studies that will hopefully one day help inform toward the design of subtype-specific drugs.

## 2.5 Materials and Methods

### *Molecular Biology*

Rat  $\alpha 6$  and  $\beta 2$  nAChRs were in the pGEMhe vector, a cDNA plasmid optimized for protein expression in *Xenopus* oocytes. Site-directed mutagenesis was performed by PCR using the Stratagene QuikChange protocol and primers ordered from Integrated DNA Technologies (Coralville, IA). Circular cDNA was linearized with SbfI (New England Biolabs, Ipswich, MA) and then transcribed *in vitro* using T7 mMessage mMachine kit (Life Technologies, Santa Clara, CA), with a purification step after each process (Qiagen, Valencia, CA). Final concentrations were quantified by UV spectroscopy.

### *Ion Channel Expression*

*Xenopus laevis* oocytes (stage V to VI) were sourced from both a Caltech facility and Ecocyte Bio Science (Austin, TX). Oocytes were injected with 50 nL solution containing either 5 or 10 ng mRNA. The  $\alpha 6:\beta 2$  ratio is presented as a mass ratio. Cells were incubated 24-48 hours at 18°C in ND96 solution (96 mM NaCl, 2mM KCl, 1 mM MgCl<sub>2</sub>, and 5mM HEPES, pH 7.5) enriched with theophylline, sodium pyruvate, gentamycine, and horse serum.

### *Whole-Cell Electrophysiological Characterization*

Acetylcholine chloride, choline chloride, carbamylcholine chloride, cytosine, and (-)-nicotine tartrate were purchased from Sigma Aldrich (St Louis, MO), ( $\pm$ )-epibatidine was purchased from Tocris (Bristol, UK), (S)-normicotine hydrochloride was purchased from Matrix Scientific (Columbia, SC), while varenicline (Pfizer) and metanicotine and TC299423 (Targacept) were generous gifts. Agonist-induced currents were recorded in TEVC mode using the OpusXpress 6000A (Molecular Devices, Sunnyvale, CA) at a holding potential of -60 mV in a running buffer of Ca<sup>2+</sup>-free ND96. Agonists were prepared in Ca<sup>2+</sup>-free ND96 and delivered to cells via a 1 mL application over 15 sec followed by a 2 min wash. Data from dose-response experiments were normalized, averaged, and fit to the Hill equation using Kaleidagraph (Synergy Software, Reading PA),

though data are visualized here with Prism (GraphPad Software, La Jolla, CA). Error bars are presented as standard error of the mean, while  $EC_{50}$  and Hill coefficient errors are reported by Kaleidagraph and represent the sum of the squared error between the data and the calculated fit.

## 2.6 References

1. Gotti, C., Zoli, M. & Clementi, F. Brain nicotinic acetylcholine receptors: native subtypes and their relevance. *Trends Pharmacol. Sci.* **27**, 482–491 (2006).
2. Zoli, M., Pistillo, F. & Gotti, C. Diversity of native nicotinic receptor subtypes in mammalian brain. *Neuropharmacology* **96**, 302–311 (2015).
3. Grady, S. R. *et al.* Structural differences determine the relative selectivity of nicotinic compounds for native  $\alpha 4\beta 2^*$ -,  $\alpha 6\beta 2^*$ -,  $\alpha 3\beta 4^*$ - and  $\alpha 7$ -nicotine acetylcholine receptors. *Neuropharmacology* **58**, 1054–1066 (2010).
4. Quik, M. & Wonnacott, S.  $\alpha 6\beta 2^*$  and  $\alpha 4\beta 2^*$  Nicotinic Acetylcholine Receptors As Drug Targets for Parkinson's Disease. *Pharmacol. Rev.* **63**, 938–966 (2011).
5. Yang, K., Jin, G. & Wu, J. Mysterious  $\alpha 6$ -containing nAChRs: function, pharmacology, and pathophysiology. *Acta Pharmacol. Sin.* **30**, 740–751 (2009).
6. Wang, J., Kuryatov, A. & Lindstrom, J. Expression of cloned  $\alpha 6^*$  nicotinic acetylcholine receptors. *Neuropharmacology* **96**, 194–204 (2015).
7. Holladay, M. W., Dart, M. J. & Lynch, J. K. Neuronal Nicotinic Acetylcholine Receptors as Targets for Drug Discovery. *J. Med. Chem.* **40**, 4169–4194 (1997).
8. Quik, M. & McIntosh, J. M. Striatal  $\alpha 6^*$  Nicotinic Acetylcholine Receptors: Potential Targets for Parkinson's Disease Therapy. *J. Pharmacol. Exp. Ther.* **316**, 481–489 (2006).
9. Bordia, T., Hrachova, M., Chin, M., McIntosh, J. M. & Quik, M. Varenicline Is a Potent Partial Agonist at  $\alpha 6\beta 2^*$  Nicotinic Acetylcholine Receptors in Rat and Monkey Striatum. *J. Pharmacol. Exp. Ther.* **342**, 327–334 (2012).
10. Kuryatov, A., Olale, F., Cooper, J., Choi, C. & Lindstrom, J. Human  $\alpha 6$  AChR subtypes: subunit composition, assembly, and pharmacological responses. *Neuropharmacology* **39**, 2570–2590 (2000).
11. Gerzanich, V., Kuryatov, A., Anand, R. & Lindstrom, J. 'Orphan'  $\alpha 6$  Nicotinic AChR Subunit Can Form a Functional Heteromeric Acetylcholine Receptor. *Mol. Pharmacol.* **51**, 320–327 (1997).
12. Papke, R. L. *et al.* Extending the analysis of nicotinic receptor antagonists with the study of  $\alpha 6$  nicotinic receptor subunit chimeras. *Neuropharmacology* **54**, 1189–1200 (2008).
13. Capelli, A. M. *et al.* Stable expression and functional characterization of a human nicotinic acetylcholine receptor with  $\alpha 6\beta 2$  properties: discovery of selective antagonists. *Br. J. Pharmacol.* **163**, 313–329 (2011).

14. Kuryatov, A. & Lindstrom, J. Expression of Functional Human  $\alpha 6\beta 2\beta 3^*$  Acetylcholine Receptors in *Xenopus laevis* Oocytes Achieved through Subunit Chimeras and Concatamers. *Mol. Pharmacol.* **79**, 126–140 (2011).
15. Ley, C. K.-K., Kuryatov, A., Wang, J. & Lindstrom, J. M. Efficient Expression of Functional ( $\alpha 6\beta 2$ ) $2\beta 3$  AChRs in *Xenopus* Oocytes from Free Subunits Using Slightly Modified  $\alpha 6$  Subunits. *PLoS ONE* **9**, e103244 (2014).
16. Gleitsman, K. R., Shanata, J. A. P., Frazier, S. J., Lester, H. A. & Dougherty, D. A. Long-Range Coupling in an Allosteric Receptor Revealed by Mutant Cycle Analysis. *Biophys. J.* **96**, 3168–3178 (2009).
17. Filatov, G. N. & White, M. M. The role of conserved leucines in the M2 domain of the acetylcholine receptor in channel gating. *Mol. Pharmacol.* **48**, 379–384 (1995).
18. Fonck, C. *et al.* Novel Seizure Phenotype and Sleep Disruptions in Knock-In Mice with Hypersensitive  $\alpha 4^*$  Nicotinic Receptors. *J. Neurosci.* **25**, 11396–11411 (2005).
19. Limapichat, W., Dougherty, D. A. & Lester, H. A. Subtype-Specific Mechanisms for Functional Interaction between  $\alpha 6\beta 4^*$  Nicotinic Acetylcholine Receptors and P2X Receptors. *Mol. Pharmacol.* **86**, 263–274 (2014).
20. Xiao, C. *et al.* Characterizing functional  $\alpha 6\beta 2$  nicotinic acetylcholine receptors in vitro: Mutant  $\beta 2$  subunits improve membrane expression, and fluorescent proteins reveal responsive cells. *Biochem. Pharmacol.* **82**, 852–861 (2011).
21. Srinivasan, R. *et al.* Nicotine up-regulates  $\alpha 4\beta 2$  nicotinic receptors and ER exit sites via stoichiometry-dependent chaperoning. *J. Gen. Physiol.* **137**, 59–79 (2011).
22. Nelson, M. E., Kuryatov, A., Choi, C. H., Zhou, Y. & Lindstrom, J. Alternate Stoichiometries of  $\alpha 4\beta 2$  Nicotinic Acetylcholine Receptors. *Mol. Pharmacol.* **63**, 332–341 (2003).
23. Moroni, M., Zwart, R., Sher, E., Cassels, B. K. & Bermudez, I.  $\alpha 4\beta 2$  Nicotinic Receptors with High and Low Acetylcholine Sensitivity: Pharmacology, Stoichiometry, and Sensitivity to Long-Term Exposure to Nicotine. *Mol. Pharmacol.* **70**, 755–768 (2006).
24. Wall, T. R. Effects of TI-299423 on Neuronal Nicotinic Acetylcholine Receptors. (California Institute of Technology, 2015).

## Chapter 3: Probing for Agonist Cation- $\pi$ Interactions

### in $\alpha 6\beta 2$ nAChRs<sup>†</sup>

#### 3.1 Abstract

A major goal of the work presented in this thesis is to characterize the binding site of the  $\alpha 6\beta 2$  nAChR subtype in an attempt to differentiate it from the other subtypes. With the  $\alpha 6\beta 2^{\ddagger}$  construct presented in Chapter 2, this is now possible. Previous studies with the  $\alpha 4\beta 2$  subtype have shown that acetylcholine and nicotine form a critical cation- $\pi$  interaction with a conserved tryptophan on loop B, while studies in the  $\alpha 7$  subtype show a functional cation- $\pi$  interaction is made between acetylcholine and a tyrosine on loop A. This chapter investigates whether acetylcholine, nicotine, and TC299423 make a functional cation- $\pi$  interaction at TrpB, TyrA, and TyrC2 using structure-function studies where the aromatic side chain is replaced with analogues containing electron-withdrawing substitutions on the ring system. When a functional cation- $\pi$  interaction is present, as negative electrostatic potential is drawn away from the center of the aromatic ring, binding should decrease. Therefore, a progressive increase in  $EC_{50}$  over the course of a fluorination series indicates a functional cation- $\pi$  interaction. Of the nine interactions probed, only acetylcholine at TrpB was observed to have such a trend. This suggests  $\alpha 6\beta 2$  has a unique binding site from the other subtypes, and raises important questions about the relevant binding interactions occurring when nicotine and TC299423 activate the receptor.

---

<sup>†</sup> A portion of the work presented in this chapter is adapted, with permission, from: Post, M. R., Limapichat, W., Lester, H. A. & Dougherty, D. A. Heterologous expression and nonsense suppression provide insights into agonist behavior at  $\alpha 6\beta 2$  nicotinic acetylcholine receptors. *Neuropharmacology* **97**, 376-382 (2015). doi:10.1016/j.neuropharm.2015.04.009

### 3.2 Introduction

The  $\alpha 6\beta 2^{\ddagger}$  construct discussed in Chapter 2 opens the door to studies that probe for binding interactions at the  $\alpha 6$ - $\beta 2$  interface. Throughout the nAChR family, a binding site forms at the interface of alpha and beta-like subunits in their extracellular domains – where  $\alpha$  forms the primary face and contributes loops A-C and  $\beta$  forms the complementary face and contributes loops D-F – and is shaped by a cluster of aromatic residues.<sup>1,2</sup> This so-

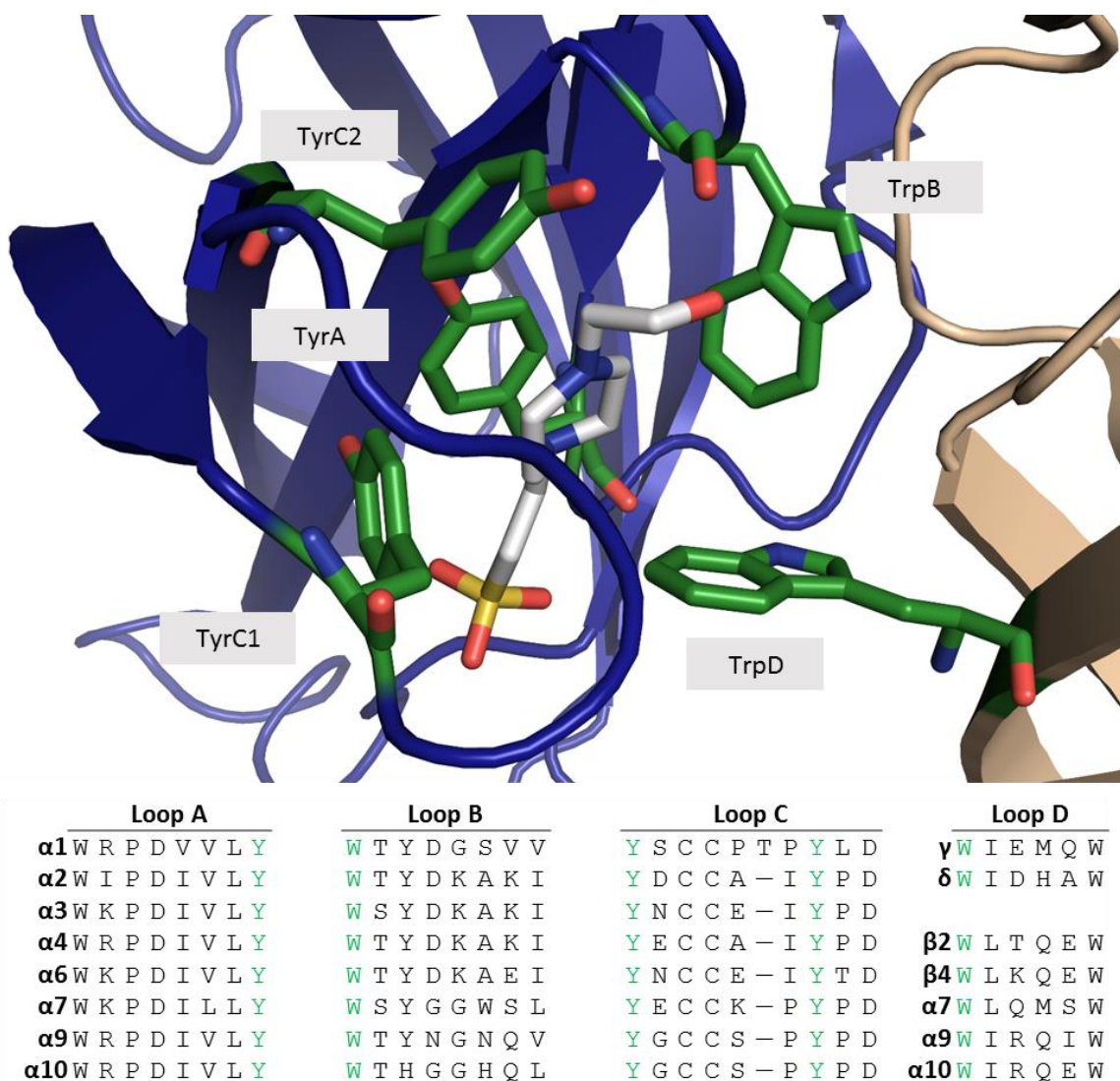


**Figure 1.** Above is a snapshot of the aromatic box region in AChB, crystallized with HEPES. The primary face is colored blue while the complementary face is tan, and the five aromatic residues that make up the box are highlighted in green. Below is an alignment of the human alpha subunits that can contribute to the primary face of the binding site as well as the subunits that can contribute loop D to the complementary face. PDB: 1I9B

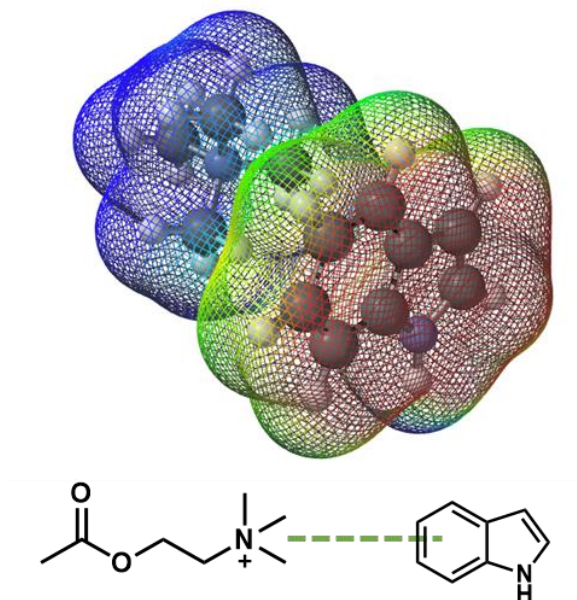


**Figure 2.** A three dimensional view of a cation- $\pi$  interaction between tetramethylammonium and an indole ring using electrostatic potential maps where red represents negative electrostatic potential and blue, positive. A structural schematic below shows a similar cation- $\pi$  interaction between the quaternary ammonium group of acetylcholine and an indole ring.

called aromatic box is formed by four of the six loops contributing five aromatic side chains – TyrA ( $\alpha$ 6:Y93), TrpB ( $\alpha$ 6:W149), TyrC1 ( $\alpha$ 6:Y190), TyrC2 ( $\alpha$ 6Y197), and TrpD ( $\beta$ 2:W57) – and is responsible for binding the cationic moiety of agonists and antagonists.<sup>3</sup> The aromatic

box has been visualized via structures of the acetylcholine binding protein (AChBP), a water soluble protein homologous to the extracellular region (Figure 1) and shows agonists positioned such that the cationic moiety is pointing

toward the face of TrpB.<sup>1</sup> The nature of the aromatic box suggests, then, that a cation- $\pi$  interaction contributes significantly to ligand binding.

The cation- $\pi$  interaction is an electrostatic interaction between a positively charged moiety – such as quaternary ammonium group of ACh – and the negative electrostatic potential concentrated on the face of an aromatic group, such as the phenol ring of tyrosine or the indole group of tryptophan (Figure 2).<sup>4,5</sup> The cation- $\pi$  interaction has been demonstrated in the gas phase, with potassium ions and ammonium binding to benzene with about 19 kcal/mol binding energy.<sup>6</sup> In addition to its significance to ligand recognition in the pLGIC receptor family,<sup>7</sup> discussed in depth in Chapter 1, the cation- $\pi$  interaction has been found to be important in general protein structure as well, with an average of one

energetically significant cation- $\pi$  interaction observed between a positively charged side chain and an aromatic side chain for every 77 residues in a protein.<sup>8</sup>

A recent computational study suggests that all five residues in the AChBP aromatic box can contribute a cation- $\pi$  interaction to the agonist, with the TrpB, TyrC2, and TyrA side chains contributing 8.3, 8.0, and 2.3 kcal/mol respectively.<sup>9</sup> It is likely that this is possible at the nAChR aromatic boxes as well; however, only certain residues have empirically been found to form a functional cation- $\pi$  interaction with agonists.<sup>7</sup> Previously reported structure-function studies with  $\alpha 4\beta 2$  and muscle-type have confirmed that a cation- $\pi$  interaction with TrpB is critical for the binding of ACh.<sup>10,11</sup> At the  $\alpha 7$ - $\alpha 7$  interface, the map is slightly different, as acetylcholine makes a functionally important cation- $\pi$  interaction with TyrA instead.<sup>12</sup> An alignment of four of the six loops (Figure 1) shows that all five aromatic residues are conserved amongst  $\alpha 6$ ,  $\alpha 4$ , and  $\alpha 1$ , suggesting that a cation- $\pi$  interaction may play a similarly important role at the  $\alpha 6$ - $\beta 2$  interface

Structure-function studies are used to probe for functional noncovalent binding interactions, wherein a small perturbation is made to the binding site, and changes in  $EC_{50}$  are monitored. For cation- $\pi$  interactions, this means substituting the aromatic residue with a non-canonical amino acid that has less concentrated negative electrostatic potential on the face of the ring, accomplished by using analogues with electron-withdrawing substituents on the ring's edge, such as fluorotryptophan and fluorophenylalanine. The effect is additive as well, with additional fluorine substituents causing a greater loss of function.

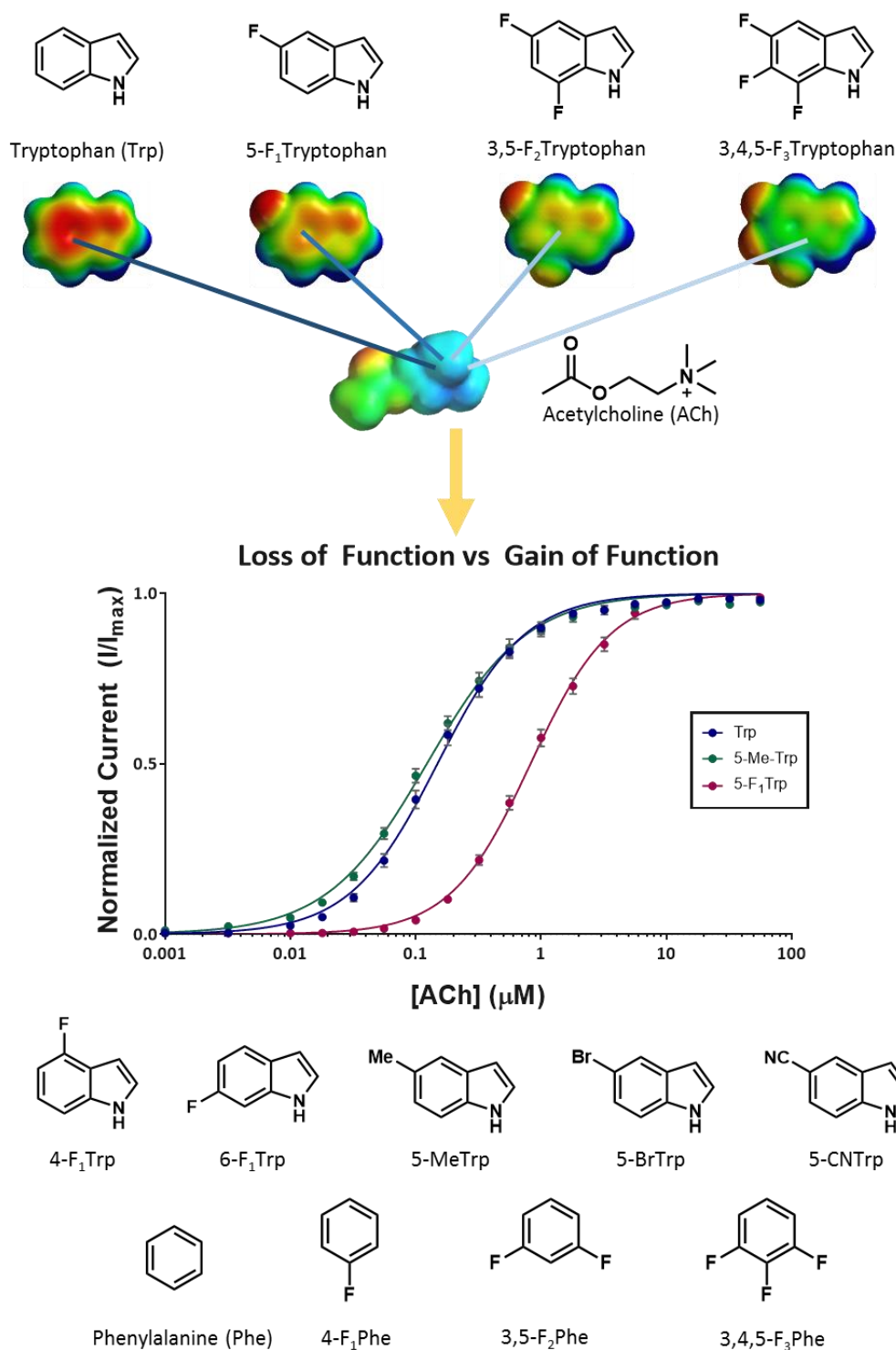


**Figure 3.** A representative schematic of the structure-function studies used to probe for cation- $\pi$  interactions wherein electron-withdrawing substituents incrementally draw negative electrostatic potential away from the face of the aromatic ring. The results from dose response experiments at each analogue are then plotted and fit to the Hill equation. A loss of function (red) causes a rightward shift in the dose response curve away from wild-type (blue) and an increase in  $EC_{50}$ , while a gain of function mutation (green) has the opposite effect. Below are the other non-canonical amino acids used in this chapter.

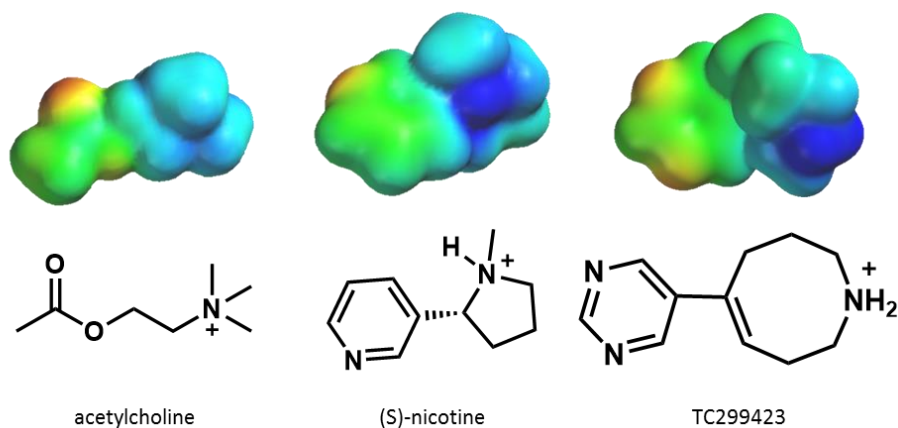


**Figure 4.** Structures and electrostatic potential maps of the agonists involved in structure-function studies, from HF 6-31G\*\* calculations ranging from -10 (red) to +150 (blue) kcal/mol

Because these mutations affect only the binding site, and gating is not perturbed,  $EC_{50}$  values can be used to measure the ligand-binding equilibrium constant for apo and bound states. Thus, the  $\log(EC_{50})$  is proportional to the binding energy, and as the binding interaction is theoretically weakened, the  $EC_{50}$  is expected to increase in the case of a functionally important cation- $\pi$  interaction. The theoretical binding energy between an agonist and each analogue in these experiments has traditionally been approximated with an *ab initio* Hartree-Fock calculation between a sodium ion and the side chain. The  $\log(EC_{50})$  for each analogue is then plotted against these values and a linear plot with a negative slope indicates a functionally important cation- $\pi$  interaction.

The work presented in this chapter takes a similar approach with ACh, nicotine, and TC299423 at three residues aligned with amino acids previously shown to form a functionally important cation- $\pi$  interaction – TrpB, TyrA, and TyrC2 – in  $\alpha 6\beta 2^{\ddagger}$ . An updated set of theoretical cation- $\pi$  binding energy values are used, calculated using M06

density functional theory instead of Hartree-Fock.<sup>‡</sup> Of all nine ligand-residue combinations tested, only ACh at TrpB shows a cation- $\pi$  interaction, suggesting the  $\alpha 6$ - $\beta 2$  interface indeed has a unique pharmacology.

### 3.3 Cation- $\pi$ Binding Studies at TrpB

#### 3.3.1 Acetylcholine binding at TrpB

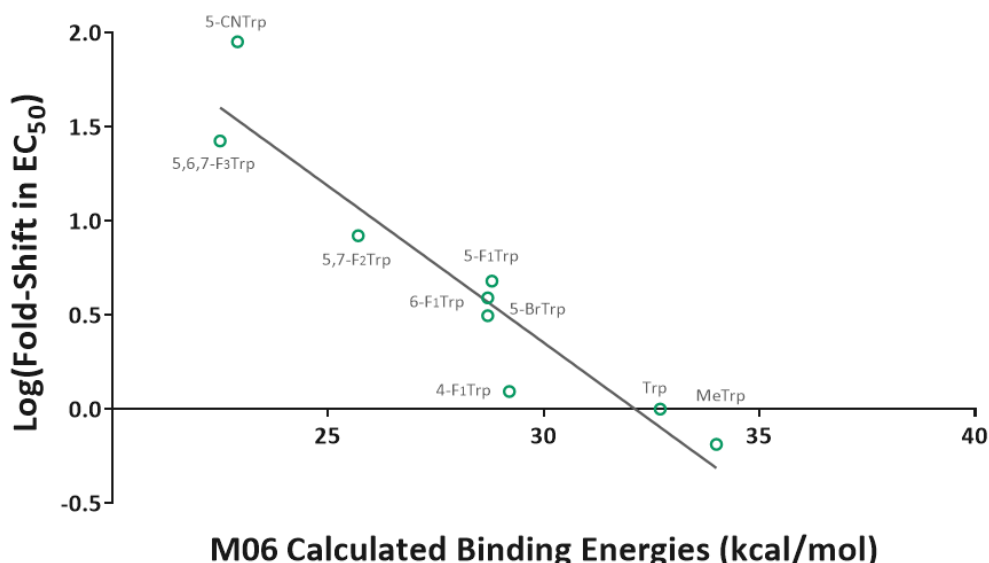
Acetylcholine has been found to make a functionally important cation- $\pi$  interaction at TrpB with every nAChR subtype investigated except  $\alpha 7$ . As such, this was the logical starting point to probe the  $\alpha 6$ - $\beta 2$  interface. For initial nonsense suppression experiments,  $\alpha 6\beta 2$ <sup>‡</sup> with an  $\alpha 6$  W149TAG mutation was injected into oocytes in a 10:1 mRNA ratio alongside tRNA acylated with the desired non-canonical tryptophan analogues. Dose response experiments were then performed with ACh, and the EC<sub>50</sub> value for each analogue was determined. Considering first the fold-shifts in EC<sub>50</sub> for 5-F<sub>1</sub>Trp, 5,7-F<sub>2</sub>Trp, and 5,6,7-F<sub>3</sub>Trp, there is a clear trend, with each additional fluorine causing greater fold-shifts. To be certain this correlation was due to electrostatic effects, 5-MeTrp, 5-F<sub>1</sub>Trp, and 5-BrTrp – all residues with a single substituent at the 5 position – were examined. The steric demands of these substituents are Br>Me>F, while the calculated cation- $\pi$  modifying ability is F $\approx$ Br>Me. The data follow the cation- $\pi$  prediction well, and therefore cannot be interpreted as a steric effect.

Figure 5 shows all the data collected at TrpB. There are some outliers in the analysis. While 5-F<sub>1</sub>Trp and 6-F<sub>1</sub>Trp show very similar results and follow the trend closely, 4-F<sub>1</sub>Trp is 3-4 times more potent than expected, producing near wild-type

---

<sup>‡</sup> Calculations were performed by Matthew Davis

## ACh-TrpB Cation- $\pi$ Interactions in $\alpha 6\beta 2$



**Figure 5.** The log of the fold-shift in  $EC_{50}$  is plotted against the M06 6-31G<sup>\*\*</sup> calculated binding energy between a sodium ion and each non-canonical side chain used at Trp B in 10:1  $\alpha 6\beta 2$ <sup>‡</sup>. The linear trend indicates the presence of a strong cation- $\pi$  interaction between the indole side chain and ACh.

**Table 1.** Investigating a Cation- $\pi$  Interaction with ACh at 10:1  $\alpha 6\beta 2$ <sup>‡</sup>

10:1	$EC_{50}$ (uM)	$n_H$	$I_{max}$ (uA)	Fold Shift	N
Trp	$0.169 \pm 0.003$	$1.36 \pm 0.03$	0.28 - 14.87	1	12
MeTrp	$0.11 \pm 0.002$	$1.18 \pm 0.02$	0.19 - 19.36	0.7	12
4-F <sub>1</sub> Trp	$0.21 \pm 0.006$	$1.25 \pm 0.04$	0.71 - 6.92	1.2	9
5-F <sub>1</sub> Trp	$0.81 \pm 0.01$	$1.37 \pm 0.03$	1.39 - 14.37	4.8	10
6-F <sub>1</sub> Trp	$0.66 \pm 0.02$	$1.30 \pm 0.04$	0.18 - 4.28	3.9	10
BrTrp	$0.53 \pm 0.01$	$1.32 \pm 0.04$	0.22 - 15.05	3.1	14
F <sub>2</sub> Trp	$1.41 \pm 0.02$	$1.43 \pm 0.02$	0.76 - 9.33	8.3	9
CNTrp	$15.1 \pm 0.6$	$1.25 \pm 0.05$	0.31 - 13.28	89	14
F <sub>3</sub> Trp	$4.5 \pm 0.2$	$1.04 \pm 0.03$	0.09 - 1.94	27	12

behavior. This is the only non-canonical amino acid studied with a substituent in the 4 position, suggesting a special interaction at this site. Also, 5-CNTrp, which is predicted to be strongly inactivating, shows the expected loss of function, but the effect is roughly 5-fold greater than expected. The cyano group is quite polar in and of itself, and therefore could be influencing the binding site in unexpected ways. Still, when taken as a whole,

these results provide strong evidence that ACh is involved in a functionally important cation- $\pi$  interaction with TrpB at the  $\alpha 6$ - $\beta 2$  interface.

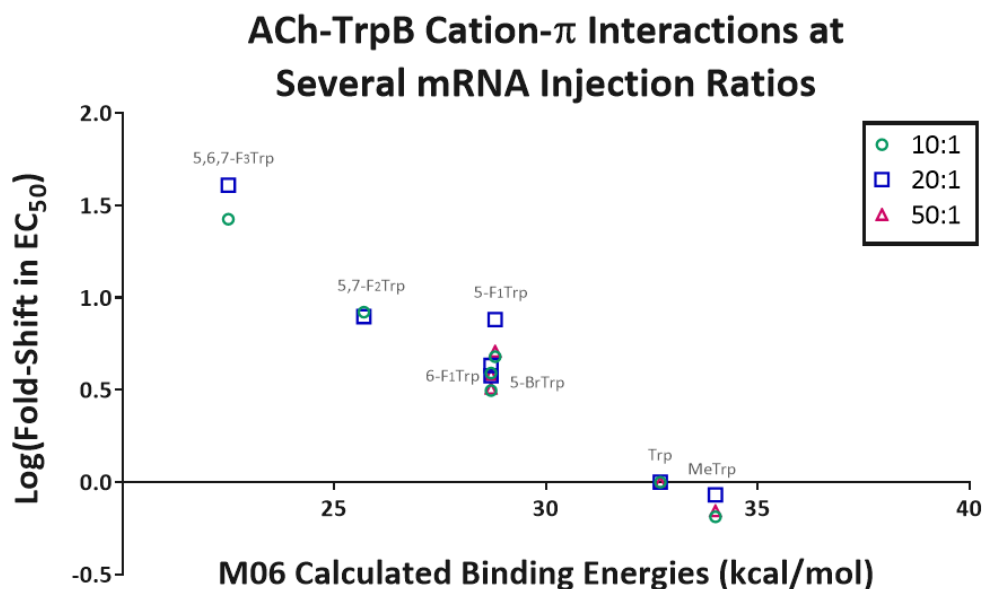


**Figure 6.** This fluorination plot shows ACh at Trp B at three different  $\alpha 6$ -biased injection ratios used  $\alpha 6\beta 2^{\ddagger}$ . Both the 20:1 and 50:1 injection ratios fit closely to the 10:1 data shown here and fit with a linear trend in Figure 3.

**Table 2.** Investigating Cation- $\pi$  Interactions at TrpB with Varying mRNA Injection Ratios

<b>20:1</b>	$EC_{50}$ (uM)	$n_H$	$I_{max}$ (uA)	Fold Shift	N
Trp	$0.17 \pm 0.01$	$1.22 \pm 0.05$	0.67 - 15.1	1	11
MeTrp	$0.145 \pm 0.004$	$1.35 \pm 0.05$	0.54 - 3.36	0.9	10
5-F <sub>1</sub> Trp	$1.29 \pm 0.04$	$1.15 \pm 0.03$	0.48 - 13.68	7.6	10
6-F <sub>1</sub> Trp	$0.73 \pm 0.01$	$1.29 \pm 0.02$	0.09 - 4.59	4.3	12
BrTrp	$0.64 \pm 0.02$	$1.24 \pm 0.03$	0.56 - 8.28	3.8	12
F <sub>2</sub> Trp	$1.34 \pm 0.03$	$1.21 \pm 0.02$	0.08 - 9.08	7.9	10
F <sub>3</sub> Trp	$6.9 \pm 0.4$	$1.03 \pm 0.05$	0.04 - 0.82	41	11
<b>50:1</b>	$EC_{50}$ (uM)	$n_H$	$I_{max}$ (uA)	Fold Shift	N
Trp	$0.180 \pm 0.004$	$1.33 \pm 0.04$	0.14 - 6.17	1.	16
MeTrp	$0.126 \pm 0.002$	$1.29 \pm 0.02$	0.2 - 6.66	0.7	13
5-F <sub>1</sub> Trp	$0.92 \pm 0.02$	$1.46 \pm 0.04$	0.05 - 7.74	5.1	12
6-F <sub>1</sub> Trp	$0.58 \pm 0.01$	$1.33 \pm 0.04$	0.06 - 2.05	3.2	9
BrTrp	$0.69 \pm 0.02$	$1.21 \pm 0.04$	0.17 - 5.59	3.8	14
F <sub>2</sub> Trp	$1.69 \pm 0.07$	$1.36 \pm 0.07$	0.11 - 0.66	9.4	10
F <sub>3</sub> Trp			No Response		

As discussed in Chapter 2,  $\alpha 6\beta 2^{\ddagger}$  exhibits an mRNA injection ratio effect, where a large increase in  $EC_{50}$  and decrease in Hill coefficient is observed with the more  $\beta 2$ -biased injection ratios. Taking this into account, one could argue that the trends presented thus far are actually due to a shift in stoichiometry as a result of the hit in translation by  $\alpha 6$  as the non-canonical amino acid strays further from wild-type. In order to ensure the results were actually due to electrostatics, the same experiments were attempted first using a more  $\beta 2$ -biased injection ratio. However, no agonist-induced currents were ever observed, suggesting functional channels were unable to form. Instead, injection ratios were pushed further into the  $\alpha 6$ -biased direction, with the same analogue progression (except 4-F<sub>1</sub> and 5-CN) tested at 20:1 and 50:1  $\alpha 6:\beta 2$  ratios. As shown in Figure 6, these results closely track those already presented at the 10:1 ratio. In all three cases, the fluorination plots have linear fits, and the Hill coefficients for each dose response curve remains greater than 1. These data confidently assert that each nonsense-suppression experiment has evaluated the same stoichiometry, and that the structure-function studies indeed prove a cation- $\pi$  interaction between ACh and TrpB.

### 3.3.2 Nicotine and TC299423 binding at TrpB

The same strategy described above was used to probe whether nicotine and TC299423 form functionally important cation- $\pi$  interactions with TrpB (Figure 7). For nicotine, the 5-F<sub>1</sub>Trp and 5-BrTrp show the expected shifts in  $EC_{50}$  based on the trend observed with ACh. However, the F<sub>2</sub>Trp and F<sub>3</sub>Trp  $EC_{50}$  values are not meaningfully different from the monosubstituted analogues. This rules out a strong cation- $\pi$  interaction between nicotine and TrpB. A more complicated result is seen with TC299423, with the monosubstituted analogues again following the trend established by ACh, but overall the

results do not show a linear trend and therefore do not support the presence of a strong cation- $\pi$  interaction. These are the exact same side chain mutations that were employed in the ACh experiments and produced a clear linear response. Thus, the receptor is able to tolerate these modest changes to structure, and while a weak interaction between these

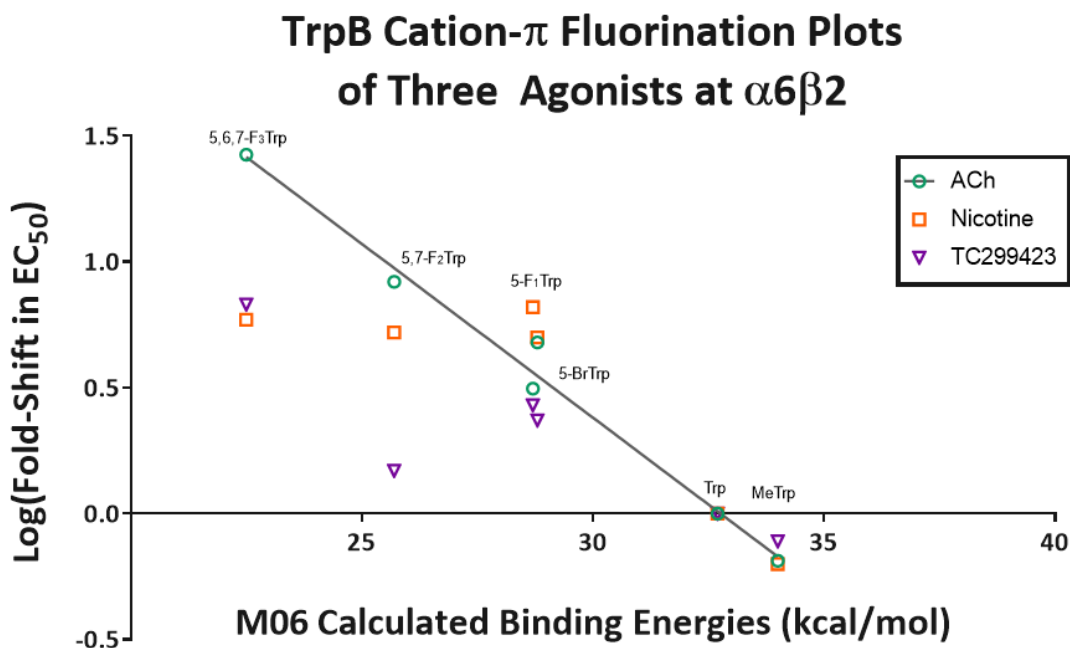


**Figure 7.** Nicotine (Nic) and TC299423 were also probed for a cation- $\pi$  interaction with Trp B, however unlike ACh, neither of these agonists form a linear trend and therefore do not form a strong cation- $\pi$  interaction

**Table 3.** Investigating Cation- $\pi$  Interactions with Nicotine and TC299423 at TrpB

Nic	EC <sub>50</sub> (uM)	n <sub>H</sub>	I <sub>max</sub> (uA)	Fold Shift	N
Trp	0.15 ± 0.006	1.43 ± 0.06	0.09 - 5.8	1	12
MeTrp	0.094 ± 0.003	1.36 ± 0.05	0.31 - 3.95	0.6	11
F <sub>1</sub> Trp	0.75 ± 0.02	1.39 ± 0.06	0.07 - 2.06	5.0	12
BrTrp	0.98 ± 0.03	1.42 ± 0.04	0.08 - 5.65	6.5	14
F <sub>2</sub> Trp	0.78 ± 0.04	1.3 ± 0.06	0.32 - 2.13	5.2	10
F <sub>3</sub> Trp	0.89 ± 0.02	1.28 ± 0.03	0.05 - 1.05	5.9	10
TC299423	EC <sub>50</sub> (uM)	n <sub>H</sub>	I <sub>max</sub> (uA)	Fold Shift	N
Trp	0.093 ± 0.004	1.09 ± 0.04	0.33 - 3.78	1	11
MeTrp	0.073 ± 0.004	0.92 ± 0.03	0.15 - 2.35	0.9	13
F <sub>1</sub> Trp	0.22 ± 0.01	1.01 ± 0.04	0.27 - 3.49	2.4	15
BrTrp	0.25 ± 0.008	1.01 ± 0.03	0.1 - 7.71	2.7	11
F <sub>2</sub> Trp	0.138 ± 0.006	0.98 ± 0.04	0.06 - 1.87	1.5	11
F <sub>3</sub> Trp	0.63 ± 0.03	0.90 ± 0.03	0.05 - 0.28	6.8	13

agonists and TrpB cannot be ruled out, the hallmark cation- $\pi$  interaction observed in many pLGICs, including nicotine at the  $\alpha 4$ - $\beta 2$  interface, is clearly absent.

While  $\alpha 6\beta 2$  is more similar to  $\alpha 4\beta 2$ , in that both subtypes are neuronal and share the  $\beta 2$  subunit, the pharmacology at  $\alpha 6\beta 2^\ddagger$  is actually more reminiscent of the  $\alpha 1\beta 1\gamma\delta$  muscle-type nAChR. In this subtype, ACh makes a cation- $\pi$  interaction with TrpB, but nicotine does not.<sup>13</sup> The difference between muscle-type and  $\alpha 4\beta 2$  subtypes was explained by the residue at the  $i + 4$  position relative to TrpB; a lysine in the  $\alpha 4$  subunit and a glycine in  $\alpha 1$ . This residue, when glycine, reshapes the binding site preventing nicotine from coming into close contact with TrpB.<sup>10</sup> However, in  $\alpha 6$ , the  $i + 4$  residue from TrpB is also a lysine, suggesting the lack of a cation- $\pi$  interaction with nicotine is due to another issue. It is also important to note that both agonists are quite efficacious at  $\alpha 6\beta 2^\ddagger$ , and that while nicotine is not very potent at muscle-type, in  $\alpha 6\beta 2^\ddagger$  it has a lower  $EC_{50}$  than ACh, further highlighting the unique nature of  $\alpha 6\beta 2$ -containing receptors.

### **3.4 Cation- $\pi$ Binding Studies at Tyrosines**

#### *3.4.1 Cation- $\pi$ Binding Studies at TyrC2*

TyrC2 is capable of forming a functionally important cation- $\pi$  interaction with epibatidine at the  $\alpha 7$ - $\alpha 7$  interface as well as secondary amine agonists at  $\alpha 4\beta 2$ , as will be shown in Chapter 5. Thus, it seemed pertinent to probe this interaction at the  $\alpha 6$ - $\beta 2$  interface, especially with the previous results suggesting nicotine and TC299423 do not make cation- $\pi$  interactions with TrpB. The strategy for probing a tyrosine cation- $\pi$  interaction is largely the same as a tryptophan with one major adjustment. Adding electron-withdrawing groups to a tyrosine phenol ring would adversely affect the pKa of the hydroxyl group. Because of this, it would be impossible to gauge whether changes in  $EC_{50}$

observed from fluorinating tyrosine were due to changes in electrostatics or the increased acidity of the phenol. Therefore, tyrosine is first substituted with phenylalanine and then

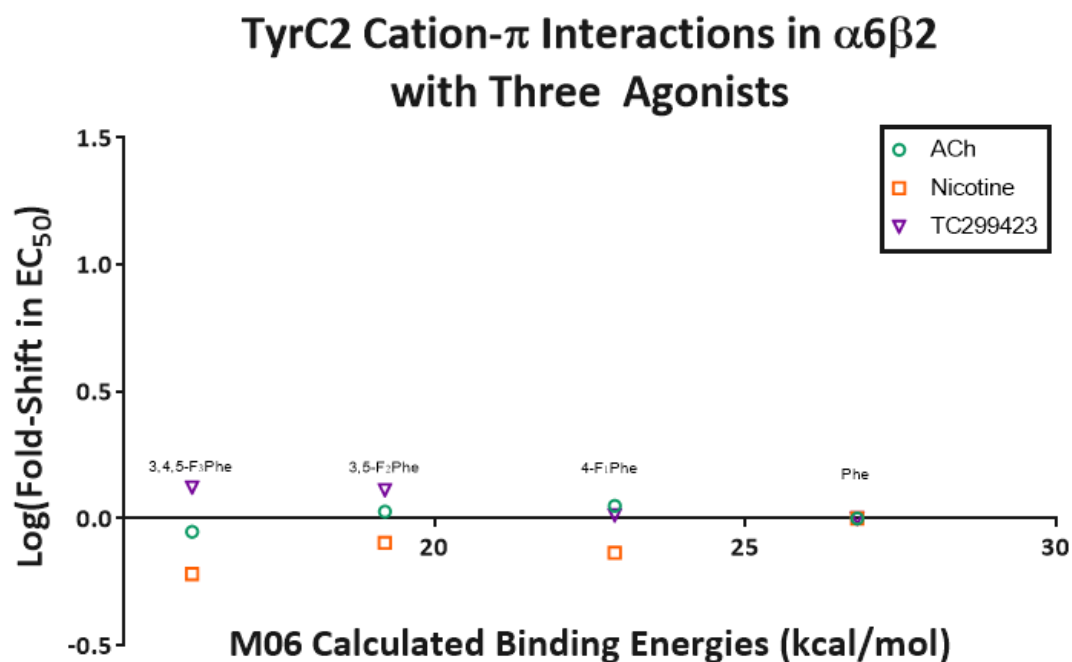


**Figure 8.** Results from structure-function studies probing for cation- $\pi$  interactions at TyrC2. Every fluorinated phenylalanine had an EC<sub>50</sub> similar to wild-type suggesting no functionally important cation- $\pi$  interactions are made with this amino acid

**Table 4.** Investigating Cation- $\pi$  Interactions at TyrC2

<b>ACh</b>	EC <sub>50</sub> (uM)	n <sub>H</sub>	I <sub>max</sub> (uA)	Fold Shift	N
Phe	1.07 ± 0.03	1.2 ± 0.03	0.19 - 11.79	1.0	13
F <sub>1</sub> Phe	1.2 ± 0.03	1.24 ± 0.03	0.13 - 5.52	1.1	13
F <sub>2</sub> Phe	1.14 ± 0.03	1.38 ± 0.04	0.29 - 9.23	1.1	8
F <sub>3</sub> Phe	0.95 ± 0.03	1.45 ± 0.05	5.09 - 15.47	0.9	5
<b>Nic</b>	EC <sub>50</sub> (uM)	n <sub>H</sub>	I <sub>max</sub> (uA)	Fold Shift	N
Phe	1.01 ± 0.04	1.23 ± 0.04	0.14 - 3.41	1.0	14
F <sub>1</sub> Phe	0.74 ± 0.02	1.53 ± 0.06	0.28 - 1.89	0.7	13
F <sub>2</sub> Phe	0.81 ± 0.02	1.46 ± 0.06	0.41 - 5.32	0.8	6
F <sub>3</sub> Phe	0.61 ± 0.04	0.91 ± 0.04	4.26 - 20.11	0.6	7
<b>TC299423</b>	EC <sub>50</sub> (uM)	n <sub>H</sub>	I <sub>max</sub> (uA)	Fold Shift	N
Phe	0.68 ± 0.02	0.88 ± 0.02	0.08 - 3.87	1.0	11
F <sub>1</sub> Phe	0.7 ± 0.04	0.92 ± 0.04	0.09 - 3.29	1.0	12
F <sub>2</sub> Phe	0.88 ± 0.1	0.96 ± 0.08	0.10 - 4.00	1.3	5
F <sub>3</sub> Phe	0.9 ± 0.08	1.2 ± 0.1	1.88 - 5.69	1.3	3

fluorinated, with quantitative fold-shifts in  $EC_{50}$  using phenylalanine as the reference.

In  $\alpha6\beta2^{\ddagger}$ , the  $\alpha6$  cDNA TyrA codon was mutated to TAG and dose response experiments were performed with Phe, 4-F<sub>1</sub>Phe, 3,5-F<sub>2</sub>Phe, and 3,4,5-F<sub>3</sub>Phe. While the initial Tyr to Phe mutation results in roughly a 7-fold loss of function, none of the fluorinated analogues show any meaningful changes in  $EC_{50}$  compared to Phe. It should be noted that nonsense suppression proved to be immensely challenging at this site, and the number of replicates are therefore lower than usually desired. However, the current wave-forms and dose response curves of successful attempts do not look unusual, and there is little reason to be skeptical of the results that none of the agonists make a cation- $\pi$  interaction with  $\alpha6$  YC2.

### 3.4.2 Cation- $\pi$ binding studies at TyrA

The  $\alpha7$ - $\alpha7$  interface has also shown that TyrA can make a functionally important cation- $\pi$  interaction with ACh; however, no agonist studied has made a cation- $\pi$  interaction with  $\alpha4\beta2$  TyrA. In  $\alpha6\beta2^{\ddagger}$ , the fluorination series yields some interesting results. The initial Tyr to Phe mutation causes a one hundred-fold shift in  $EC_{50}$ . This enormous loss of function suggests the tyrosine phenol group makes a critical interaction with either the agonist (which is unlikely) or another amino acid. This theory is supported by the recovery in binding (a 2 to 10 fold-shift gain of function relative to Phe) that occurs when a fluorine atom is substituted in the 4 position, as seen in 4-F<sub>1</sub>Phe and 3,4,5-F<sub>3</sub>Phe. The 3,5-F<sub>2</sub>Phe substitutions show varying results, with a 5-fold gain of function relative to Phe with ACh, and near-Phe  $EC_{50}$  values for nicotine and TC299423. Overall, these data suggest that TyrA plays an important role in  $\alpha6\beta2$  function, but that role likely does not involve making a cation- $\pi$  with the agonist.

## TyrA Cation- $\pi$ Interactions in $\alpha 6\beta 2$ at Three Agonists

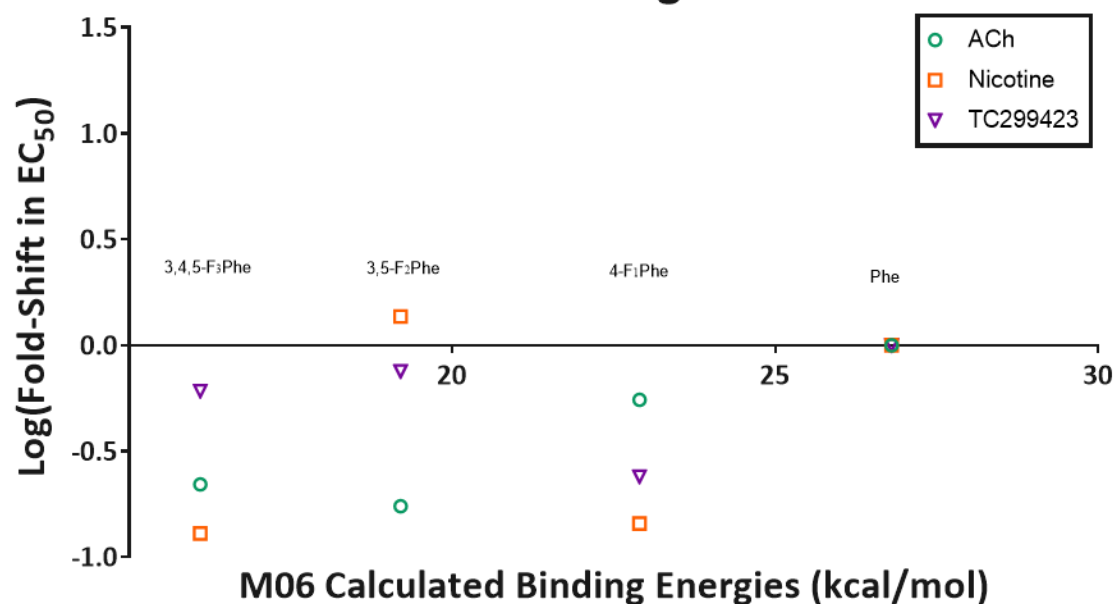


**Figure 9.** Results from structure-function studies probing for cation- $\pi$  interactions at TyrA show interesting results that suggest the 4 position of the phenyl ring is important for receptor function, but that a functionally important cation- $\pi$  interaction with these agonists is not present.

**Table 5.** Investigating Cation- $\pi$  Interactions at TyrA

ACh	EC <sub>50</sub> (uM)	n <sub>H</sub>	I <sub>max</sub> (uA)	Fold Shift	N
Phe	15.0 ± 0.7	1.28 ± 0.06	0.09 - 14.40	1.0	13
F <sub>1</sub> Phe	8.3 ± 0.4	1.24 ± 0.07	0.13 - 2.19	0.6	12
F <sub>2</sub> Phe	2.61 ± 0.08	1.35 ± 0.05	0.23 - 1.29	0.2	13
F <sub>3</sub> Phe	3.31 ± 0.09	1.07 ± 0.03	0.04 - 2.77	0.2	12
Nic	EC <sub>50</sub> (uM)	n <sub>H</sub>	I <sub>max</sub> (uA)	Fold Shift	N
Phe	1.39 ± 0.07	1.07 ± 0.04	0.07 - 3.98	1.0	11
F <sub>1</sub> Phe	0.20 ± 0.01	1.35 ± 0.07	0.06 - 2.00	0.1	10
F <sub>2</sub> Phe	1.9 ± 0.1	1.24 ± 0.06	0.10 - 0.75	1.4	10
F <sub>3</sub> Phe	0.18 ± 0.01	1.4 ± 0.1	0.09 - 1.05	0.1	10
TC299423	EC <sub>50</sub> (uM)	n <sub>H</sub>	I <sub>max</sub> (uA)	Fold Shift	N
Phe	6.5 ± 0.7	1.2 ± 0.1	0.04 - 0.14	1.0	9
F <sub>1</sub> Phe	1.56 ± 0.04	1.06 ± 0.03	0.21 - 1.41	0.2	10
F <sub>2</sub> Phe	4.9 ± 0.3	1.18 ± 0.07	0.05 - 0.28	0.8	13
F <sub>3</sub> Phe	3.95 ± 0.4	1.01 ± 0.07	0.01 - 1.11	0.6	10

### 3.4 Conclusion

Testing ACh, nicotine, and TC299423 at three different aromatic residues at the  $\alpha 6$ - $\beta 2$  interface – TrpB, TyrA, and TyrC2 – has yielded nine different fluorination series. Yet, only one of these plots supports a cation- $\pi$  interaction: ACh with TrpB. That only one of these interactions is functionally important is quite surprising. Of the 22 TrpB-agonist combinations tested in a pLGIC, 18 produced linear fluorination plots.<sup>7</sup> This suggests that the binding site of  $\alpha 6\beta 2$  has a unique pharmacology. TyrC1 was the last residue where nonsense suppression was attempted, but the technique proved unable to work at this site. Future work should investigate what specific role the TyrA and TyrC2, as well as if TrpD contributes any meaningful interactions. The next chapter will investigate the role hydrogen bonding has on agonist binding and will answer some, but not all of the questions raised here.

### 3.6 Materials and Methods

#### *Molecular Biology*

Rat  $\alpha 6L9'S$  and  $\beta 2L9'S_{LFM/AAQA}$  nAChRs were in the pGEMhe vector, a cDNA plasmid optimized for protein expression in *Xenopus* oocytes. Site-directed mutagenesis was performed by PCR using the Stratagene QuikChange protocol and primers ordered from Integrated DNA Technologies (Coralville, IA). Circular cDNA was linearized with SbfI (New England Biolabs, Ipswich, MA) and then transcribed *in vitro* using T7 mMessage mMachine kit (Life Technologies, Santa Clara, CA), with a purification step after each process (Qiagen, Valencia, CA). Final concentrations were quantified by UV spectroscopy.

#### *Ion Channel Expression*

*Xenopus laevis* oocytes (stage V to VI) were sourced from both a Caltech facility and Ecocyte Bio Science (Austin, TX). Oocytes were injected with 50 nL solution containing

either 5 or 10 ng mRNA. The  $\alpha 6:\beta 2$  ratio is presented as a mass ratio. Cells were incubated 24-48 hours at 18°C in ND96 solution (96 mM NaCl, 2mM KCl, 1 mM MgCl<sub>2</sub>, and 5mM HEPES, pH 7.5) enriched with theophylline, sodium pyruvate, gentamycine, and horse serum.

### *Non-canonical Amino Acid Incorporation*

The cyanomethylester form of NVOC-protected tryptophan and phenylalanine analogues was coupled to dinucleotide dCA and enzymatically ligated to UAG-suppressor 74-mer THG73 tRNA<sub>CUA</sub> as previously described.<sup>14</sup> The product was verified by MALDI time-of-flight mass spectrometry on a 3-hydroxypicolinic acid matrix. The non-canonical amino acid-coupled tRNA was deprotected by photolysis on a 500 W Hg/Xe arc lamp, filtered with Schott WG-320 and UG-11 filters, immediately prior to coinjection with mRNA containing the UAG mutation at the site of interest. mRNA and tRNA were typically injected in a 1:1 or 1:2 volume ratio in a total volume of 50 or 75 nL respectively so that 25 ng of mRNA was injected per cell. In cases where observed agonist-induced currents were low after 48 hour incubation – likely due to low receptor protein expression – a second injection of mRNA and tRNA was performed after 24 hours. The fidelity of non-canonical amino acid incorporation was confirmed at Trp with a wild-type recovery experiment where tryptophan was loaded onto tRNA. If this experiment yielded similar to EC<sub>50</sub> to wild-type then the cell incorporated the charged residue and nothing else. This was accomplished with the Tyr sites by comparing tRNA charged with Phe to a conventional Y-Phe mutation. A read-through/reaminoacylation test served a negative control by injecting unacylated full-length 76-mer tRNA. Lack of current proved no detectable reaminoacylation at the TrpB site.

### *Whole-Cell Electrophysiological Characterization*

Acetylcholine chloride and (-)-nicotine tartrate were purchased from Sigma Aldrich (St Louis, MO), while TC299423 (Targacept) was a generous gift. Agonist-induced currents were recorded in TEVC mode using the OpusXpress 6000A (Molecular Devices, Sunnyvale, CA) at a holding potential of -60 mV in a running buffer of Ca<sup>2+</sup>-free ND96. Agonists were prepared in Ca<sup>2+</sup>-free ND96 and delivered to cells via a 1 mL application over 15 sec followed by a 2 min wash. Data from dose-response experiments were normalized, averaged, and fit to the Hill equation using Kaleidagraph (Synergy Software, Reading PA), though data are visualized here with Prism (GraphPad Software, La Jolla,

CA). Error bars are presented as standard error of the mean, while  $EC_{50}$  and Hill coefficient errors are reported by Kaleidagraph and represent the sum of the squared error between the data and the calculated fit.

### 3.7 References

1. Brejc, K., *et al.* Crystal structure of an ACh-binding protein reveals the ligand-binding domain of nicotinic receptors. *Nature* **411**, 269–276 (2001).
2. Lester, H. A., Dibas, M. I., Dahan, D. S., Leite, J. F. & Dougherty, D. A. Cys-loop receptors: new twists and turns. *Trends Neurosci.* **27**, 329–336 (2004).
3. Corringer, P.-J., Novère, N. L. & Changeux, J.-P. Nicotinic Receptors at the Amino Acid Level. *Annu. Rev. Pharmacol. Toxicol.* **40**, 431–458 (2000).
4. Dougherty, D. A. Cation- $\pi$  Interactions in Chemistry and Biology: A New View of Benzene, Phe, Tyr, and Trp. *Science* **271**, 163–168 (1996).
5. Dougherty, D. A. The Cation- $\pi$  Interaction. *Acc. Chem. Res.* **46**, 885–893 (2013).
6. Meot-Ner, M. & Deakyne, C. A. Unconventional ionic hydrogen bonds. 2.  $\text{NH}_3^+\cdots\text{C}\equiv\text{N}\cdots\text{C}\equiv\text{N}\cdots\text{N}^+$ . Complexes of onium ions with olefins and benzene derivatives. *J. Am. Chem. Soc.* **107**, 474–479 (1985).
7. Van Arnam, E. B. & Dougherty, D. A. Functional Probes of Drug-Receptor Interactions Implicated by Structural Studies: Cys-Loop Receptors Provide a Fertile Testing Ground. *J. Med. Chem.* **57**, 6289–6300 (2014).
8. Gallivan, J. P. & Dougherty, D. A. Cation- $\pi$  interactions in structural biology. *Proc. Natl. Acad. Sci.* **96**, 9459–9464 (1999).
9. Davis, M. R. & Dougherty, D. A. Cation- $\pi$  interactions: computational analyses of the aromatic box motif and the fluorination strategy for experimental evaluation. *Phys. Chem. Chem. Phys.* **17**, 29262–29270 (2015).
10. Xiu, X., Puskar, N. L., Shanata, J. A. P., Lester, H. A. & Dougherty, D. A. Nicotine binding to brain receptors requires a strong cation- $\pi$  interaction. *Nature* **458**, 534–537 (2009).
11. Zhong, W. *et al.* From ab initio quantum mechanics to molecular neurobiology: A cation- $\pi$  binding site in the nicotinic receptor. *Proc. Natl. Acad. Sci.* **95**, 12088–12093 (1998).
12. Puskar, N. L., Xiu, X., Lester, H. A. & Dougherty, D. A. Two Neuronal Nicotinic Acetylcholine Receptors,  $\alpha 4\beta 4$  and  $\alpha 7$ , Show Differential Agonist Binding Modes. *J. Biol. Chem.* **286**, 14618–14627 (2011).
13. Beene, D. L. *et al.* Cation- $\pi$  Interactions in Ligand Recognition by Serotonergic (5-HT<sub>3A</sub>) and Nicotinic Acetylcholine Receptors: The Anomalous Binding Properties of Nicotine†. *Biochemistry (Mosc.)* **41**, 10262–10269 (2002).

14. Dougherty, D. A. & Van Arnem, E. B. In Vivo Incorporation of Non-canonical Amino Acids by Using the Chemical Aminoacylation Strategy: A Broadly Applicable Mechanistic Tool. *ChemBioChem* **15**, 1710–1720 (2014).

## Chapter 4: Probing for Agonist Hydrogen Bonds in $\alpha 6\beta 2$

### 4.1 Abstract

Designing agonists that are selective for specific subtypes of the nicotinic acetylcholine receptor is a major goal in nicotine addiction research. Intricate knowledge of how agonists bind at the  $\alpha 6\beta 2$  interface, as well as how this binding site differs from other neuronal subtypes such as  $\alpha 4\beta 2$ , is therefore important. The previous chapter showed acetylcholine makes a functionally important cation- $\pi$  interaction with Trp149, but nicotine and TC299423 do not. Furthermore, no cation- $\pi$  interactions were observed at TyrC2 or TyrA with any of the agonists. The cation- $\pi$  interaction at TrpB is one that has been observed in a majority of the agonists investigated in neuronal nAChR subtypes, and therefore a different mode of binding for these two is likely in  $\alpha 6\beta 2$ . Chapter 4 explores the role of hydrogen binding between the cationic amine moiety of agonists and the backbone carbonyl associated with TrpB. Probing this interaction is accomplished by substituting the  $i + 1$  residue, Thr150, to threonine  $\alpha$ -hydroxy acid (Tah). This mutates the backbone amide bond to an ester bond, thereby attenuating the carbonyl's hydrogen bond accepting ability. With the  $\alpha 6\beta 2^{\ddagger}$  T150Tah mutant, nicotine shows a 24-fold loss of function, TC299423 shows a modest loss, and acetylcholine shows no effect. The effect at nicotine was further analyzed via a double-mutant cycle analysis wherein N'-methylnicotinium was utilized as the second "mutant". In  $\alpha 6\beta 2^{\ddagger}$ , the double-mutant demonstrates a loss of function that is non-additive with an  $\Omega$  value of 88 and a  $\Delta\Delta G$  of -2.6 kcal/mol. This suggests that nicotine makes a strong enough hydrogen bond with the TrpB backbone carbonyl to explain why a cation- $\pi$  interaction was not previously observed there; however, the picture for TC299423 remains murky.

## 4.2 Introduction

Previous work, discussed in detail in Chapter 3, has shown that at the  $\alpha 6$ - $\beta 2$  interface, while ACh makes a functionally important cation- $\pi$  interaction, nicotine and TC299423 do not.<sup>1</sup> This binding mode differs greatly from the  $\alpha 4$  $\beta 2$  subtype, and specifically the  $\alpha 4$ - $\beta 2$  interface, which has been studied in depth with structure-function studies over the last several years.<sup>2</sup> Those studies revealed three key binding interactions: the canonical cation- $\pi$  interaction with  $\alpha 4$  TrpB, a hydrogen bond with the backbone carbonyl associated with TrpB, and an additional hydrogen bond between nicotine's pyridine nitrogen and a backbone NH on loop E of the  $\beta 2$  subunit.

This chapter investigates the role of that second interaction in  $\alpha 6\beta 2$ , the hydrogen bond between an agonist's amine moiety and the backbone carbonyl associated with TrpB. While quaternary amine agonists such as acetylcholine are unable to make a hydrogen bond, such interactions have been observed in both stoichiometries of  $\alpha 4\beta 2$  for nicotine, varenicline, and cytisine.<sup>3,4</sup> Nicotine also shows a strong hydrogen bond interaction in  $\alpha 4\beta 4$ , but not at the muscle-type.<sup>5,6</sup> In each of those instances, evidence of the hydrogen bond was accompanied by a linear fluorination plot at TrpB; however, because nicotine did not show evidence of making a strong cation- $\pi$  interaction at TrpB with  $\alpha 6\beta 2^{\ddagger}$ , it was not necessarily obvious if it could make the hydrogen bond at this residue in that subtype. This chapter will describe how structure-function studies using an  $\alpha$ -hydroxy acid substitution reveal that nicotine indeed makes a functional hydrogen bond with this backbone carbonyl at the  $\alpha 6$ - $\beta 2$  interface. The interaction will be further supported and quantified by a double mutant cycle analysis utilizing *N*'-methylnicotinium.

### 4.3 Probing for Hydrogen Bonds in $\alpha 6\beta 2$ at the TrpB Carbonyl

#### 4.3.1 The $\alpha$ -hydroxy acid Strategy

To probe for hydrogen bonds between an agonist and the nAChR protein backbone, nonsense suppression-based, site specific, non-canonical amino acid mutagenesis is once again employed. In this structure-function study, the hydrogen bond accepting ability of the backbone carbonyl is attenuated by making a mutation one amino acid downstream from the residue of interest, i.e. at the  $i + 1$  residue to TrpB. Due to the loss of resonance when the nitrogen is replaced with an oxygen, an ester carbonyl is a weaker hydrogen bond acceptor.<sup>7</sup> An amide-to-ester mutation of this type is achieved not through an amino acid, but an  $\alpha$ -hydroxy acid substitution at the  $i + 1$  residue from the carbonyl of interest (Figure 1).<sup>8</sup> Remarkably, the *Xenopus* oocyte ribosome accepts the Tah-bound tRNA and inserts the hydroxy acid into the nascent strand as though it were an amino acid and continues translation as per usual leading to functional receptors at the cell surface.

If the agonist is indeed making a functionally important hydrogen bond with the backbone in this location, an amide-to-ester backbone mutation would weaken this interaction. Therefore, an increase in  $EC_{50}$  upon mutation to the  $\alpha$ -hydroxy acid confirms the presence of a functionally important hydrogen bond. This strategy will be applied at  $\alpha 6\beta 2^{\ddagger}$  with ACh, nicotine, and TC299423 in an attempt to further clarify some of the surprising results seen in Chapter 3. If nicotine and TC299423 show strong hydrogen bonding interactions, it might explain the lack of cation- $\pi$  interactions observed in the previous chapter and further develop the binding map at the  $\alpha 6$ - $\beta 2$  interface.

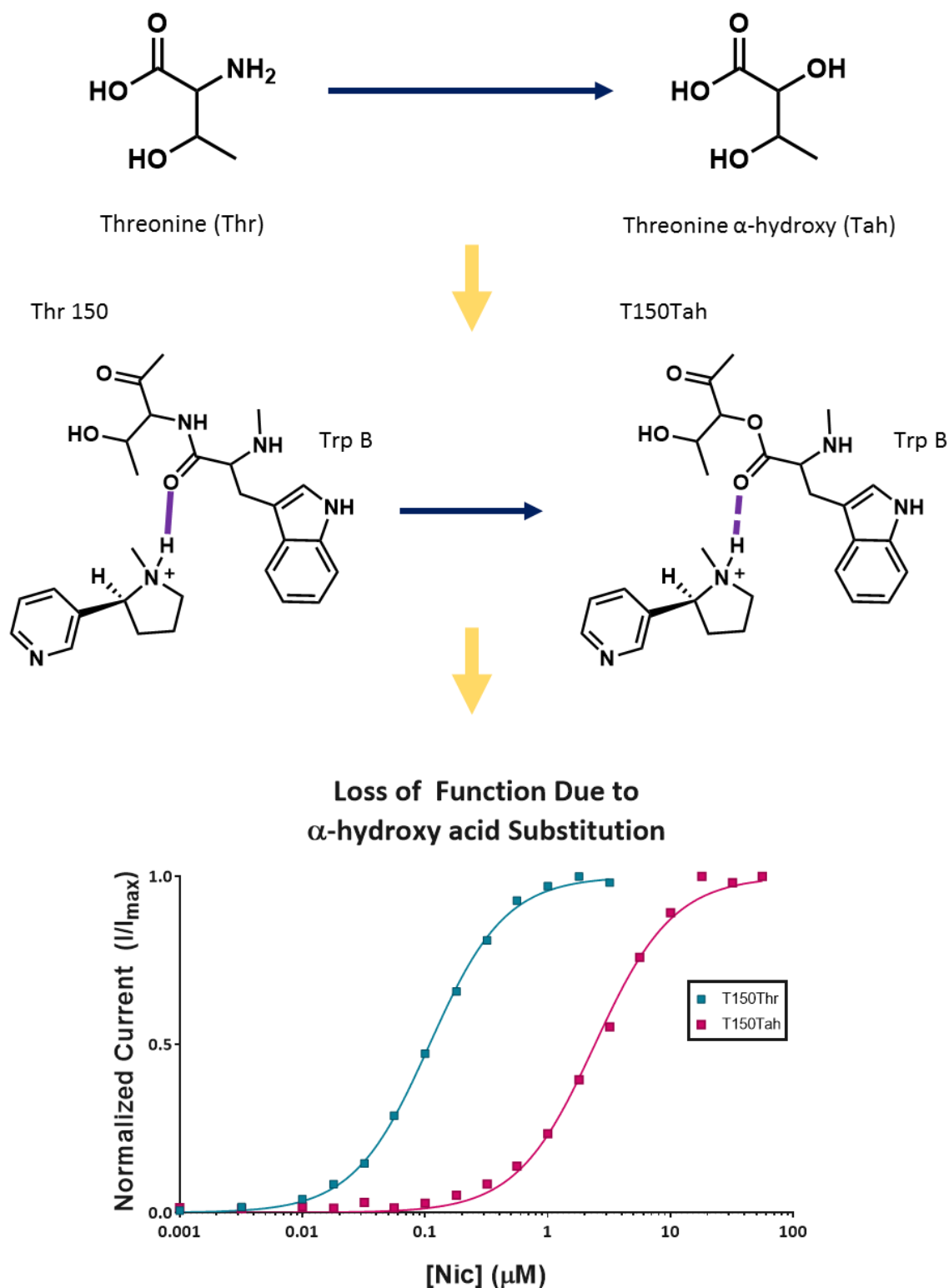


**Figure 1.** The Thr to Tah mutation shown at the top leads to an amide-to-ester backbone mutation in the protein. This mutation has the effect of attenuating the hydrogen bonding ability of the carbonyl one amino acid up from the site of mutation. In this case, a T150Tah mutation causes attenuation in the hydrogen bond accepting ability of the carbonyl associated with TrpB (Trp149) that leads to an increase in  $EC_{50}$  as shown with nicotine (Nic) in the dose response curves at the bottom.

### 4.3.2 $\alpha$ -hydroxy acid Substitution at T150

In  $\alpha 6$ , TrpB is at position 149, and Thr150 was substituted with threonine  $\alpha$ -hydroxy (Tah) to produce the desired amide-to-ester bond mutation. As with the cation- $\pi$  experiments, the  $EC_{50}$  of the agonist is determined at the wild-type and Tah mutant, and a loss of function indicates a functional hydrogen bonding interaction is present. Typically, for these types of experiments, at least a 2-fold shift in  $EC_{50}$  is required to be considered meaningful. Once the T150TAG mutation was made, the corresponding  $\alpha 6\beta 2^{\ddagger}$  mRNA was injected into oocytes alongside Thr- or Tah-bound tRNA, followed by dose response experiments with nicotine, acetylcholine, and TC299423.

Nicotine experiences a 24-fold loss in function at the T150Tah mutant, suggesting it makes a potent hydrogen bond with the backbone carbonyl of TrpB. To put such a loss of function into context, a similar shift in  $EC_{50}$  for ACh was observed when the cation- $\pi$  interaction was ablated at TrpB, as described in Chapter 3. ACh, on the other hand, did not experience any loss in function when applied to the Tah mutant. This result was expected as ACh is a quaternary amine and has no hydrogen atom for which to donate into a hydrogen bond. Finally, only a 4-fold loss of function was observed for TC299423. This modest shift in  $EC_{50}$  indicates the agonist makes a hydrogen bond here, as it passes the

**Table 1.** Investigating Hydrogen Bonding at  $\alpha 6\beta 2$  TrpB Carbonyl

<b>ACh</b>	$EC_{50}$ ( $\mu$ M)	$n_H$	$I_{max}$ ( $\mu$ A)	Fold	N
Thr	$0.156 \pm 0.004$	$1.31 \pm 0.04$	0.32 - 3.76		10
Tah	$0.199 \pm 0.007$	$0.91 \pm 0.03$	0.48 - 3.27	1.3	10
<b>Nicotine</b>	$EC_{50}$ ( $\mu$ M)	$n_H$	$I_{max}$ ( $\mu$ A)	Fold	N
Thr	$0.11 \pm 0.003$	$1.36 \pm 0.04$	0.19 - 2.69		16
Tah	$2.7 \pm 0.1$	$1.24 \pm 0.06$	0.09 - 2.71	24	10
<b>TC299423</b>	$EC_{50}$ ( $\mu$ M)	$n_H$	$I_{max}$ ( $\mu$ A)	Fold	N
Thr	$0.078 \pm 0.002$	$1.07 \pm 0.03$	0.21 - 3.57		11
Tah	$0.30 \pm 0.01$	$0.94 \pm 0.03$	0.12 - 4.13	3.8	13

two-fold threshold, but not as strong as nicotine. Perhaps, then, a different non-covalent interaction is primarily responsible for the binding of TC299423 to  $\alpha 6\beta 2$ .

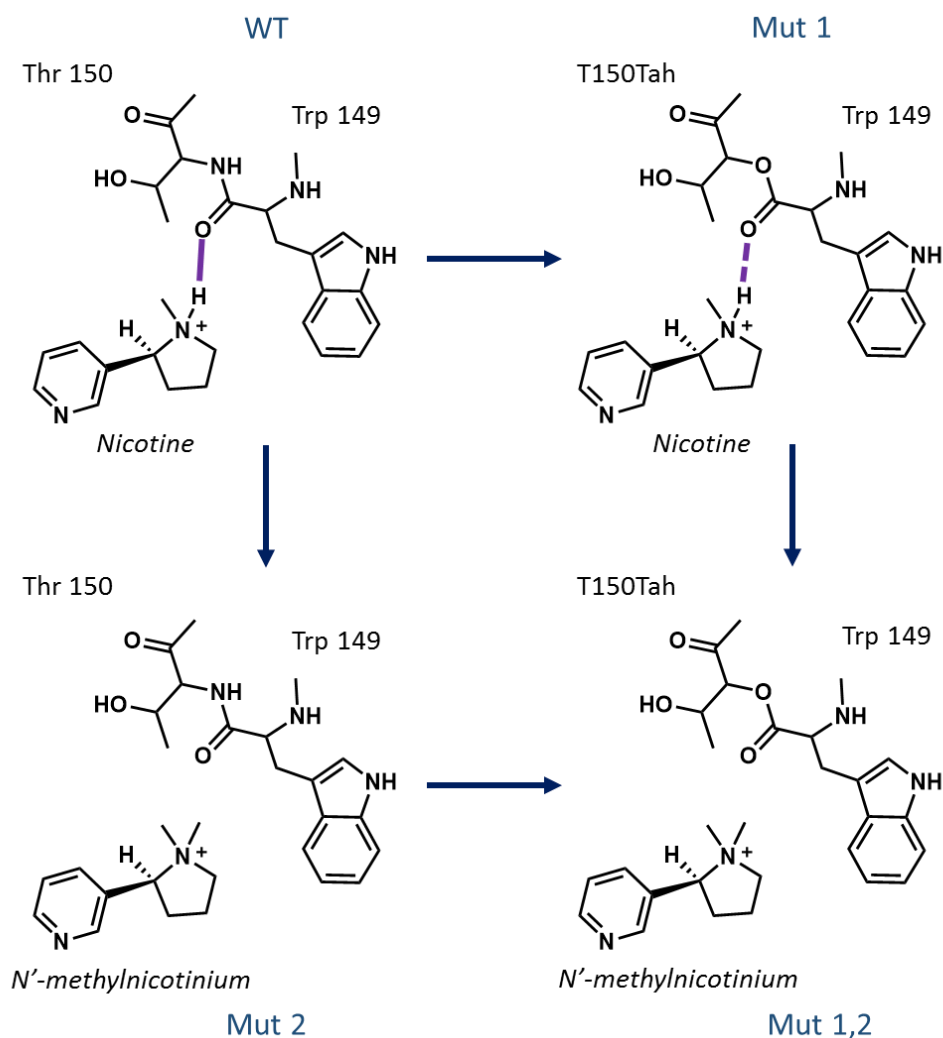
## 4.4 Quantifying the $\alpha 6\beta 2$ -nicotine Hydrogen Bond

### 4.4.1 *The Double-Mutant Cycle Analysis*

A classic technique in determining a functional coupling interaction between amino acids in a protein is the double-mutant cycle analysis.<sup>9-11</sup> In this type of experiment, the two amino acids of interest are each mutated in a way that would attenuate the same non-covalent interaction, both independently (as single-mutants) and simultaneously (as a double-mutant). Changes in function for both the single-mutants and the double-mutant are then compared to wild-type. If the fold-shift in  $EC_{50}$  of the double-mutant is merely a sum of each single-mutant fold-shift – that is, if the effects are additive – the single-mutant perturbations act independently of each other, and the two amino acids do not participate in a functionally coupled interaction. If, on the other hand, the effect of the double-mutant proves to be non-additive, the amino acids are indeed functionally coupled. The degree to which the double-mutant is additive or non-additive is expressed by an  $\Omega$  value, which is defined as the product of the wild-type and double-mutant  $EC_{50}$  values divided by the product of the single-mutant  $EC_{50}$  values (Figure 2). An  $\Omega$  value other 1 indicates functional coupling between amino acids. Because  $\Omega$  is a ratio of  $EC_{50}$  values, and  $EC_{50}$  is directly related to the binding energy,  $\Omega$  values can be inserted into the free energy relationship to calculate a  $\Delta\Delta G$  for the coupling energy between amino acids.

To assess the nicotine hydrogen bond with the TrpB backbone carbonyl, a riff on the double-mutant cycle analysis was designed. The first mutant in the analysis is the T150Tah substitution that results in an amide-to-ester backbone mutation. The second

“mutant” uses a nicotine analog, wherein the pyrrolidine nitrogen is methylated to yield *N'*-methylnicotinium (*N'*MeNic in data tables). As a quaternary amine, this compound is similar to ACh in that it is unable to donate a hydrogen bond. By finding  $EC_{50}$  values for each condition – nicotine at wild-type, nicotine at T150Tah, *N'*-methylnicotinium at wild-type, and *N'*-methylnicotinium at T150Tah – and determining whether or not the double-



$$\Omega = \frac{[EC_{50}(WT) \times EC_{50}(Mut\ 1,2)]}{[EC_{50}(Mut\ 1) \times EC_{50}(Mut\ 2)]} \quad \Delta\Delta G = -RT \ln(\Omega)$$

**Figure 2.** Schematic of the double-mutant cycle analysis used to confirm and quantify a functional hydrogen bond between nicotine and the  $\alpha 6$ - $\beta 2$  interface. An  $\Omega$  value other than 1 indicates functional coupling between the mutants and provides conclusive evidence of a functional hydrogen bond. Below are the equations used to calculate  $\Omega$  and  $\Delta\Delta G$  values.

mutant shows an additive loss of function, this mutant cycle will not only strengthen evidence that nicotine makes a hydrogen bond with the backbone carbonyl of Trp149 but will also quantify the strength of the hydrogen bond.

#### 4.4.2 Proof of Concept in $\alpha 4\beta 2$

As a proof of concept, the double-mutant cycle analysis described above was first performed in the  $\alpha 4\beta 2$ , because this subtype is more extensively studied and has a better understood binding map for nicotine than  $\alpha 6\beta 2$ . At  $\alpha 4\beta 2$ , nicotine shows a 27-fold shift in  $EC_{50}$  at the T150Tah mutant, a major loss of function. When N'methylnicotinium is tested at the wild-type receptor, in this case the second "mutant" in the analysis, a 6-fold loss of function is observed. If these two mutations were independent of each other and loss of function was due to an effect other than attenuating the hydrogen bond, an additive loss of function would be expected at the double-mutant close to 160-fold. Instead, an  $EC_{50}$  of 0.40  $\mu M$  is observed, a 4-fold loss of function compared to wild-type that is not meaningfully different from the  $EC_{50}$  of N'methylnicotinium at wild-type (0.62  $\mu M$ ). This lack of additivity is quantified with an  $\Omega$  value of 42, which when entered into the free energy relationship reveals a  $\Delta\Delta G$  value of -2.2 kcal/mol. This value agrees with empirically determined hydrogen bond strengths of *N*-methylacetamide aggregates in carbon tetrachloride ( $\Delta H^\circ = -4.2$  kcal/mol) and benzene ( $\Delta H^\circ = -3.6$  kcal/mol).<sup>12,13</sup>

**Table 2.** Bond Double Mutant Cycle Analysis of the Nicotine-TrpB Carbonyl Hydrogen in  $\alpha 4\beta 2$

$\alpha 4L9'\beta 2$	Agonist	T150	$EC_{50}$ ( $\mu M$ )	$n_H$	$I_{max}$ ( $\mu A$ )	Fold	N
WT	Nicotine	Thr	0.10 $\pm$ 0.01	1.4 $\pm$ 0.2	0.05 - 1.23	1	15
Mut1	Nicotine	Tah	2.7 $\pm$ 0.1	1.34 $\pm$ 0.04	0.11 - 1.23	27	6
Mut2	N'MeNic	Thr	0.62 $\pm$ 0.03	1.22 $\pm$ 0.07	0.02 - 0.60	6.2	10
Mut1,2	N'MeNic	Tah	0.40 $\pm$ 0.04	1.1 $\pm$ 0.1	0.08 - 0.42	4	12
						$\Omega$	42
						$\Delta\Delta G$ (kcal/mol)	-2.2

#### 4.4.3 Quantifying the Nicotine Hydrogen Bond in $\alpha 6\beta 2^{\ddagger}$

The same approach was taken in  $\alpha 6\beta 2^{\ddagger}$ , for which nicotine has already been shown to experience a 24-fold loss of function at T150Tah. The other single-mutant in this analysis, which is N'-methylnicotinium at wild-type  $\alpha 6\beta 2^{\ddagger}$ , shows an even larger loss of function, with a 38-fold shift in EC<sub>50</sub>. If these losses in function were not due to hydrogen bonding and instead were independent of each other, the double-mutant fold-shift would be totally additive with a nearly 900-fold increase in EC<sub>50</sub> with respect to wild-type. The double-mutant, N'-methylnicotinium at T150Tah, has instead an EC<sub>50</sub> of 1.2  $\mu$ M, a 10-fold shift away from wild-type. This fold shift is not meaningfully different from the EC<sub>50</sub> of nicotine at T150Tah (2.7  $\mu$ M), and is only modestly different than N'-methylnicotinium at wild-type (4.2  $\mu$ M), showing the effect is non-additive. Overall, the mutant cycle has an  $\Omega$  value of 88 and a  $\Delta\Delta G$  of -2.6 kcal/mol, suggesting nicotine makes an even stronger bond with  $\alpha 6\beta 2$  than  $\alpha 4\beta 2$ .

**Table 3.** Bond Double Mutant Cycle Analysis of the Nicotine-TrpB Carbonyl Hydrogen in  $\alpha 4\beta 2$

$\alpha 6\beta 2^{\ddagger}$	Agonist	T150	EC <sub>50</sub> ( $\mu$ M)	n <sub>H</sub>	I <sub>max</sub> ( $\mu$ A)	Fold	N
WT	Nic	Thr	0.11 $\pm$ 0	1.36 $\pm$ 0.04	0.19 - 2.69	1	16
Mut1	Nic	Tah	2.7 $\pm$ 0.1	1.24 $\pm$ 0.06	0.09 - 2.71	24	10
Mut2	N'MeNic	Thr	4.22 $\pm$ 0.19	1.03 $\pm$ 0.03	0.1 - 2.07	38	11
Mut1,2	N'MeNic	Tah	1.17 $\pm$ 0.08	0.93 $\pm$ 0.04	0.08 - 1.12	11	10

$\Omega$  88

$\Delta\Delta G$  (kcal/mol) -2.6

## 4.5 Conclusion

The work described in this chapter shows that nicotine makes a strong, quantifiable hydrogen bond with the backbone carbonyl of TrpB, though the effects with TC299423 are more modest. These results offer an explanation for the lack of cation- $\pi$  interaction observed between nicotine and the indole side chain of TrpB. Such a strong hydrogen bond

might compensate for any losses of function that might have occurred by making cation- $\pi$ -attenuating mutations. However, because the loss of function for TC299423 was so modest, and because a double mutant cycle is untenable with TC299423, the binding map for this agonist remains murky, with no perturbation made to the binding site causing more than a 6.7-fold loss in function. What is clear is that as the picture of how agonists bind at the  $\alpha 6$ - $\beta 2$  interface develops, the  $\alpha 6\beta 2$  subtype continues to present a unique and interesting pharmacology.

## 4.6 Materials and Methods

### *Molecular Biology*

Rat  $\alpha 6$ L9'S,  $\alpha 4$ L9'A (denoted as  $\alpha 4$  throughout the section),  $\beta 2$ L9'S<sub>LFM/AAQA</sub> and  $\beta 2$  nAChRs were in the pGEMhe vector, a cDNA plasmid optimized for protein expression in *Xenopus* oocytes. Site-directed mutagenesis was performed by PCR using the Stratagene QuikChange protocol and primers ordered from Integrated DNA Technologies (Coralville, IA). Circular cDNA was linearized with SbfI (New England Biolabs, Ipswich, MA) and then transcribed *in vitro* using T7 mMessage mMachinE kit (Life Technologies, Santa Clara, CA), with a purification step after each process (Qiagen, Valencia, CA). Final concentrations were quantified by UV spectroscopy.

### *Ion Channel Expression and $\alpha$ -hydroxy Acid Incorporation*

The cyanomethylester form of threonine  $\alpha$ -hydroxy was synthesized, coupled to the dinucleotide dCA, and enzymatically ligated to UAG-suppressor 74-mer THG73 tRNA<sub>CUA</sub> as previously described.<sup>2</sup> The product was verified by MALDI time-of-flight mass spectrometry on a 3-hydroxypicolinic acid matrix. *Xenopus laevis* oocytes (stage V to VI) were sourced from both a Caltech facility and Ecocyte Bio Science (Austin, TX). The Tah-tRNA was injected alongside  $\alpha 6\beta 2^{\ddagger}$   $\alpha 6$ -T150UAG mRNA into oocytes at a 1:1 volume ratio, with an  $\alpha 6$ : $\beta 2$  mRNA mass ratio of 10:1, resulting in 25 ng each of mRNA and tRNA injected per cell. Cells were incubated 24-48 hours at 18°C in ND96 solution (96 mM NaCl, 2mM KCl, 1 mM MgCl<sub>2</sub>, and 5mM HEPES, pH 7.5) enriched with theophylline, sodium pyruvate, and gentamycine. The fidelity of incorporation of Tah was confirmed

by charging tRNA with Thr in a wild-type recovery experiment. Data from these experiments (reported as Thr in the data tables above) matched wild-type data, reported in previous chapters. A read-through/reaminoacylation test serves as a negative control wherein a 76-mer tRNA is injected alongside mRNA. Lack of current proved no detectable reaminoacylation at the Thr150 site.

### *N*'-methylnicotinium Synthesis

Synthesis of *N*'-methylnicotinium was based on previously reported methods.<sup>14</sup> All reagents were purchased from Sigma Aldrich (St. Louis, MO). In a roundbottom flask, 19.8 mL of nicotine was added to 250 mL of acetonitrile and excess sodium carbonate. Methyl iodide was added dropwise while stirring until 5.76 mL were added. The reaction was stirred at room temperature for three days. The reaction solution was filtered by vacuum and solids were discarded. Solvent from the filtrate was removed by rotary evaporation until tan oil remained. Deionized water, 50 mL, was added to the oil and dissolved forming an orange solution. Continuous chloroform extraction was performed on the orange solution for five days. The aqueous layer was isolated and solvent was removed by rotary evaporation upon which crystals formed. Product was recrystallized three consecutive times with hot isopropanol for an over 40% yield. Further purification was achieved by iterative preparative HPLC (Waters, Milford, MA) using a 100% water solvent profile.

<sup>1</sup>H NMR (500 MHz, Acetonitrile-*d*<sub>3</sub>) δ 8.80 (dd, *J* = 2.5, 0.8 Hz, 1H), 8.71 (dd, *J* = 4.8, 1.6 Hz, 1H), 8.12 – 8.00 (m, 1H), 7.50 (ddd, *J* = 8.0, 4.8, 0.9 Hz, 1H), 5.06 (dd, *J* = 11.5, 8.0 Hz, 1H), 3.95 – 3.69 (m, 2H), 3.12 (s, 3H), 2.75 (s, 3H), 2.74 – 2.63 (m, 1H), 2.57 – 2.42 (m, 1H), 2.39 – 2.19 (m, 2H).

### *Whole-Cell Electrophysiological Characterization*

Acetylcholine chloride and (-)-nicotine tartrate were purchased from Sigma Aldrich (St Louis, MO), while TC299423 (Targacept) was a generous gift. *N*'-methylnicotinium iodide was prepared according to the procedure above. Agonist-induced currents were recorded in TEVC mode using the OpusXpress 6000A (Molecular Devices, Sunnyvale, CA) at a holding potential of -60 mV in a running buffer of Ca<sup>2+</sup>-free ND96. Agonists were prepared in Ca<sup>2+</sup>-free ND96 and delivered to cells via a 1 mL application over 15 sec followed by a 2 min wash. Data from dose-response experiments were normalized, averaged, and fit to the Hill equation using Kaleidagraph (Synergy Software, Reading PA),

though data are visualized here with Prism (GraphPad Software, La Jolla, CA). Error bars are presented as standard error of the mean, while  $EC_{50}$  and Hill coefficient errors are reported by Kaleidagraph and represent the sum of the squared error between the data and the calculated fit.

## 4.7 References

1. Post, M. R., Limapichat, W., Lester, H. A. & Dougherty, D. A. Heterologous expression and nonsense suppression provide insights into agonist behavior at  $\alpha 6\beta 2$  nicotinic acetylcholine receptors. *Neuropharmacology* **97**, 376–382 (2015).
2. Van Arnam, E. B. & Dougherty, D. A. Functional Probes of Drug–Receptor Interactions Implicated by Structural Studies: Cys-Loop Receptors Provide a Fertile Testing Ground. *J. Med. Chem.* **57**, 6289–6300 (2014).
3. Tavares, X. D. S. *et al.* Variations in Binding Among Several Agonists at Two Stoichiometries of the Neuronal,  $\alpha 4\beta 2$  Nicotinic Receptor. *J. Am. Chem. Soc.* **134**, 11474–11480 (2012).
4. Xiu, X., Puskar, N. L., Shanata, J. A. P., Lester, H. A. & Dougherty, D. A. Nicotine binding to brain receptors requires a strong cation– $\pi$  interaction. *Nature* **458**, 534–537 (2009).
5. Puskar, N. L., Xiu, X., Lester, H. A. & Dougherty, D. A. Two Neuronal Nicotinic Acetylcholine Receptors,  $\alpha 4\beta 4$  and  $\alpha 7$ , Show Differential Agonist Binding Modes. *J. Biol. Chem.* **286**, 14618–14627 (2011).
6. Cashin, A. L., Petersson, E. J., Lester, H. A. & Dougherty, D. A. Using Physical Chemistry To Differentiate Nicotinic from Cholinergic Agonists at the Nicotinic Acetylcholine Receptor. *J. Am. Chem. Soc.* **127**, 350–356 (2005).
7. Deechongkit, S. *et al.* Context-dependent contributions of backbone hydrogen bonding to  $\beta$ -sheet folding energetics. *Nature* **430**, 101–105 (2004).
8. England, P. M., Zhang, Y., Dougherty, D. A. & Lester, H. A. Backbone Mutations in Transmembrane Domains of a Ligand-Gated Ion Channel: Implications for the Mechanism of Gating. *Cell* **96**, 89–98 (1999).
9. Horovitz, A. Double-mutant cycles: a powerful tool for analyzing protein structure and function. *Fold. Des.* **1**, R121–R126 (1996).
10. Daeffler, K. N.-M., Lester, H. A. & Dougherty, D. A. Functionally Important Aromatic–Aromatic and Sulfur– $\pi$  Interactions in the D2 Dopamine Receptor. *J. Am. Chem. Soc.* **134**, 14890–14896 (2012).
11. Blum, A. P., Lester, H. A. & Dougherty, D. A. Nicotinic pharmacophore: The pyridine N of nicotine and carbonyl of acetylcholine hydrogen bond across a subunit interface to a backbone NH. *Proc. Natl. Acad. Sci.* **107**, 13206–13211 (2010).
12. Klotz, I. M. & Franzen, J. S. Hydrogen Bonds between Model Peptide Groups in Solution. *J. Am. Chem. Soc.* **84**, 3461–3466 (1962).

13. Davies, M., Evans, J. C. & Jones, R. L. Molecular interaction and infra-red absorption spectra. Part 4 — Methyl acetamide. *Trans. Faraday Soc.* **51**, 761 (1955).
14. Seeman, J. I. & Whidby, J. F. The iodomethylation of nicotine. An unusual example of competitive nitrogen alkylation. *J. Org. Chem.* **41**, 3824–3826 (1976).

## Chapter 5: Investigating a Dual Cation- $\pi$ Interaction Trend with Secondary Amines at $\alpha 4\beta 2$ <sup>§</sup>

### 5.1 Abstract

Results presented thus far have shown that in  $\alpha 6\beta 2$ , while ACh makes a functional cation- $\pi$  interaction with TrpB, and nicotine makes a strong compensatory hydrogen bond with the backbone carbonyl of TrpB, the binding mode of TC299423 remains a mystery. In an effort to further understand TC299423 binding in other subtypes, the binding interactions of TC299423 with  $\alpha 4\beta 2$  were probed, and an interesting dual cation- $\pi$  interaction with both TrpB and TyrC2 was observed. This effect was reminiscent of results observed with metan nicotine several years prior and revealed a possible trend amongst secondary amine agonists. Varenicline, also a secondary amine, was probed at TrpB and TyrC2 to support that hypothesis and was shown to indeed form cation- $\pi$  interactions at both residues.

Finally, a structure-function study of sorts was designed with the secondary amine norm nicotine, which only deviates in structure from nicotine by one methyl group on the pyrrolidine ring causing a shift from a tertiary amine to a secondary amine. Norm nicotine was found to form a cation- $\pi$  interaction at TrpB, and preliminary results suggest it forms a functional cation- $\pi$  interaction at TyrC2 as well. This result, if confirmed with more data, suggests that a dual cation- $\pi$  interaction with TrpB and TyrC2 is a general feature of secondary amines, and offers new insight into the pharmacology of  $\alpha 4\beta 2$  nAChRs.

---

<sup>§</sup> Much of the work described in this chapter was completed by Gabrielle S Tender (Caltech '18) including structure-function studies of TC299423 (TrpB and TyrC2), Varenicline (TyrC2), and Norm nicotine (TyrC2).

## 5.2 Introduction

The previous three chapters have investigated the binding patterns of ACh, nicotine, and TC299423 at  $\alpha 6\beta 2$  with results revealing that this nAChR subtype has a unique pharmacology. Of particular interest, though, is TC299423, an agonist that was originally developed as a possible  $\alpha 6\beta 2$ -selective agonist with properties showing promise for therapeutic use.<sup>1</sup> However, whereas acetylcholine makes the canonical cation- $\pi$  interaction with TrpB, nicotine and TC299423 do not.<sup>2</sup> For nicotine, this is partially explained by a strong hydrogen bond was made with the backbone carbonyl of TrpB that might compensate for the attenuating effects of a fluorination series. For TC299423, only a modest hydrogen bond was found at this site, and therefore further work is needed to explain its binding and activation of  $\alpha 6\beta 2$ .

In order to understand more about TC299423, its binding interactions were studied in  $\alpha 4\beta 2$ , which has been thoroughly characterized in previous work.<sup>3</sup> The  $\alpha 4\beta 2$  binding site lies at the  $\alpha 4$ - $\beta 2$  interface, and like all nAChR binding sites, it is composed of an aromatic box motif. Five aromatic residues are contributed by four loops – TyrA ( $\alpha 4$ : 93), Trp B ( $\alpha 4$ : 149), TyrC1 ( $\alpha 4$ : 190), TyrC2 ( $\alpha 4$ :197), and TrpD ( $\beta 2$ : 57).<sup>4</sup> All agonists that have previously been studied at  $\alpha 4\beta 2$  demonstrate a cation- $\pi$  interaction with TrpB, highlighting the anomalous nature the  $\alpha 6\beta 2$  results.<sup>5,6</sup>

A recent computational study looking at the predicted cation- $\pi$  binding ability of each aromatic residue in the AChBP aromatic box shows that each of these side chains can theoretically contribute cation- $\pi$  binding energy to the overall binding energy of the ACh-AChBP complex (modeled as tetramethylammonium): TyrA contributes 2.3 kcal/mol, TrpB contributes 8.3 kcal/mol, TyrC1 contributes 7.5 kcal/mol, TyrC2 contributes 8.0

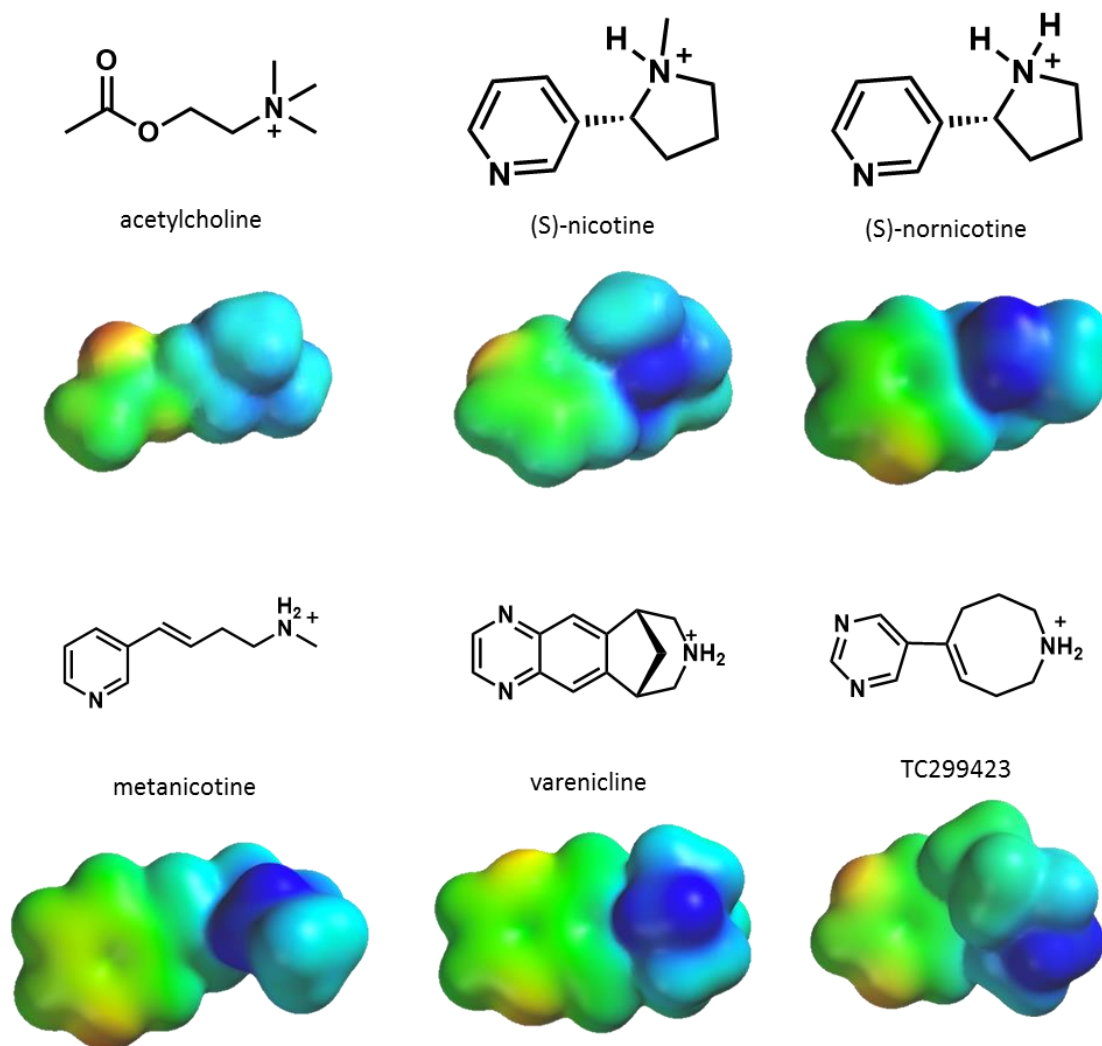


**Figure 1.** The structures and electrostatic potential maps of acetylcholine and nicotine are shown here for comparison to the secondary amine agonists used in this chapter: TC299423, metanicotine, nornicotine, and varenicline. Maps are calculated with Hartree Fock 6-31G\*\* and are shown on a scale of -10 to +150 kcal/mol.

kcal/mol, and TrpD contributes 4.8 kcal/mol.<sup>7</sup> Though these predicted energy values suggest each member of the aromatic box plays some role in binding, previously reported structure-function studies show that they do not. In studies investigating the behavior of nicotine at  $\alpha 4\beta 2$ , the phenol group of TyrA was shown to form an important hydrogen bond, likely with another amino acid; a result determined from an O-methyltyrosine substitution causing a large loss of function. However, TyrA shows no meaningful changes in  $EC_{50}$  when replaced with electron-withdrawing analogues and therefore does not make

a cation- $\pi$  interaction with nicotine. TyrC2 shows no important phenol hydrogen bonding effects, as well as no cation- $\pi$  interaction with nicotine. This was established with a CN-Phe substitution, which has similar electron-withdrawing effects as F<sub>2</sub>Phe but only causes a modest 2.7 fold-shift in EC<sub>50</sub> (whereas metanicotine with CNPhe demonstrates a 6.1-fold shift in EC<sub>50</sub>).<sup>8</sup>

As TC299423 and nicotine showed in  $\alpha 6\beta 2$ , binding patterns may differ from agonist to agonist and subtype to subtype. This makes sense since it is well known that each subtype has a different pharmacology, function, and localization in the brain.<sup>9,10</sup> Thus, it would be interesting and important to know if the variations in binding observed with TC299423 in  $\alpha 6\beta 2$  are consistent in  $\alpha 4\beta 2$ . This chapter will discuss work done making it evident that TC299423 makes a cation- $\pi$  interaction with both TrpB *and* TyrC2, and it will explore whether this dual cation- $\pi$  pattern is a general one for secondary amines. Of the secondary amine agonists interrogated, all made a cation- $\pi$  interaction with both TrpB and TyrC2. This includes nornicotine – a nicotine analogue with the pyrrolidine methyl group eliminated – proving that the additional cation- $\pi$  interaction is indeed a feature of secondary amines at  $\alpha 4\beta 2$ .

### **5.3 Binding Studies of TC299423 at $\alpha 4\beta 2$**

TC299423 was found to not make a cation- $\pi$  interaction with any aromatic residues probed in  $\alpha 6\beta 2$  as shown in Chapter 3. Furthermore, it was only shown to make a modest hydrogen bond with the backbone carbonyl of TrpB in  $\alpha 6\beta 2$  as shown in Chapter 4. These results showed TC299423 to behave quite differently than ACh and nicotine. An important question to answer then, is if TC299423 also behaves uniquely at other subtypes, including  $\alpha 4\beta 2$ . This is an especially interesting question considering TC299423 was designed to be

an  $\alpha 6\beta 2$ -selective ligand. In order to learn the answer, TC299423 was probed for a cation- $\pi$  interaction with all of the aromatic residues using methods discussed in previous chapters.

At TrpB, TC299423 yet again shows some interesting results (Figure 2, Table 3).

While there is a marked increase in  $EC_{50}$  with each additional fluorine substituent on the

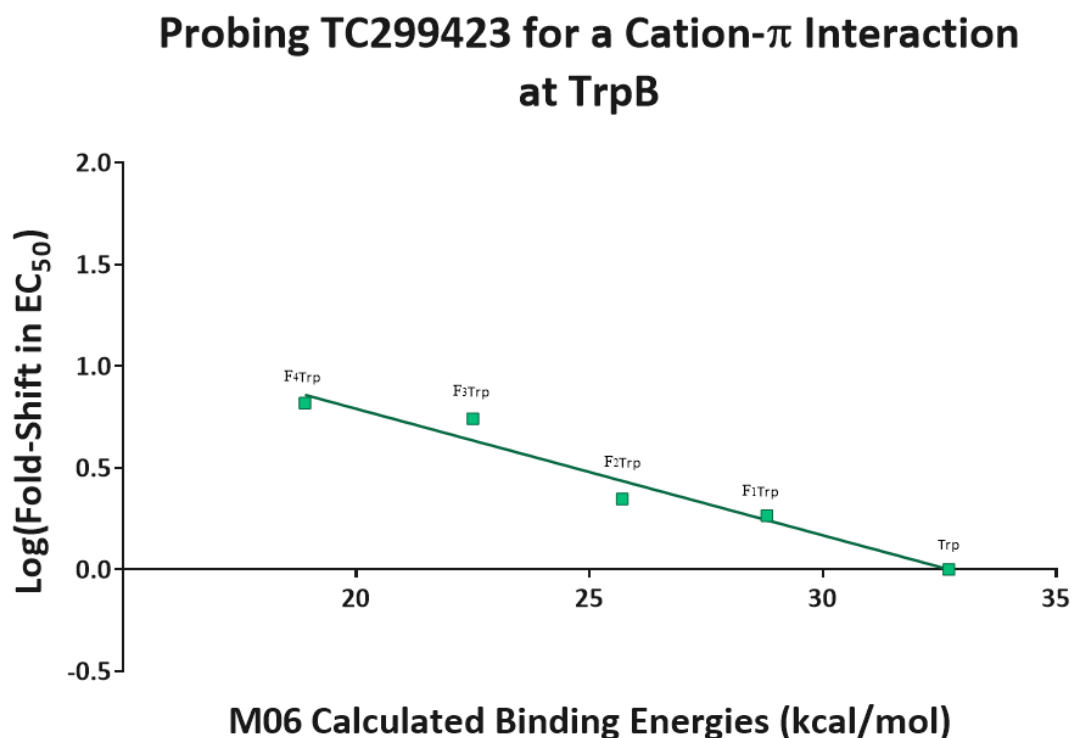


**Figure 2.** For this and all fluorination plots presented in this chapter, the log of the fold-shift in  $EC_{50}$  is plotted against the M06 6-31G<sup>\*\*</sup> calculated binding energy between a sodium ion and each non-canonical side chain for TC299423 at TrpB in  $\alpha 4\beta 2$ . While the maximum fold-shift at F<sub>4</sub>Trp is rather small for these types of experiments, the linear trend indicates the presence of a functional cation- $\pi$  interaction between the indole side chain and the cationic agonist.

**Table 1.** Investigating a Cation- $\pi$  Interaction between TC299423 and TrpB in  $\alpha 4\beta 2$

TrpB	$EC_{50}$ ( $\mu$ M)	$n_H$	$I_{max}$ ( $\mu$ A)	Fold Shift	N
Trp	$0.0234 \pm 0.0009$	$1.39 \pm 0.06$	0.22 - 1.46	1	15
F <sub>1</sub> Trp	$0.0431 \pm 0.0008$	$1.26 \pm 0.03$	0.12 - 1.2	1.8	11
F <sub>2</sub> Trp	$0.052 \pm 0.001$	$1.21 \pm 0.04$	0.05 - 0.62	2.2	14
F <sub>3</sub> Trp	$0.129 \pm 0.003$	$1.24 \pm 0.03$	0.11 - 1.41	5.5	12
F <sub>4</sub> Trp	$0.154 \pm 0.007$	$1.12 \pm 0.05$	0.15 - 0.77	6.6	14

## Probing TC299423 for a Cation- $\pi$ Interaction at TyrC2

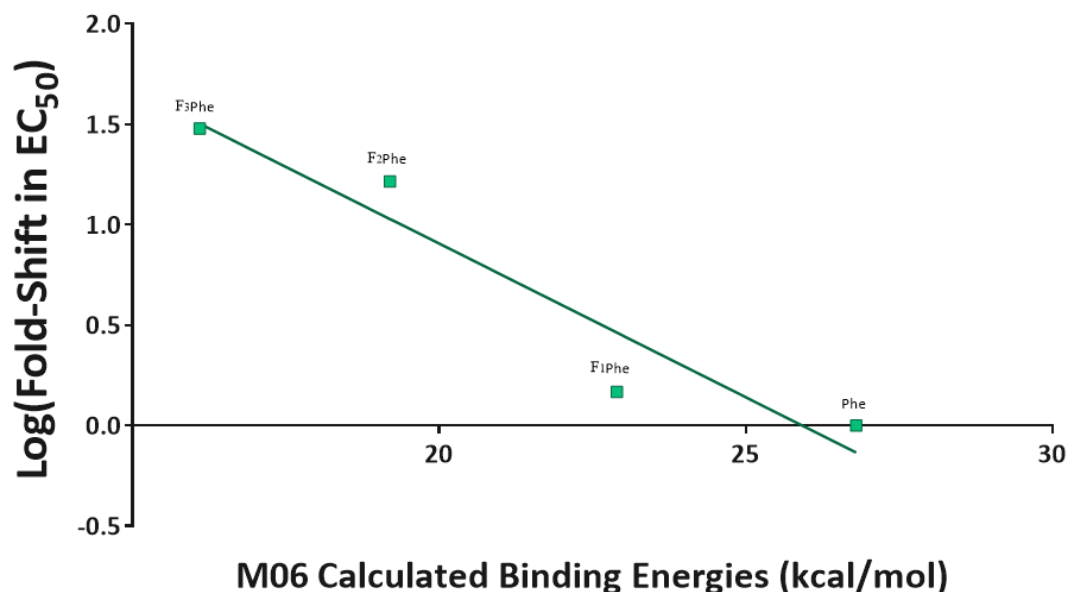


**Figure 3.** A fluorination plot for TC299423 at TyrC2 in  $\alpha 4\beta 2$ . The linear trend indicates the presence of a strong cation- $\pi$  interaction between the indole side chain and the cationic agonist.

**Table 2.** Investigating a Cation- $\pi$  Interaction between TC299423 and TyrC2 in  $\alpha 4\beta 2$

TyrC2	EC <sub>50</sub> ( $\mu$ M)	n <sub>H</sub>	I <sub>max</sub> ( $\mu$ A)	Fold Shift	N
Phe	0.098 $\pm$ 0.003	1.09 $\pm$ 0.03	0.06 - 1.08	1	17
F <sub>1</sub> Phe	0.144 $\pm$ 0.005	1.19 $\pm$ 0.04	0.05 - 0.38	1.5	12
F <sub>2</sub> Phe	1.61 $\pm$ 0.07	1.28 $\pm$ 0.06	0.05 - 0.57	16	9
F <sub>3</sub> Phe	2.95 $\pm$ 0.25	1.28 $\pm$ 0.11	0.07 - 0.18	30	7

ring, the maximum fold-shift in EC<sub>50</sub> observed was at F<sub>4</sub>Trp and was only a 6.6-fold increase. While this is a modest loss of function – ACh experiences a 66-fold loss of function at F<sub>4</sub>Trp in the same subtype<sup>5</sup> – there is nevertheless a linear trend when the log(fold-shift) of each mutation is plotted against M06-calculated theoretical binding energies between a sodium ion and each side chain. Thus, it can be said that TC299423 makes a functional, if only modest, cation- $\pi$  interaction with TrpB in  $\alpha 4\beta 2$ .

TyrA was then probed for a cation- $\pi$  interaction with TC299423, and yielded the same results previously published for nicotine. That is, no functional cation- $\pi$  interaction

was found. TyrC2, though, showed an unexpected trend (Figure 3, Table 4). While F<sub>1</sub>Phe only showed a modest 1.5-fold increase in EC<sub>50</sub>, the other points in the fluorination series showed large fold-shifts. F<sub>2</sub>Phe resulted in a 16-fold increase, and F<sub>3</sub>Phe caused a 30-fold increase in EC<sub>50</sub>. When translated into a fluorination plot, these results show a distinctly linear trend, showing that in addition to a cation- $\pi$  interaction with TrpB, TC299423 makes an even stronger functional cation- $\pi$  interaction at TyrC2.

### 5.3 Binding Studies of Metanicotine at $\alpha 4\beta 2$

The second cation- $\pi$  interaction observed with TC299423 while surprising, was actually reminiscent of work done with metanicotine. Metanicotine (also known as rivanieline, TC-2403, and RJR-2403) is an isomer of nicotine in which the pyrrolidine ring has been opened.<sup>11</sup> This compound has antinociceptive effects in mice and is more potent and efficacious than ACh at  $\alpha 4\beta 2$  receptors.<sup>12,13</sup> It had been proposed as a relatively selective activator of human  $\alpha 4\beta 2$  receptors, and therefore was of some interest to fully characterize at the  $\alpha 4\beta 2$  binding site. This study was completed early on relative to other projects presented in the thesis, and the results seemed anomalous until the data from TC299423 at  $\alpha 4\beta 2$  were collected several years later.

When metanicotine was used in a fluorination series at TrpB in  $\alpha 4\beta 2$  (Figure 4, Table 5), a strong cation- $\pi$  interaction was observed, with F<sub>4</sub>Trp resulting in a 25-fold shift in EC<sub>50</sub>. Though F<sub>1</sub>Trp is close to wild-type, the remaining points in the series show additive losses in function to form a linear trend when the log(fold-shift) is plotted against M06-calculated binding energies. TyrC2 also shows a linear fluorination plot, with the F<sub>3</sub>Phe mutation causing 51-fold shift relative to Phe. TyrA showed no meaningful changes

in metanicotine  $EC_{50}$  for fluorinated Phe residues relative to Phe. Thus, metanicotine also forms dual functional cation- $\pi$  interactions at both TrpB and TyrC2 in  $\alpha 4\beta 2$ .

At the time these studies were completed, this dual cation- $\pi$  feature, while remarkable, had no clear rationale. However, once the same effect was observed with TC299423, both structures were compared to look for similarities that create a trend. Both agonists are typical nicotinic pharmacophores in that they have a cationic amine moiety, a hydrogen bond donor associated with that amine, and a hydrogen bond acceptor several

### Probing Metanicotine for a Cation- $\pi$ Interaction at TrpB

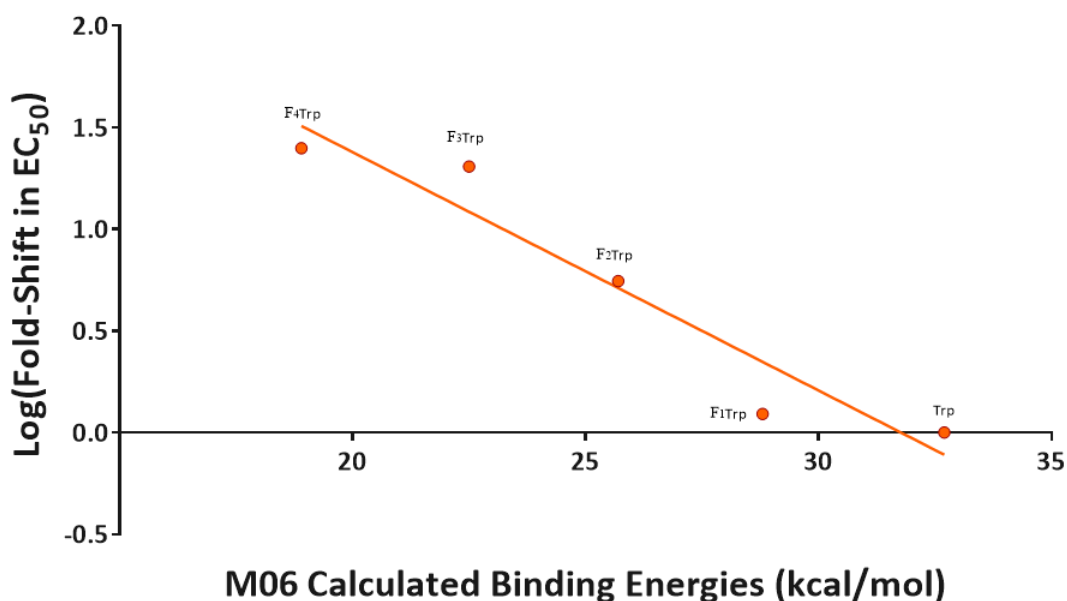


**Figure 4.** A fluorination plot for metanicotine at TrpB in  $\alpha 4\beta 2$ . The linear trend indicates the presence of a strong cation- $\pi$  interaction between the indole side chain and the cationic agonist.

**Table 3.** Investigating a Cation- $\pi$  Interaction between metanicotine and TrpB in  $\alpha 4\beta 2$

TrpB	$EC_{50}$ ( $\mu$ M)	$n_H$	$I_{max}$ ( $\mu$ A)	Fold Shift	N
Trp	$0.64 \pm 0.02$	$1.32 \pm 0.04$	0.08 - 0.89	1	13
F <sub>1</sub> Trp	$0.79 \pm 0.02$	$1.38 \pm 0.03$	0.12 - 0.80	1.2	16
F <sub>2</sub> Trp	$3.6 \pm 0.1$	$1.54 \pm 0.06$	0.15 - 0.56	5.6	14
F <sub>3</sub> Trp	$13 \pm 1$	$1.6 \pm 0.1$	0.07 - 0.30	20	12
F <sub>4</sub> Trp	$16 \pm 2$	$1.3 \pm 0.1$	0.03 - 0.11	25	12

## Probing Metanicotine for a Cation- $\pi$ Interaction at TyrC2

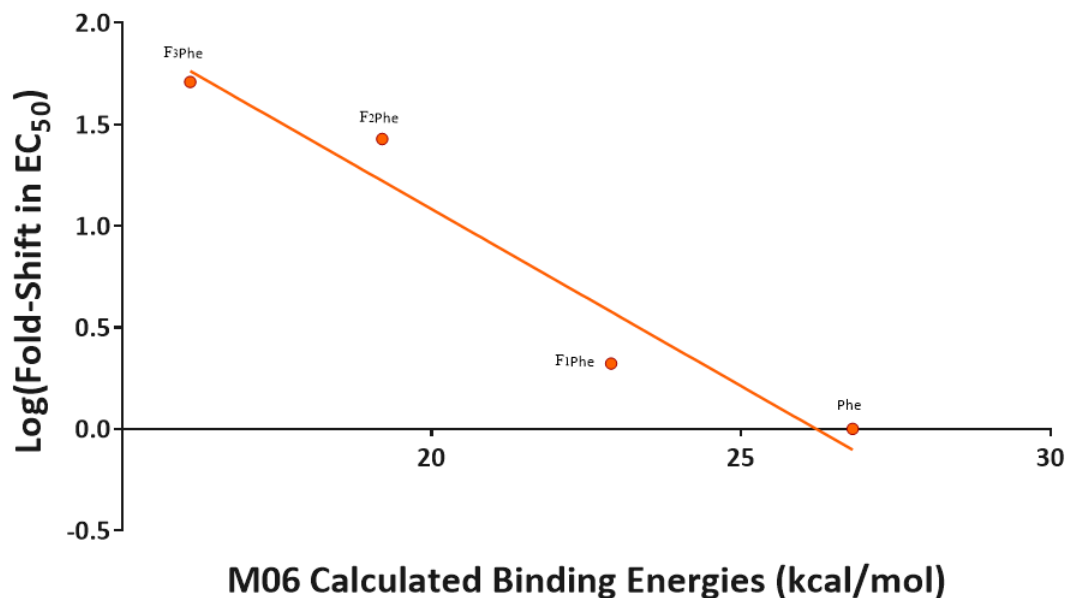


**Figure 5.** A fluorination plot for metanicotine at TyrC2 in  $\alpha 4\beta 2$ . The linear trend indicates the presence of a strong cation- $\pi$  interaction between the indole side chain and the cationic agonist.

**Table 4.** Investigating a Cation- $\pi$  Interaction between metanicotine and TrpB in  $\alpha 4\beta 2$

TyrC2	EC <sub>50</sub> (μM)	n <sub>H</sub>	I <sub>max</sub> (μA)	Fold Shift	N
Phe	0.41 ± 0.03	1.16 ± 0.07	0.06 - 2.78	1	17
F <sub>1</sub> Phe	0.86 ± 0.06	1.15 ± 0.08	0.04 - 0.07	2.1	11
F <sub>2</sub> Phe	11 ± 1	0.6 ± 0.1	0.03 - 0.13	27	8
F <sub>3</sub> Phe	21 ± 1	1.4 ± 0.2	0.04 - 0.24	51	12

angstroms away.<sup>14</sup> While metanicotine and TC299423 have critical differences in the moieties that make up these features – a pyridine versus a pyrimidine ring for the hydrogen bond acceptor, and a linear amine versus a hexahydroazocine – they are both secondary amines. The question was then raised whether other secondary amines also had this interesting dual cation- $\pi$  interaction. If so, this would present an interesting and novel feature of secondary amine agonists and build on the current understanding of  $\alpha 4\beta 2$  pharmacology.

## 5.4 Establishing a Binding Trend for Secondary Amines

The agonists discussed above, TC299423 and metanicotine, are both secondary amines and both make functional cation- $\pi$  interactions with TrpB and TyrC2. In order to determine whether these features are correlated – that is, whether a dual cation- $\pi$  interaction is a defining feature of the secondary amine – more agonists must be tested. Varenicline, sold and marketed by Pfizer as Chantix<sup>®</sup>, is an FDA-approved smoking cessation drug that

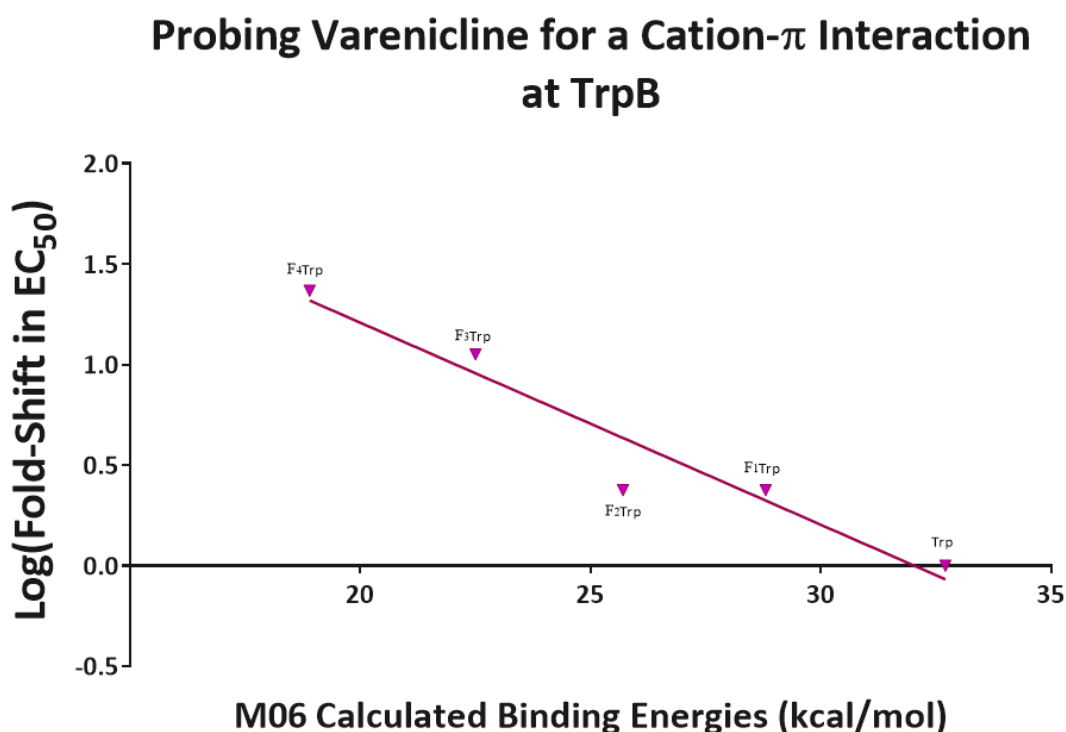


**Figure 6.** A fluorination plot for Varenicline at TrpB in  $\alpha 4\beta 2$  as previously reported in Tavares da Silva et al. The linear trend indicates the presence of a strong cation- $\pi$  interaction between the indole side chain and the cationic agonist.

**Table 5.** Previously Reported Cation- $\pi$  Interaction between Varenicline and TrpB\*

TrpB	EC <sub>50</sub> ( $\mu$ M)	n <sub>H</sub>	Fold Shift	N
Trp	0.0024 $\pm$ 0.0001	1.2 $\pm$ 0.1	1	15
F <sub>1</sub> Trp	0.0057 $\pm$ 0.0002	1.2 $\pm$ 0.1	2.4	11
F <sub>2</sub> Trp	0.0057 $\pm$ 0.0021	1.2 $\pm$ 0.1	2.4	14
F <sub>3</sub> Trp	0.027 $\pm$ 0.001	1.3 $\pm$ 0.1	11	12
F <sub>4</sub> Trp	0.056 $\pm$ 0.005	1.1 $\pm$ 0.1	23	14

\*Data as reported in Tavares da Silva et al

## Probing Varenicline for a Cation- $\pi$ Interaction at TyrC2

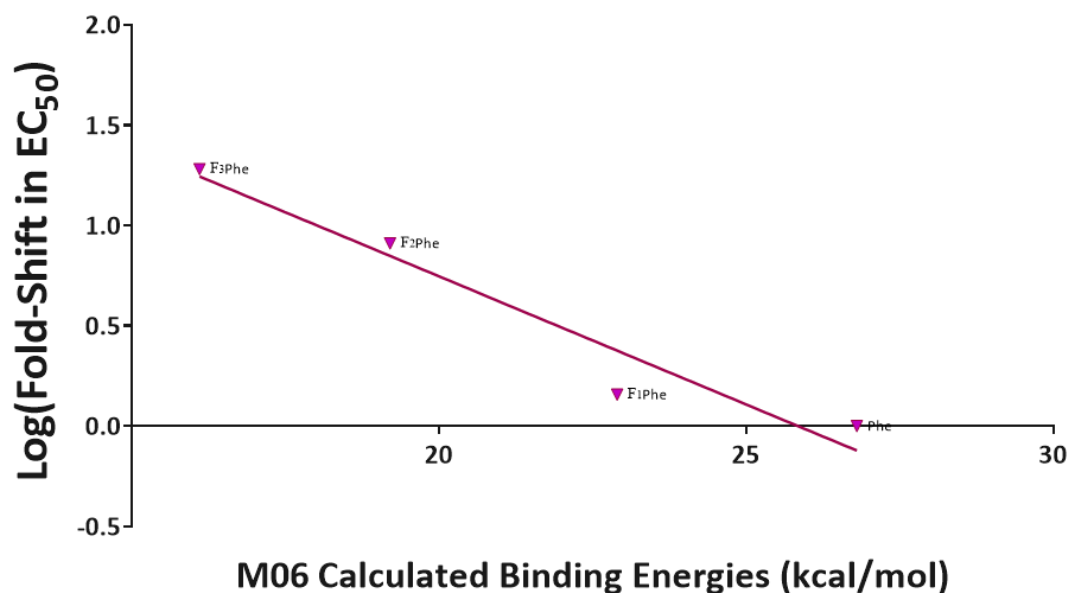


**Figure 7.** A fluorination plot for varenicline at TyrC2 in  $\alpha 4\beta 2$ . The linear trend indicates the presence of a strong cation- $\pi$  interaction between the indole side chain and the cationic agonist.

**Table 6.** Investigating a Cation- $\pi$  Interaction between Varenicline and TyrC2 in  $\alpha 4\beta 2$

TyrC2	EC <sub>50</sub> ( $\mu$ M)	n <sub>H</sub>	I <sub>max</sub> ( $\mu$ A)	Fold Shift	N
Phe	0.0014 $\pm$ 0.0002	1.3 $\pm$ 0.14	0.04 - 0.14	1	10
F <sub>1</sub> Phe	0.00201 $\pm$ 0.00009	1.45 $\pm$ 0.09	0.02 - 0.08	1.4	8
F <sub>2</sub> Phe	0.0114 $\pm$ 0.00097	1.21 $\pm$ 0.11	0.02 - 0.1	8.1	12
F <sub>3</sub> Phe	0.0267 $\pm$ 0.0016	1.08 $\pm$ 0.06	0.02 - 0.09	19	8

is thought to work by serving as a partial agonist to  $\alpha 4\beta 2$ .<sup>15,16</sup> Varenicline has a pyrazine hydrogen bond acceptor fused to a bridged tetrahydrobenzazepine group that serves as the cationic secondary amine group in the pharmacophore model. This drug has previously been shown to form a cation- $\pi$  interaction at TrpB (Figure 6, Table 5)<sup>6</sup> in  $\alpha 4\beta 2$ , with a 23-fold shift in EC<sub>50</sub> at F<sub>4</sub>Trp, but had never been analyzed at TyrC2.

Nonsense-suppression based fluorination studies were conducted for varenicline at TyrC2. Once again, F<sub>1</sub>Phe showed only a modest 1.4-fold shift in EC<sub>50</sub> relative to Phe, but F<sub>2</sub>Phe and F<sub>3</sub>Phe showed 8.1-fold and 19-fold shifts in EC<sub>50</sub>, respectively (Figure 7, Table

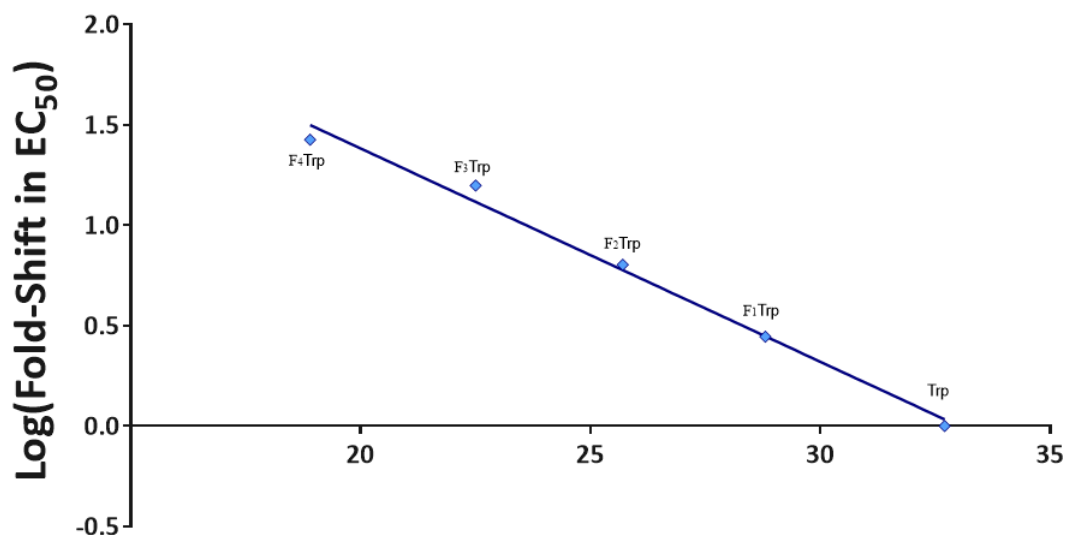
6). The corresponding fluorination plot shows a linear trend confirming that varenicline makes a strong cation- $\pi$  interaction with TyrC2 in  $\alpha 4\beta 2$ .

With the results from varenicline, three agonists have now been demonstrated to form functional cation- $\pi$  interactions with both TrpB and TyrC2 in  $\alpha 4\beta 2$ . These three drugs have distinctly varied structural features at both their hydrogen bond acceptor and cationic ends (Figure 1). However, they all share in common a secondary amine moiety. While having three secondary amine agonists display dual cation- $\pi$  interactions is highly indicative of a trend, it does not definitively prove a correlation. To do this, a structure-function study of sorts was designed. Transforming nicotine – which has been shown to only form a cation- $\pi$  interaction at TrpB in  $\alpha 4\beta 2$  – into a secondary amine should establish that it is solely the difference in the order of the amine that is responsible for the dual cation- $\pi$  interaction effect. The demethylated, secondary amine version of nicotine is nornicotine, a natural component of tobacco that is a precursor to the well-documented carcinogen *N*'-nitrosonicotine that is a byproduct of the curing process.<sup>17</sup> This compound is available commercially and was probed for binding interactions at TrpB and TyrC2.

Nornicotine has an EC<sub>50</sub> of 1.8  $\mu$ M, a 20-fold shift compared to nicotine, showing that it is a significantly less potent agonist. The fluorination plot of nornicotine at TrpB shows a cation- $\pi$  interaction, with F<sub>4</sub>Trp resulting in a 27-fold shift in EC<sub>50</sub> (Figure 8, Table 7). Compared to nicotine, which shows a 47-fold loss in function at F<sub>4</sub>Trp, this is perhaps a less strong but still functionally important cation- $\pi$  interaction. Preliminary data for TyrC2 shows the same type of trend seen for other secondary amine agonists analyzed in this chapter (Figure 9, Table 8). The YC2Phe mutant has an EC<sub>50</sub> of 3.7  $\mu$ M, only a slight loss of function from wild-type. The F<sub>1</sub>Phe and F<sub>2</sub>Phe mutants have EC<sub>50</sub> values of 5.6

and 26  $\mu\text{M}$  respectively. These mutations represent a 1.5-fold and 7-fold shift in  $\text{EC}_{50}$  from wild-type, results that are consistent with the other agonists (varenicline had 1.4-fold and 8.1-fold shifts in  $\text{EC}_{50}$  at these mutants). The fluorination plot for these three values shows a fairly linear trend ( $R^2 = 0.89$ ) that can be used to predict a fold-shift for  $\text{F}_3\text{Phe}$  of 12.7, and an  $\text{EC}_{50}$  of 46  $\mu\text{M}$ . While this theoretical fold-shift is lower than other secondary amine agonists (summarized in Table 9), it is still indicative of a functional cation- $\pi$  interaction. If future data collected at  $\text{F}_3\text{Phe}$  substantiates the trend, it would provide definitive proof that a unique and general feature of secondary amine agonists is the formation of dual cation- $\pi$  interactions with TrpB and TyrC2.

### Probing Nornicotine for a Cation- $\pi$ Interaction at TrpB



### M06 Calculated Binding Energies (kcal/mol)

**Figure 8.** A fluorination plot for nornicotine at TrpB in  $\alpha 4\beta 2$ . The linear trend indicates the presence of a strong cation- $\pi$  interaction between the indole side chain and the cationic agonist.

**Table 7.** Investigating a Cation- $\pi$  Interaction between Nornicotine and TrpB in  $\alpha 4\beta 2$

TrpB	$\text{EC}_{50}$ ( $\mu\text{M}$ )	$n_H$	$I_{\max}$ ( $\mu\text{A}$ )	Fold Shift	N
Trp	$1.65 \pm 0.06$	$1.29 \pm 0.05$	1.33 - 9.37	1	13
$\text{F}_1\text{Trp}$	$4.6 \pm 0.2$	$1.26 \pm 0.05$	0.27 - 0.9	2.8	16
$\text{F}_2\text{Trp}$	$10.5 \pm 0.7$	$1.31 \pm 0.08$	0.04 - 0.11	6.4	8
$\text{F}_3\text{Trp}$	$26 \pm 2$	$1.5 \pm 0.1$	0.05 - 1.28	16	16
$\text{F}_4\text{Trp}$	$44 \pm 4$	$1.15 \pm 0.08$	0.95 - 1.51	27	8

## Probing Nornicotine for a Cation- $\pi$ Interaction at TyrC2

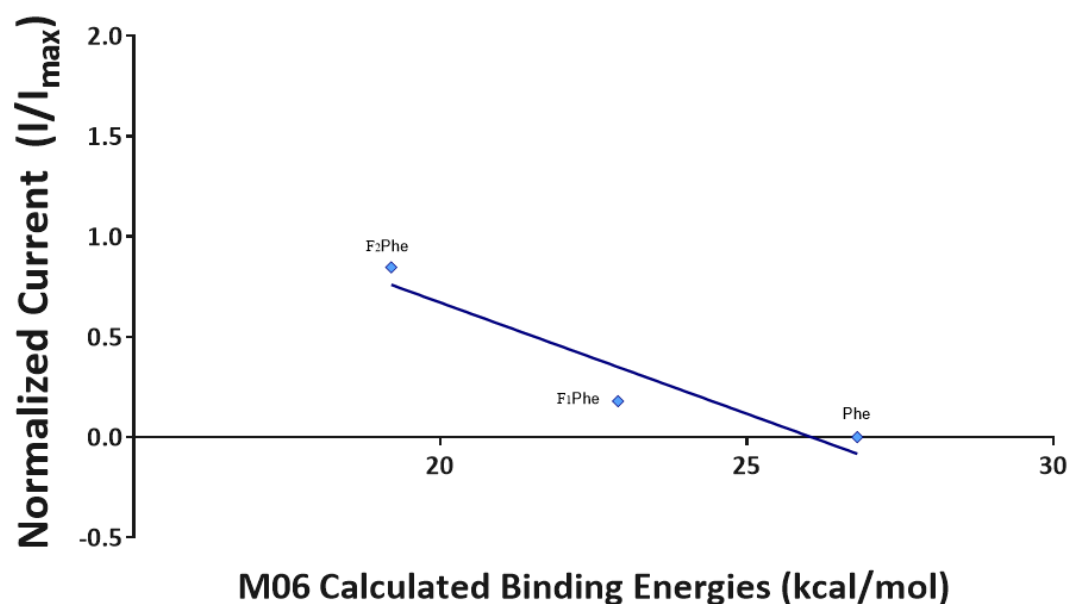


**Figure 9.** A preliminary fluorination plot for nornicotine at TyrC2 in  $\alpha 4\beta 2$ . The linear trend indicates the presence of a strong cation- $\pi$  interaction between the indole side chain and the cationic agonist though data at F<sub>3</sub>Phe would make this case stronger. If the trend holds with more data, it would be especially strong evidence that secondary amines follow a dual cation- $\pi$  interaction trend in  $\alpha 4\beta 2$  as the only difference between this agonist and nicotine is the shift from a tertiary amine to a secondary amine.

**Table 8.** Investigating a Cation- $\pi$  Interaction between Nornicotine and TyrC2 in  $\alpha 4\beta 2$

TyrC2	EC <sub>50</sub> ( $\mu$ M)	n <sub>H</sub>	I <sub>max</sub> ( $\mu$ A)	Fold Shift	N
Phe	3.7 $\pm$ 0.4	1.2 $\pm$ 0.1	0.07 - 1.42	1	20
F <sub>1</sub> Phe	5.6 $\pm$ 0.6	1.2 $\pm$ 0.1	0.06 - 0.1	1.5	4
F <sub>2</sub> Phe	26 $\pm$ 2	1.6 $\pm$ 0.1	0.05 - 0.08	7.0	5
F <sub>3</sub> Phe			No Data		

### 5.5 Conclusions

Structure-function studies of four different agonists, with a variety of structural features but a common secondary amine moiety, have each demonstrated a functional cation- $\pi$  interaction with both TrpB and TyrC2 in  $\alpha 4\beta 2$ . The computational studies of AChBP discussed earlier are predictive of this effect (TrpB contributed 8.3 kcal/mol and TyrC2 contributed 8.0 kcal/mol to the overall binding of tetramethylammonium), but it has

not been observed with either ACh or nicotine. While the nornicotine experiments could definitively show the dual cation- $\pi$  interaction to be a feature of secondary amines, they do not offer substantial evidence explaining why.

A likely hypothesis is that the secondary amine has less local steric bulk, and therefore Loop C is able to come closer to the agonist forming a strong and functionally important cation- $\pi$  interaction. Along the same lines, the agonist may be freer to move around the binding site with one less methyl group and orient in a way that brings the cation closer to both aromatic residues than a tertiary or quaternary amine would allow. An alignment of two AChBP structures, one crystallized with the tertiary amine nicotine and the other with varenicline, could potentially add extra insight. However, as seen in Figure 10, the positions of TrpB in each structure superimpose almost perfectly, and TyrC2 only shows a slight rotation of the phenol ring, though not enough to cause any changes in cation- $\pi$  binding ability. The positions of the cationic center of each agonist also overlap closely. This could be a result of differences between AChBP and  $\alpha 4\beta 2$ ; recall that that their extracellular regions only share about 30% sequence identity. It is also important to remember that crystal structures only offer a snapshot of one confirmation, and that the lack of the methyl group may allow a conformation shifts not visualized by the crystal structure. Thus, the crystal structures neither substantiate the sterics-based hypothesis nor rule it out.

**Table 9:** Summary of Relative Cation- $\pi$  Interaction Strengths at TrpB and YC2 for Secondary Amines

Agonist	Fold Shift: F <sub>4</sub> Trp	Fold Shift: F <sub>3</sub> Phe
ACh	66	---
Nicotine	47	---
TC299423	6.6	30
metanicotine	25	51
varenicline	23	19
nornicotine	27	12.7*

\*predicted using linear regression result from Figure 9

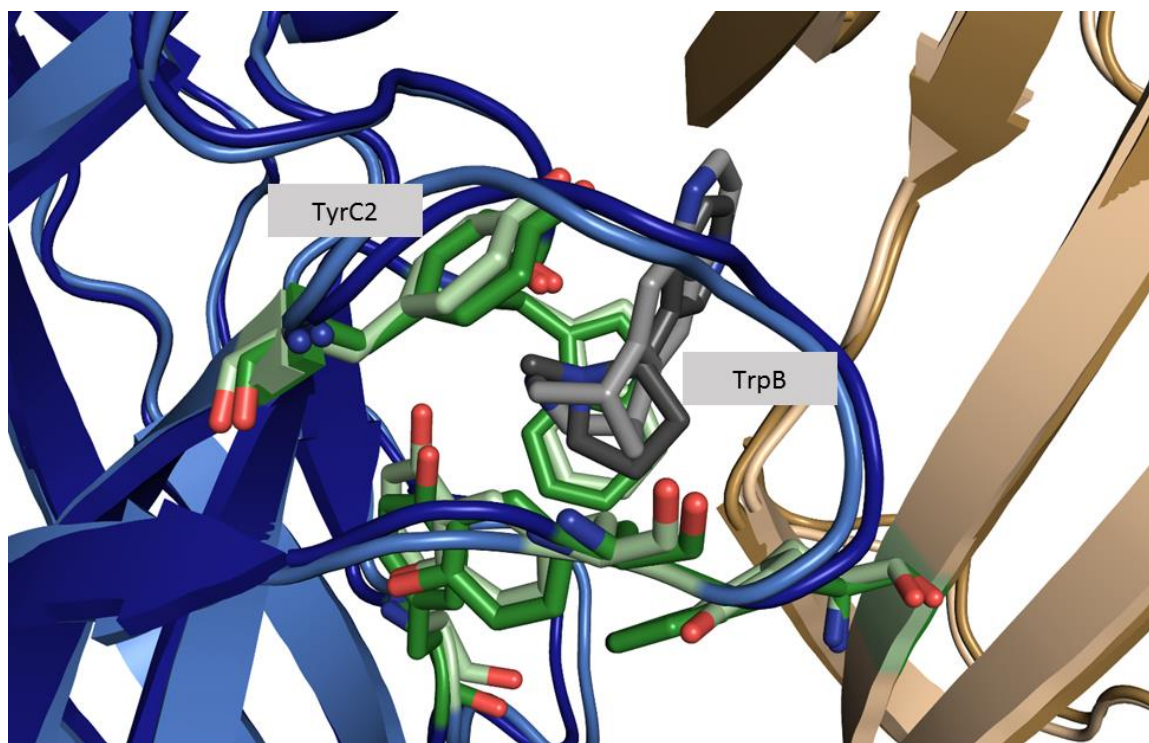


**Figure 10.** Structures of AChBP crystallized with varenicline (lighter shades) and nicotine (darker shades) from PDBs 1UW6 and 4AFT. The primary face is in blue, the complementary face is in tan, and the aromatic box is highlighted in green. Note that neither TrpB nor TyrC2 show any meaningful movement. It is important to note, however, that AChBP only shares 30% identity with the extracellular region of  $\alpha 4\beta 2$  and does not rule out any possible explanations for differences in binding. Structures were aligned with PyMol Molecular Graphics System.

Future studies should investigate the cause of the dual cation- $\pi$  interaction feature of secondary amine agonists described here. They should also determine whether this effect is present in other subtypes such as muscle-type,  $\alpha 7$ , and  $\alpha 6\beta 2$  (though TC299423 was not observed to form a cation- $\pi$  interaction at TyrA or TyrC2). If the dual cation- $\pi$  interaction is unique to  $\alpha 4\beta 2$ , which evidence in this chapter suggests, it may be an intriguing feature to consider when designing subtype-selective agonists. If it proves to be universal, or at least common amongst several subtypes, an important aspect of nAChR function will have been revealed. Either way, this is a new and novel pharmacological phenomenon of a ligand gated ion channel that offers exciting new ways of thinking about ligand-binding.

## 5.6 Materials and Methods

### *Molecular Biology*

Rat  $\alpha 4L9'A$  (described as wild-type and/or  $\alpha 4$  throughout this chapter) and  $\beta 2$  nAChRs were in the pGEMhe vector, a cDNA plasmid optimized for protein expression in *Xenopus* oocytes. Site-directed mutagenesis was performed by PCR using the Stratagene QuikChange protocol and primers ordered from Integrated DNA Technologies (Coralville, IA). Circular cDNA was linearized with SbfI (New England Biolabs, Ipswich, MA) and then transcribed *in vitro* using T7 mMessage mMachine kit (Life Technologies, Santa Clara, CA), with a purification step after each process (Qiagen, Valencia, CA). Final concentrations were quantified by UV spectroscopy.

### *Ion Channel Expression*

*Xenopus laevis* oocytes (stage V to VI) were sourced from both a Caltech facility and Ecocyte Bio Science (Austin, TX). Oocytes were injected with 50 nL solution containing either 5 or 10 ng mRNA, injected in a 1:2 ratio. Cells were incubated 24-48 hours at 18°C in ND96 solution (96 mM NaCl, 2mM KCl, 1 mM MgCl<sub>2</sub>, and 5mM HEPES, pH 7.5) enriched with theophylline, sodium pyruvate, and gentamycine.

### *Non-canonical Amino Acid Incorporation*

The cyanomethylester form of NVOC-protected tryptophan and phenylalanine analogues was coupled to dinucleotide dCA and enzymatically ligated to UAG-suppressor 74-mer THG73 tRNA<sub>CUA</sub> as previously described.<sup>18</sup> The product was verified by MALDI time-of-flight mass spectrometry on a 3-hydroxypicolinic acid matrix. The non-canonical amino acid-coupled tRNA was deprotected by photolysis either on a 500 W Hg/Xe arc lam, filtered with Schott WG-320 and UG-11 filters, or with an M365LP1 365 nm 1150 mW LED lamp (Thor Labs, Newton, NJ) immediately prior to coinjection with mRNA containing the UAG mutation at the site of interest. mRNA and tRNA were typically injected in a 1:1 or 1:2 volume ratio in a total volume of 50 or 75 nL respectively so that 25 ng of mRNA was injected per cell. In cases where observed agonist-induced currents were low after 48 hour incubation – likely due to low receptor protein expression – a second injection of mRNA and tRNA was performed after 24 hours. The fidelity of non-canonical amino acid incorporation was confirmed at Trp with a wild-type recovery experiment where tryptophan was loaded onto tRNA. If this experiment yielded similar to EC<sub>50</sub> to

wild-type then the cell incorporated the charged residue and nothing else. This was accomplished with the Tyr sites by comparing tRNA charged with Phe to a conventional Y-Phe mutation. A read-through/reaminoacylation test served a negative control by injecting unacylated full-length 76-mer tRNA. Lack of current proved no detectable reaminoacylation at the TrpB site.

#### *Whole-Cell Electrophysiological Characterization*

(S)-nornicotine hydrochloride was purchased from Matrix Scientific (Columbia, SC) while varenicline (Pfizer), metanicotine and TC299423 (Targacept) were generous gifts. Agonist-induced currents were recorded in TEVC mode using the OpusXpress 6000A (Molecular Devices, Sunnyvale, CA) at a holding potential of -60 mV in a running buffer of Ca<sup>2+</sup>-free ND96. Agonists were prepared in Ca<sup>2+</sup>-free ND96 and delivered to cells via a 1 mL application over 15 sec followed by a 2 min wash. Data from dose-response experiments were normalized, averaged, and fit to the Hill equation using Kaleidagraph (Synergy Software, Reading PA), though data are visualized here with Prism (GraphPad Software, La Jolla, CA). Error bars are presented as standard error of the mean, while EC<sub>50</sub> and Hill coefficient errors are reported by Kaleidagraph and represent the sum of the squared error between the data and the calculated fit.

## 5.7 References

1. Wall, T. R. Effects of TI-299423 on Neuronal Nicotinic Acetylcholine Receptors. (California Institute of Technology, 2015).
2. Post, M. R., Limapichat, W., Lester, H. A. & Dougherty, D. A. Heterologous expression and nonsense suppression provide insights into agonist behavior at  $\alpha 6\beta 2$  nicotinic acetylcholine receptors. *Neuropharmacology* **97**, 376–382 (2015).
3. Van Arnam, E. B. & Dougherty, D. A. Functional Probes of Drug–Receptor Interactions Implicated by Structural Studies: Cys-Loop Receptors Provide a Fertile Testing Ground. *J. Med. Chem.* **57**, 6289–6300 (2014).
4. Corringer, P.-J., Novère, N. L. & Changeux, J.-P. Nicotinic Receptors at the Amino Acid Level. *Annu. Rev. Pharmacol. Toxicol.* **40**, 431–458 (2000).
5. Xiu, X., Puskar, N. L., Shanata, J. A. P., Lester, H. A. & Dougherty, D. A. Nicotine binding to brain receptors requires a strong cation– $\pi$  interaction. *Nature* **458**, 534–537 (2009).
6. Tavares, X. D. S. *et al.* Variations in Binding Among Several Agonists at Two Stoichiometries of the Neuronal,  $\alpha 4\beta 2$  Nicotinic Receptor. *J. Am. Chem. Soc.* **134**, 11474–11480 (2012).
7. Davis, M. R. & Dougherty, D. A. Cation– $\pi$  interactions: computational analyses of the aromatic box motif and the fluorination strategy for experimental evaluation. *Phys. Chem. Chem. Phys.* **17**, 29262–29270 (2015).
8. Puskar, N. L. Structure-function studies of nicotinic acetylcholine receptors using unnatural amino acids. (California Institute of Technology, 2012).
9. Gotti, C., Zoli, M. & Clementi, F. Brain nicotinic acetylcholine receptors: native subtypes and their relevance. *Trends Pharmacol. Sci.* **27**, 482–491 (2006).
10. Zoli, M., Pistillo, F. & Gotti, C. Diversity of native nicotinic receptor subtypes in mammalian brain. *Neuropharmacology* **96, Part B**, 302–311 (2015).
11. Wilson, K. L., Chang, R. S., Bowman, E. R. & McKennis, H. Nicotine-like actions of cis-metanicotine and trans-metanicotine. *J. Pharmacol. Exp. Ther.* **196**, 685–696 (1976).
12. Damaj, M. I., Patrick, G. S., Creasy, K. R. & Martin, B. R. Pharmacology of Lobeline, A Nicotinic Receptor Ligand. *J. Pharmacol. Exp. Ther.* **282**, 410–419 (1997).
13. Papke, R. L., Webster, J. C., Lippiello, P. M., Bencherif, M. & Francis, M. M. The Activation and Inhibition of Human Nicotinic Acetylcholine Receptor by RJR-2403 Indicate a Selectivity for the  $\alpha 4\beta 2$  Receptor Subtype. *J. Neurochem.* **75**, 204–216 (2000).

14. Blum, A. P., Lester, H. A. & Dougherty, D. A. Nicotinic pharmacophore: The pyridine N of nicotine and carbonyl of acetylcholine hydrogen bond across a subunit interface to a backbone NH. *Proc. Natl. Acad. Sci.* **107**, 13206–13211 (2010).
15. Coe, J. W. *et al.* 3,5-Bicyclic aryl piperidines: a novel class of alpha4beta2 neuronal nicotinic receptor partial agonists for smoking cessation. *Bioorg. Med. Chem. Lett.* **15**, 4889–4897 (2005).
16. Coe, J. W. *et al.* Varenicline: an alpha4beta2 nicotinic receptor partial agonist for smoking cessation. *J. Med. Chem.* **48**, 3474–3477 (2005).
17. Siminszky, B., Gavilano, L., Bowen, S. W. & Dewey, R. E. Conversion of nicotine to nornicotine in *Nicotiana tabacum* is mediated by CYP82E4, a cytochrome P450 monooxygenase. *Proc. Natl. Acad. Sci. U. S. A.* **102**, 14919–14924 (2005).
18. Dougherty, D. A. & Van Arnem, E. B. In Vivo Incorporation of Non-canonical Amino Acids by Using the Chemical Aminoacylation Strategy: A Broadly Applicable Mechanistic Tool. *ChemBioChem* **15**, 1710–1720 (2014).

## Chapter 6: Evaluating a Predicted Interfacial Hydrogen Bond Interaction Across the $\alpha 4$ - $\beta 2$ Interface\*\*

### 6.1 Abstract

Several AChBP crystal structures report a predicted hydrogen bond between the indole NH of TrpB and lobeline, a compound with potential for use as a smoking cessation aid. In  $\alpha 4\beta 2$ , the naphthylalanine (NpAla) substitution used to probe this hydrogen bond interaction yielded inconclusive results for lobeline, but showed an interesting gain-of-function when tested with acetylcholine. One possible explanation for that gain of function is that the indole NH is actually hydrogen bonding with a backbone carbonyl on Loop E and stabilizing the closed state. Thus, when the interaction is eliminated, the state equilibrium shifts more toward the open state and causes a decrease in  $EC_{50}$ . This Loop B-Loop E hydrogen bond was tested using several different double-mutant cycle analysis strategies, made complicated because the carbonyl of interest is associated with a leucine that is followed by two conserved prolines. The only approach taken that worked preserved the Pro-Pro motif and instead substituted Leu119 with trifluoroalanine ( $F_3$ Ala), which due to inductive effects weakens the carbonyl's ability to serve as a hydrogen bond acceptor. After this strategy was validated by both computational and empirical NMR studies, a double mutant cycle was executed using NpAla and  $F_3$ Ala as the two mutants. The double-mutant proved to be additive, with an  $\Omega$  value of 1.7 and a  $\Delta\Delta G$  of -0.3 kcal/mol, thus

---

\*\* Work presented in this chapter was borne out of a wonderful collaboration with Matthew R Davis, who performed all of the computational and NMR studies and contributed to project direction and experimental design.

disproving the hypothesis that the TrpB NH makes a hydrogen bond with a backbone carbonyl on Loop E; however, a useful hydrogen bond probe was developed in the process.

## 6.2 Introduction

Since the first crystal structure of AChBP was published,<sup>1</sup> the number of pLGIC receptors and corresponding homologues in the protein database has increased rapidly.<sup>2,3</sup> These structures offer a wealth of information, and knowing the position and proximity of amino acids in relation to each other allows for predictions to be made about the types of interactions that might influence protein structure and

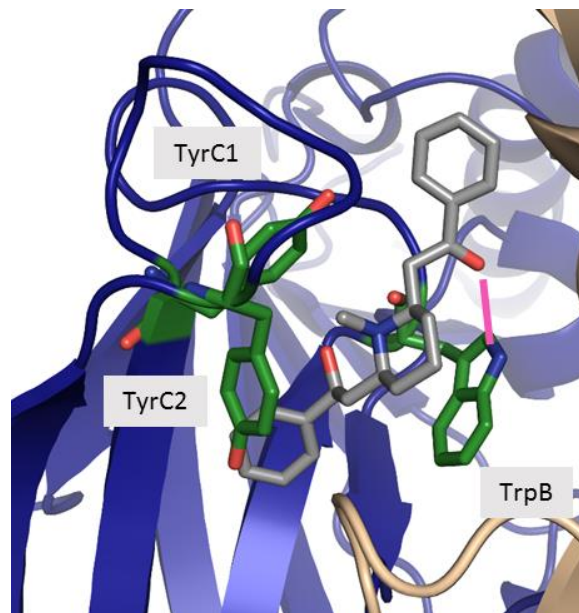


**Figure 1.** Shown above is the crystal structure (PDB: 4AFH) of ct-AChBP bound to lobeline (in gray) that predicts a hydrogen bond between the 2-keto-ethyl group and the indole NH of TrpB (shown in pink).

function. Two of these structures, both of lobeline bound to AChBP from two different organisms, published six years apart, predict a hydrogen bond between lobeline and the indole NH of a tryptophan that would align with TrpB (Figure 1).<sup>4,5</sup> Lobeline is a natural component of Indian tobacco (*Lobelia inflata*) and consists of two phenyl rings linked to a methylated piperidine ring by a 2-keto-ethyl and a 2-hydroxyethyl group. It has been shown to exhibit both agonist and antagonist properties at  $\alpha 4\beta 2$  depending on the concentration.<sup>6</sup> Lobeline has previously been examined as a smoking cessation drug, as well as a possible lead compound for vesicular monoamine transporter ligands.<sup>7,8</sup> Therefore, there is some interest in determining whether these predicted interactions are functionally important in  $\alpha 4\beta 2$ .

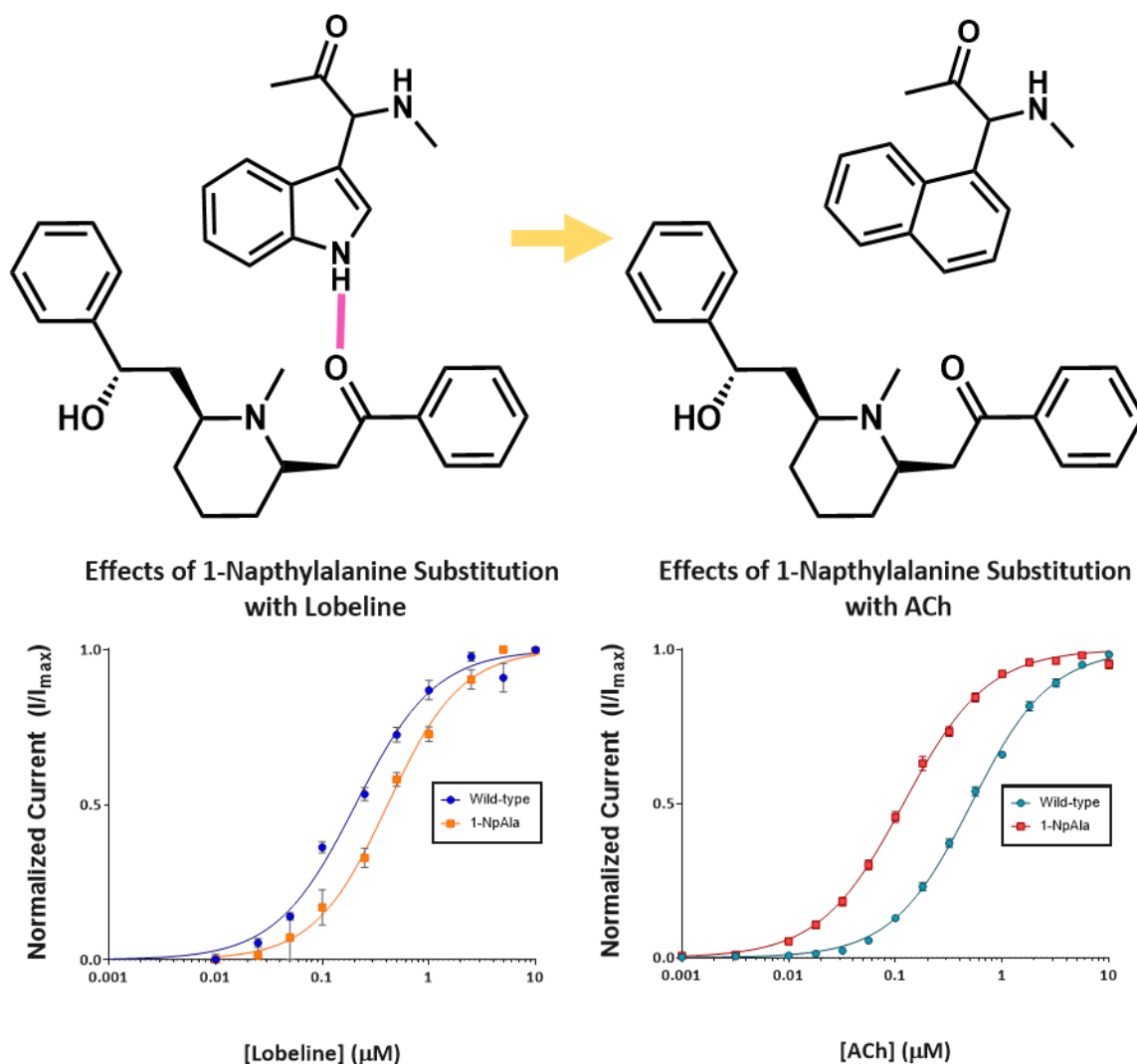


**Figure 2.** A Trp NH hydrogen bond can be probed using 1-naphthylalanine (NpAla), which replaces the indole side chain with a naphthyl ring. Shown below the structural schematic are results from dose response experiments at wild-type and the NpAla with both lobeline and ACh. Note that the agonists experience a shift in  $EC_{50}$  in opposite directions.

To probe for an interaction between the indole NH of a tryptophan and an agonist carbonyl, the simplest structure-function study eliminates the NH all together by substituting the tryptophan of interest with 1-naphthylalanine (NpAla). If the 2-keto-ethyl group of lobeline is indeed making a hydrogen bond with the TrpB in  $\alpha 4\beta 2$ , then upon mutation to NpAla, there should be an increase in  $EC_{50}$ . Instead, the fold-shift in  $EC_{50}$  with lobeline at this mutation is just at the two-fold threshold. Thus, there is likely not a meaningfully important hydrogen bond between lobeline and the indole ring. As a negative

**Table 1.** Investigating hydrogen bonding at TrpB NH

<b>Lobeline</b>	EC50 (uM)	$n_H$	$I_{max}$ (uA)	Fold Shift	N
WT	0.20 ± 0.03	1.2 ± 0.1	0.12 - 0.57	1	10
NpAla	0.40 ± 0.05	1.18 ± 0.03	0.03 - 0.10	2.0	3
<b>ACh</b>	EC50 (uM)	$n_H$	$I_{max}$ (uA)	Fold Shift	N
WT	0.5 ± 0.01	1.19 ± 0.03	4.25 - 30.31	1	10
NpAla	0.11 ± 0.003	1.16 ± 0.03	0.05 - 19.77	0.2	18

control, ACh was also tested at this mutant, which has been previously been explored at the muscle-type nAChR NpAla mutant and shown to have no shift in the  $EC_{50}$ .<sup>9</sup> Interestingly, a different effect was observed with ACh at  $\alpha 4\beta 2$  than either the muscle-type or lobeline experiments yielded, and a five-fold decrease in  $EC_{50}$  was observed. Because ACh is a quaternary amine and cannot form a hydrogen bond, the gain of function shift is likely not due to ligand-binding. Furthermore, gain of function mutations are not commonly encountered when employing non-canonical amino acid mutagenesis in the binding region of pGLIC receptors,<sup>10</sup> and so this NpAla mystery warranted further investigation, as it could potentially reveal important details about  $\alpha 4\beta 2$  function.

Because  $EC_{50}$  is a composite measurement of both binding and gating, if the NpAla gain-of-function result is not due to changes in ligand-binding, it is then likely due to gating. One way to conceptualize nAChR function is through an oversimplified three state model (Figure 3).<sup>11</sup> The first state consists of a closed inactive ion channel and unbound ligand. In the second state, the receptor is bound to ligand, but still in a closed and inactive state. In the third state, the receptor is bound to ligand and open to conduct a flow of positively charged ions. The receptor is in a dynamic equilibrium between the three states, with  $K_d$  serving as the equilibrium constant describing the binding event, and  $\Theta$  serving as the equilibrium constant describing the gating event.  $EC_{50}$  is equal to  $K_d$  divided by  $(1 + \Theta)$ ; therefore if  $K_d$  is unchanged by a mutant, and a decrease in  $EC_{50}$  is observed, that must

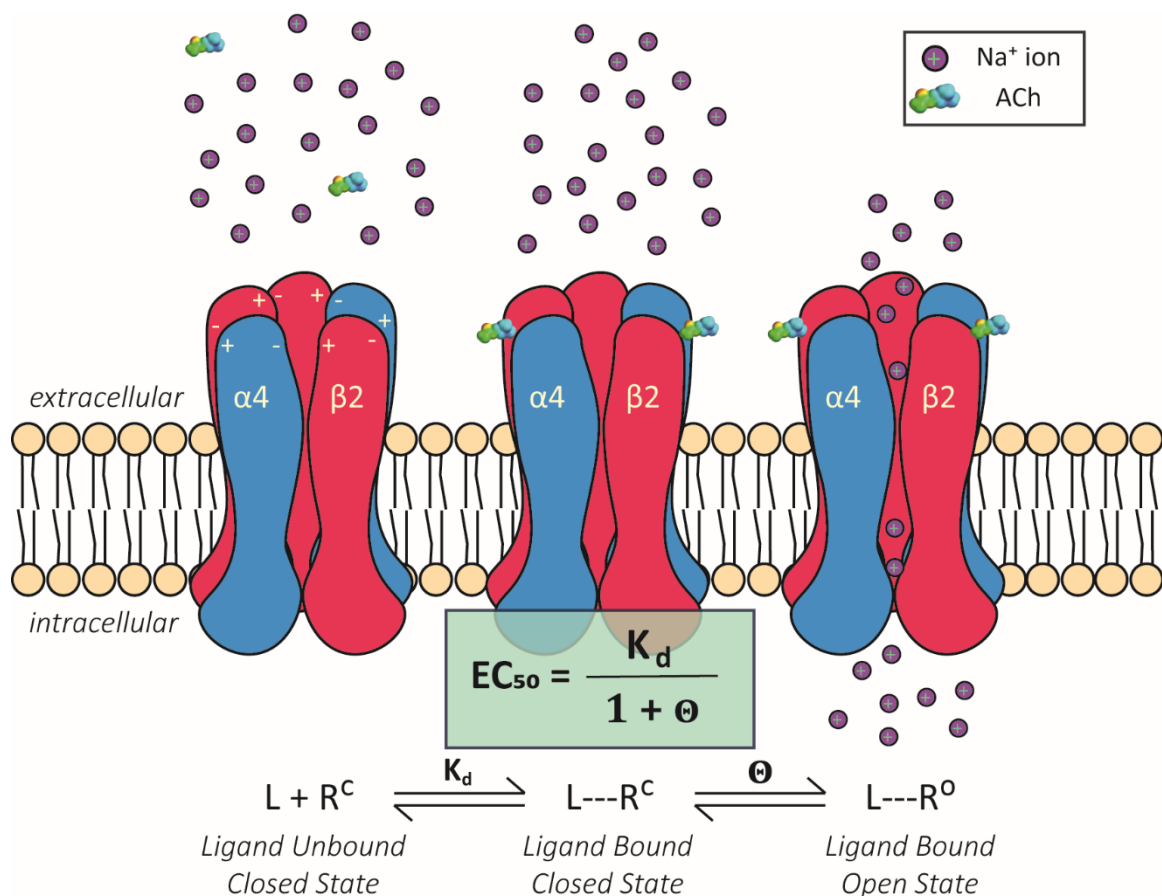


**Figure 3.** This schematic depicts the simple three state model used to describe ligand-gated ion channel function. The receptor, in this case  $\alpha 4\beta 2$  nAChR, is in a dynamic equilibrium among all three. The binding event is characterized by  $K_d$ , while the gating event is characterized by  $\Theta$ .  $EC_{50}$  is a composite measurement taking into account both binding ( $K_d$ ) and gating ( $\Theta$ ).

be due to an increase in  $\Theta$ . Such an increase in  $\Theta$  is then likely to be caused by either a destabilization of the closed ligand-bound state, or a stabilization of the open ligand-bound state.

In the case of the Trp-to-NpAla mutation, a hydrogen bond donor is eliminated, resulting in a five-fold gain of function, and so it seems likely that the resulting decrease in  $EC_{50}$  is due to a destabilization of the closed state. To put this in simpler terms, one possible hypothesis is that the indole NH makes a hydrogen bond with another amino acid, and when that binding interaction is eliminated with NpAla, the closed state is destabilized, and it becomes easier for the receptor to open upon ligand-binding. A greater proportion

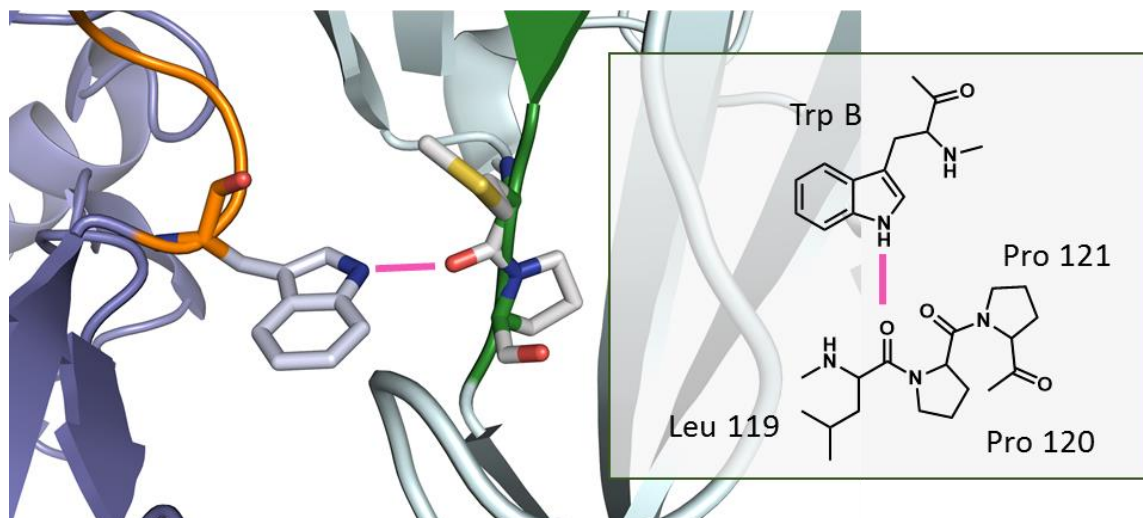


**Figure 4.** This crystal structure (PDB: 1UX2) view predicts a hydrogen bond between Trp149 (on Loop B, in orange) and Leu119 (on Loop E, in green)

of receptors in the open state upon ligand binding means a higher  $\Theta$ , which results in a lower  $EC_{50}$ .

In order to prove this hypothesis, the indole ring's hydrogen bond partner must be identified and confirmed. A crystal structure of AChBP bound to nicotine shows that the TrpB indole ring is in proximity to a carbonyl associated with a leucine on Loop E of the  $\beta 2$  subunit, L119 (Figure 4).<sup>12</sup> If a closed-state-stabilizing hydrogen bond exists between TrpB and another amino acid, it is most likely Leu119. As shown in Chapter 4, a good way to determine whether amino acids participate in a coupled interaction, such as a hydrogen bond, is via a double-mutant cycle analysis. Attenuating or eliminating the hydrogen bond by mutating the TrpB indole NH and the Leu119 carbonyl, both independently and together, will provide the necessary information to determine if this interaction is important, and furthermore, if it is responsible for the gain of function discussed above.

The typical structure-function strategy for attenuating a carbonyl's ability to serve as a hydrogen bond acceptor has been described in Chapter 4 as well. By substituting the  $i + 1$  residue to the carbonyl of interest with an  $\alpha$ -hydroxy acid, the backbone is mutated from an amide to an ester. Because of the loss of resonance when the nitrogen is replaced with an oxygen, the carbonyl becomes a weaker hydrogen bond acceptor, and the binding energy of the interaction decreases. This strategy can theoretically work in any situation as long as the  $i + 1$  residue can be converted to an  $\alpha$ -hydroxy acid. In the Loop B-Loop E hydrogen bond under investigation, herein lies a massive issue: Leu119 is part of a conserved Leu-Pro-Pro motif, and proline  $\alpha$ -hydroxy is not an option.

The primary goal of this chapter is then two-fold – develop a new means of probing for hydrogen bonding for the Leu-Pro-Pro motif, and use this technique to determine whether TrpB makes a closed state-stabilizing hydrogen bond to LeuE. Ultimately, it seems the best approach is to use fluorinated side chains at the same position ( $i + 0$ ) to withdraw electron density away from the carbonyl. Using this method, it is evident that the hydrogen bonding interaction predicted by structure and hypothesized to explain the gain of function seen with NpAla is not actually functionally relevant, and that this mysterious effect requires other rationale.

### **6.3 Strategies to Probe for Hydrogen Bonding at Loop E Leu-Pro-Pro**

The hypothesis being tested is that the reason NpAla causes a gain-of-function response from the receptor is due to a functional hydrogen bond that stabilizes the closed state. Therefore, NpAla is always an element in the cycle. The chief issue to overcome is attenuating the hydrogen bonding ability of the LeuE carbonyl, since the  $i + 1$  residue is a proline and cannot be simply mutated to an  $\alpha$ -hydroxy acid. Thus, each of the following

strategies follow a similar road map. They all propose a double-mutant cycle analysis where the first mutant substitutes TrpB with NpAla, and the second mutant attenuates the ability of the LeuE carbonyl to form a strong hydrogen bond using methods beyond what have already been established. If the hypothesis is correct, then attenuating that carbonyl should also result in a gain of function; however, the double mutant cycle analysis ensures those fold-shifts are due to this specific proposed hydrogen bond, and not extraneous effects.

### 6.3.1 The $\delta$ -amino acid Strategy

The first approach taken to determine if Loop B and Loop E make an interfacial hydrogen bond was also conceptually and practically the most complicated. Because the Leu-Pro-Pro motif is so well conserved (the vicinal di-proline is found in almost every nAChR subunit from almost every organism in which the gene has been cloned), a strategy was conceived that retained both side chains while eliminating the carbonyl all together.

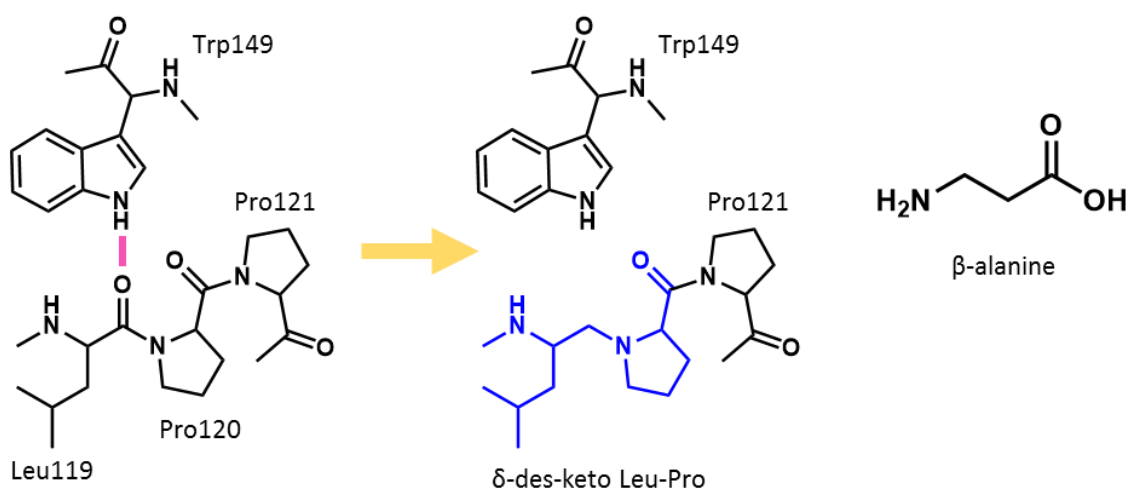


**Figure 5.** The proposed hydrogen bond that is stabilizing the closed state is between the indole NH of Trp149 (Trp B) and Leu119 (of Loop E). Typically an  $\alpha$ -hydroxy acid at the  $i + 1$  position would be used to attenuate the hydrogen bond, but in this case that position is occupied by a highly conserved proline. The strategy depicted here proposes a  $\delta$ -amino acid containing the Leu and Pro side chains but lacking a carbonyl group. This idea was quickly demonstrated to be impossible when the ribosome was unable to insert  $\beta$ -alanine at even the most promiscuous sites.

However, replacing the carbonyl with a methylene group would also destroy the peptide bond and require the incorporation of a  $\delta$  amino in place of Leu119 and Pro120 (Figure 5).

It was unclear, and perhaps unlikely, that the oocyte ribosome (or any ribosome for that matter) would be able to incorporate an amino acid with an extended backbone, let alone a  $\delta$ -amino acid with two relatively bulky side chains. Therefore, initial nonsense suppression experiments tested  $\beta$ -alanine, a  $\beta$ -amino acid with no side chain structurally more similar to glycine than alanine. The appropriate dCA- $\beta$ -alanine was synthesized and ligated to THG73 and then tested at various glycine sites in the muscle-type nAChR. These tests either resulted in no functional expression or in observed agonist-induced currents at both  $\beta$ -alanine and 76mer control conditions. These results suggested that not even a  $\beta$ -amino acid could make it through the translation machinery, and further attempts to incorporate the Leu-Pro  $\delta$ -amino acid were subsequently abandoned in favor of simpler approaches.

### 6.3.2 *The Gly-Gah Strategy*

After attempting such a shoot-the-moon strategy, in deference to Occam's razor, the perhaps simplest approach was attempted next. Here, any potential importance of the conserved vicinal di-proline motif was disregarded, and a double mutant cycle was designed where Pro120 is first mutated to a glycine. The P120Gly mutant would then serve as the cycle's "wild-type" and provide a baseline for calculating the single- and double-mutant fold shifts in  $EC_{50}$ . In this analysis, the first single-mutant consists of the NpAla substitution at TrpB in the  $\alpha 4$  subunit and the P120Gly mutation in the  $\beta 2$  subunit. The other single-mutant is a glycine to glycine  $\alpha$ -hydroxy (Gah) mutation in the  $\beta 2$  subunit. Since P120Gly is  $i + 1$  to Leu119, a Gah substitution causes an amide-ester backbone

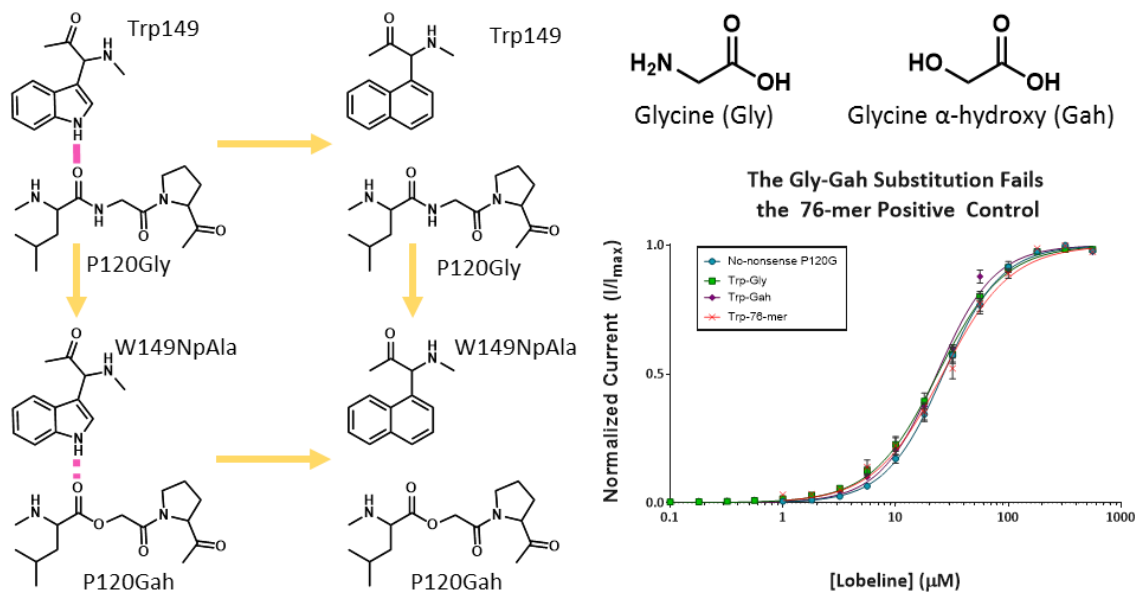


**Figure 6.** On the left is the proposed double mutant cycle using a P120Gly mutant as the “wild-type” and Gah and NpAla as the single-mutants. This strategy failed as the 76-mer control had the same exact  $EC_{50}$  as the conventional P120G mutant as shown by the overlapping dose response curves. Above the plot are the structures of Gly and Gah.

mutation, and makes the carbonyl of interest a weaker hydrogen bond acceptor. If the predicted hydrogen bond is present, this mutation should be accompanied with a decrease in  $EC_{50}$ . Finally, the  $EC_{50}$  of a NpAla-L119 double-mutant is evaluated for additivity. If the Gly-Gah mutation alone causes a gain of function, and the cycle shows an  $\Omega$  value other than one, the closed-state hypothesis would be proven correct.

The double-mutant in this case requires incorporation of two different non-canonical amino acids in two different protein chains – NpAla in  $\alpha 4$  and Gah in  $\beta 2$ . Double- and triple-incorporations have previously been reported in the muscle-type nAChR. In one example, two adjacent residues in the  $\alpha 1$  subunit were substituted using nonsense suppression, with the codon of Phe135 mutated to TAG and Pro136 to TGA (a TAA stop codon was used to terminate translation).<sup>13</sup> Two different suppressor tRNAs, THG73 (UAG) and TQOPS' (UGA), were then used to incorporate a different non-

**Table 2.** Investigating an Interfacial Hydrogen Bond with a Gly-Gah Mutant Cycle

$\alpha 4\beta 2$	W149	P120	EC <sub>50</sub> ( $\mu$ M)	n <sub>H</sub>	I <sub>max</sub> ( $\mu$ A)	Fold Shift	N
WT	Trp	Gly	31.7 $\pm$ 0.8	1.49 $\pm$ 0.04	2.13 - 18.41	1	13
Mut1	NpAla	Gly	9 $\pm$ 0.3	1.34 $\pm$ 0.05	0.04 - 0.53	0.3	14
Mut2	Trp	Gah	23.3 $\pm$ 0.8	1.69 $\pm$ 0.09	0.68 - 9.59	0.7	6
Mut1,2	NpAla	Gah	9 $\pm$ 1	1.09 $\pm$ 0.13	0.17 - 0.33	0.3	2
						$\Omega$	1.4
						$\Delta\Delta G$ (kcal/mol)	-0.2

canonical amino acid at each site. In the other example, a different non-canonical amino acid was simultaneously incorporated into each of the  $\alpha 1$ ,  $\beta 1$ , and  $\delta$  subunits using both nonsense suppression and frameshift suppression.<sup>14</sup> Both strategies proved to be quite effective, though it was not certain that either would work in a neuronal subtype.

In the Gly-Gah double-mutant studies,  $\alpha 4$  Trp149 was mutated to a TAG stop codon and suppressed with THG73 tRNA, and  $\beta 2$  Leu119 was mutated to a TGA stop codon and suppressed with TQOPS' tRNA. The TQOPS' suppressor tRNA has an added benefit of being less likely to get reaminoacylated with endogenous amino acid.<sup>15</sup> This characteristic is important, as sites on Loop E are often quite promiscuous in that they can tolerate a wide range of amino acid substitutions, and they are therefore more likely to have an issue with reaminoacylation.

In the case of this current study, that issue proved to be fatal for the Gly-Gah strategy. All four scenarios of the double mutant cycle analysis showed high currents and monophasic dose response curves. The Trp-Gly and Trp-Gah EC<sub>50</sub> values were not meaningfully different, the NpAla cases showed the same five-fold decrease in EC<sub>50</sub>, and no changes were observed between the Gly-NpAla and Gah-NpAla mutation. These results would have proven that no hydrogen bond exists – the calculated  $\Omega$  value only results in a  $\Delta\Delta G$  of 0.2 kcal/mol. However, the critical reaminoacylation positive control failed. The

dose response curve that was generated from injecting both Trp-bound THG73 and 76-mer TQOPS' (full length, but non-acylated) alongside the double stop codon mutant mRNA were identical to the Trp-Gly and Trp-Gah experiments. Additionally, a no-nonsense experiment using wild-type  $\alpha 4$  and conventionally mutated P120G  $\beta 2$  had a dose response curve that overlapped perfectly with the previous two conditions (Figure 6).

The endogenous amino acid found to reacylate both THG73 and TQOPS' is glutamine,<sup>16</sup> which suggests that Pro120 can tolerate mutation to both glycine and glutamine, and that both substitutions have the same effect on  $EC_{50}$ . That in and of itself might be interesting, but for the purposes of identifying and confirming an interfacial hydrogen bond between TrpB and Leu119, the Gly-Gah double mutant strategy is not viable.

### 6.3.3 The Fluorination Strategy

Clearly, the vicinal di-proline of the conserved Leu-Pro-Pro motif is important for protein function and should not be manipulated. Taking this into account, the next strategy attempts to attenuate the hydrogen bond accepting ability of the carbonyl from the other side; that is, by mutating the actual residue associated with the carbonyl. The goal here is to attenuate the hydrogen bond interaction without affecting the protein backbone. No matter the approach, the electronegativity of the carbonyl oxygen needs to be decreased. On first principles, adding electron-withdrawing groups in close proximity to the carbonyl group can potentially cause such an effect. Adding electron-withdrawing substituents like

**Table 3.** Conventional Mutagenesis Results at  $\beta 2$  L119

$\alpha 4\beta 2$	$EC_{50}$ ( $\mu M$ )	$n_H$	$I_{max}$ ( $\mu A$ )	N
WT	$0.50 \pm 0.01$	$1.19 \pm 0.03$	4.24 - 30.31	10
L119A	$1.49 \pm 0.08$	$1.21 \pm 0.06$	3.05 - 15.98	11
L119V	$1.73 \pm 0.06$	$1.12 \pm 0.03$	5.93 - 26.20	11

fluorine at the  $\alpha$ -carbon runs the risk of causing an elimination reaction forming an imino acid. However,  $\beta$ - and  $\gamma$ - substituted trifluoro groups should still have an inductive attenuating effect while avoiding potential elimination reactions.

Leucine has a  $\beta$ -carbon methylene group that could possibly be fluorinated, but using trifluoroalanine (F<sub>3</sub>Ala) and hexafluorovaline (F<sub>6</sub>Val) provided an approach with more electron withdrawing atoms and less challenging synthetic routes. The fluorination strategy for probing a Loop B-Loop E interfacial hydrogen bond thus employs a double-mutant cycle analysis that substitutes these fluorinated amino acids at Leu119 as one of the single-mutants. Of course this requires using the L119Ala or L119Val mutants as the cycle's "wild-type" reference. Conventional mutagenesis shows the receptor experiences a roughly 3-fold gain in EC<sub>50</sub> with both the Ala and Val mutations, a modest loss of function that should not create problems for the double-mutant cycle (Table 3). As per other proposed cycles, the TrpB NpAla mutation serves as the second mutation. A NpAla-F<sub>3</sub>Ala or NpAla-F<sub>6</sub>Val double-mutant would then serve as a way to measure additivity and confirm the presence of a functional hydrogen bond between these two residues.

Initial experiments show that nonsense suppression is possible at both sites simultaneously. In these wild-type recovery tests, well-behaved large current traces are observed with monophasic dose response curves. A 76-mer ne control experiment does not result in functional expression at the Trp149 site, but does show large agonist-induced currents at L119. The latter, however, produces a dose response curve that never turns over as the ACh concentration approaches 1000  $\mu$ M. While these initial results are promising, this method of attenuating the hydrogen bond is new, and relies on first principles. In order to be certain any results from the double-mutant cycle are meaningful,

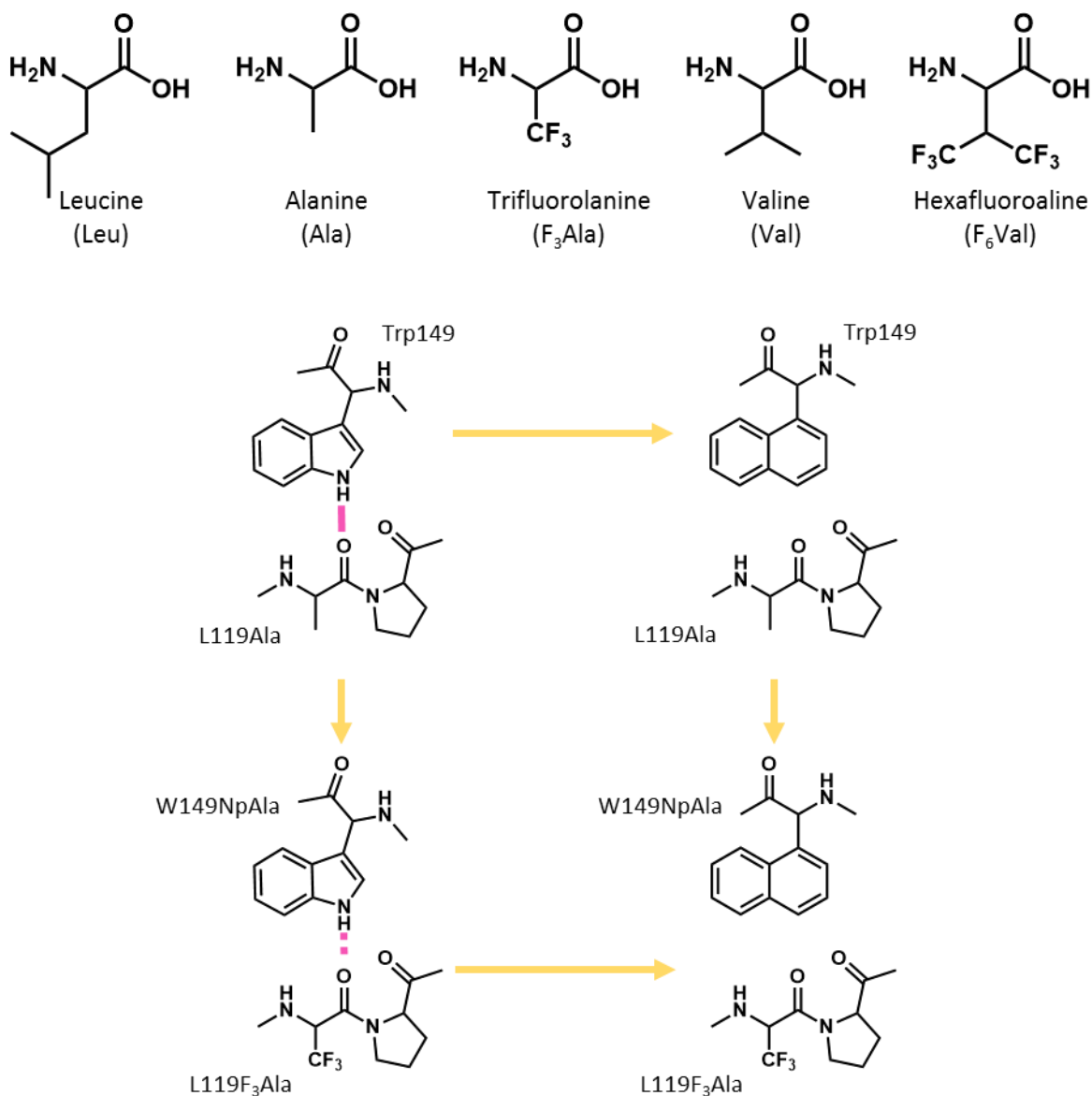


**Figure 7.** Above are structures of all the amino acids proposed to be used in the fluorination strategy for probing indole NH – backbone carbonyl hydrogen bonds in across the  $\alpha 4$ - $\beta 2$  interface. Below is an example of the type of double mutant cycle that could be conducted using NpAla and F<sub>3</sub>Ala.

the fluoro-analogues must be tested to ensure they are causing the desired effect. This will be done through computational as well as NMR-based studies. If these analyses prove that F<sub>3</sub>Ala and F<sub>6</sub>Val are an appropriate strategy, then data from the double-mutant cycle analysis can be collected and used to prove the closed-state hypothesis described above.

## 6.4 Computational and Experimental Support for the Fluorination Strategy

### 6.4.1 Electrostatic Potential Maps to Predict Hydrogen Bonding Attenuation

The hydrogen bond, such as the Loop B-Loop E interaction in question, is inherently electrostatic in nature, with the partial positive charge of the hydrogen making a stabilizing interaction with the partial negative charge of the hydrogen bond acceptor. This phenomenon can be described by the equation  $\log(K) = c_1\alpha_2^H\beta_2^H + c_2$  where  $K$  is an association constant,  $c_1$  and  $c_2$  are solvent-dependent constants, and  $\alpha_2^H$  and  $\beta_2^H$  are constants that characterize the properties of the hydrogen bond donor and acceptors respectively.<sup>17</sup>

This relationship can then be rearranged to determine the energetic cost of a hydrogen bond donor switching from interacting with solvent to the hydrogen bond acceptor.<sup>18</sup> Doing so is akin to predicting the free energy of the hydrogen-bonding interaction ( $\Delta\Delta G_{\text{H-bond}}$ ), and using the equation  $\Delta\Delta G_{\text{H-bond}} = -(\alpha - \alpha_s)(\beta - \beta_s)$  will allow will allow for the calculation of a hydrogen bond in any solvent provided once these four variables are known, as described by Hunter. All of these parameters can be derived from empirically determined  $\alpha_2^H$  and  $\beta_2^H$ ; however, the dimensionless  $\alpha$  and  $\beta$  values also correspond to the  $E_{\text{max}}$  and  $E_{\text{min}}$  of electrostatic potential maps determined by density functional theory. The solvent parameters,  $\alpha_s$  and  $\beta_s$  follow the same characteristics, but their values have been determined and reported for almost all solvents commonly used in the laboratory.

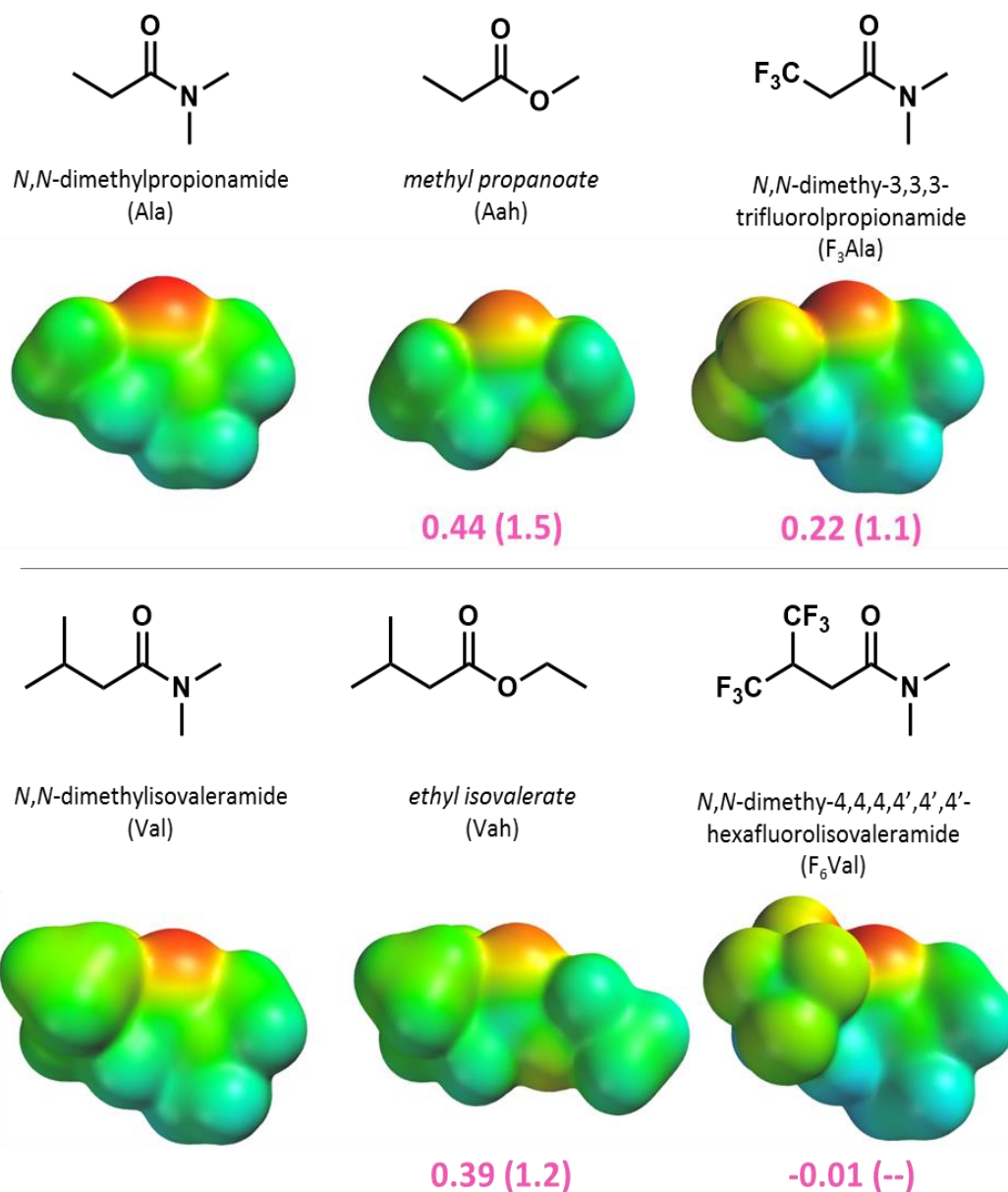


**Figure 8.** Shown are structures and electrostatic potential maps (where red is negative and blue is positive) for each compound analyzed by computational methods and NMR experiments with their corresponding amino acid in parentheses. Below each electrostatic potential map in pink are the theoretical shifts in binding energy in kcal/mol with the empirical NMR result in parentheses.

**Table 4.** Results from Computational Electrostatic Potential Map Hydrogen Bond Prediction Studies

	$E_{\min/\max}$ (kJ/mol)	$\alpha$ or $\beta$ *	$\Delta\Delta G_{\text{H-bond}}$ (kcal/mol)					
			<i>Water</i>	<i>Hexanes</i>	<i>CCl<sub>4</sub></i>	<i>DMSO</i>	<i>Acetonitrile</i>	<i>DMF</i>
<b>Indole</b>	236.8	4.5						
<b>EtAc</b>	175.4	3.4	0.5	-3.1	-2.1	2.1	0.9	0.9
<b>Ala</b>	205.7	4	0.2	-3.6	-2.5	1.8	0.5	0.5
<b>Aah</b>	175.3	3.4	0.5	-3.1	-2.1	2.1	0.9	0.9
<b><math>F_3</math>Ala</b>	191.1	3.7	0.3	-3.3	-2.3	1.9	0.7	0.7
<b>Val</b>	191.5	3.7	0.3	-3.4	-2.3	1.9	0.7	0.7
<b>Vah</b>	164.5	3.2	0.6	-2.8	-1.9	2.1	1.0	1.1
<b><math>F_6</math>Val</b>	192.4	3.7	0.3	-3.4	-2.3	1.9	0.7	0.7

\*  $\alpha$  is calculated for hydrogen bond donors like indole using  $E_{\max}$  and  $\beta$  for hydrogen bond acceptors using  $E_{\min}$

Thus, the theoretical hydrogen bond strength between an amino acid (or an  $\alpha$ -hydroxy acid) and an indole NH can be determined by generating electrostatic potential maps for each molecule and finding the  $E_{\max}$  or  $E_{\min}$  (depending on whether it is a donor or acceptor, respectively). These energy values are then divided by a correction factor of 52 kJ/mol to determine the unitless  $\alpha$  and  $\beta$  values. Finally, depending on the solvent of interest,  $\Delta\Delta G_{\text{H-bond}}$  can then be calculated based on the equation above.

The specific compounds used in these calculations were the same used in the NMR studies detailed in the following subsection. Each compound, except ethyl acetate which serves as a control and indole which is the hydrogen bond donor, is an analogue for the amino acids proposed in the fluorination strategy double-mutant cycle analysis. For each compound, an electrostatic potential map was generated via an M06 density functional theory calculation using a 6-31G(d,p) basis set. The  $E_{\max}$  for indole and  $E_{\min}$  for the amino/hydroxy acid analogues were then determined and used to calculate  $\alpha$  and  $\beta$ , ultimately leading to  $\Delta\Delta G_{\text{H-bond}}$  values for various solvents.

Because the penultimate read-out in a double-mutant cycle analysis is a fold-shift in  $EC_{50}$ , the value of interest in these calculations is the relative shift in  $\Delta\Delta G_{\text{H-bond}}$  from the wild-type amino acid to the non-canonical residue, i.e.  $\Delta\Delta G_{\text{H-bond}}(\text{non-canonical}) - \Delta\Delta G_{\text{H-bond}}(\text{wild-type})$ . Thus, the choice of solvent is slightly arbitrary as long as it remains consistent in each calculation. The theoretical  $\Delta\Delta G_{\text{H-bond}}$  values are reported in Table 4 for a wide array of solvents, though carbon tetrachloride was ultimately used to determine shifts in  $\Delta\Delta G_{\text{H-bond}}$ , given in Figure 8. For the  $F_3\text{Ala}$  analogue, the calculated shift in  $\Delta\Delta G_{\text{H-bond}}$  was determined to be 0.22 kcal/mol, about half as attenuating as alanine  $\alpha$ -hydroxy (Aah). There was no meaningful calculated shift in  $\Delta\Delta G_{\text{H-bond}}$  of  $F_6\text{Val}$  compared to Val,

with a value of -0.01 kcal/mol. Valine  $\alpha$ -hydroxy (Vah), on the other hand, showed a shift in  $\Delta\Delta G_{\text{H-bond}}$  of 0.39 kcal/mol. The lack of theoretical hydrogen bond attenuation in F<sub>6</sub>Val is likely due to the weak or nonexistent inductive effects of adding electron-withdrawing groups to the  $\gamma$ -carbon. While these values seem lower than intuition would suggest, these computational studies show that relative to Aah, F<sub>3</sub>Ala is still a promising option for probing hydrogen bonds when the  $i + 1$  residue cannot be mutated to an  $\alpha$ -hydroxy acid. Furthermore, F<sub>6</sub>Val can serve as a valuable negative control, as it adds electron withdrawing fluorine atoms to the side chain without affecting the hydrogen bond.

#### 6.4.2 Evaluating F<sub>3</sub>Ala with <sup>19</sup>F-NMR

Although the previously discussed computational studies show that F<sub>3</sub>Ala is likely a useful non-canonical amino acid for perturbing hydrogen bonds, empirical evidence would make this claim stronger. A 1969 paper by Gurka and Taft reports that the formation constant of the hydrogen bond,  $K_f$ , can be calculated experimentally through <sup>19</sup>F-NMR.<sup>19</sup> In this experiment, the <sup>19</sup>F chemical shift of *p*-fluorophenol is monitored as a hydrogen bond acceptor is added to solution and a donor-acceptor complex is formed. The fluorophenol serves as the hydrogen bond donor, and as the equilibrium of fluorophenol and acceptor moves more toward towards donor-acceptor complex, i.e. as the concentration of acceptor is increased, the chemical shift of the fluorine will move upfield. This study also showed empirically that  $K_f$  follows a van't Hoff relationship and can be used to determine the  $\Delta G$  of the hydrogen bond interaction. Precise and accurate  $K_f$  measurements can be made provided concentrations of the fluorophenol are kept low and that the acceptor-donor ratio does not exceed 1:1. Furthermore, to account for instrument variations and other substituent effects, a 0.01 M solution of *p*-fluoroanisole is used as an

internal reference, with changes in chemical shift reported as  $\delta$  ( $p$ -fluoroanisole) –  $\delta$  ( $p$ -fluorophenol).

Using this strategy, a dose-response experiment of sorts was conducted by incrementally increasing the concentration of hydrogen bond acceptor in a carbon tetrachloride solution containing 0.01 M  $p$ -fluorophenol and  $p$ -fluoroanisole. As concentration of the acceptor was increased, the  $^{19}\text{F}$  chemical shift of both the  $p$ -fluorophenol and  $p$ -fluoroanisole was monitored, until a 1:1 phenol-acceptor ratio was achieved. The changes in chemical shift follow a sigmoidal shape, with the maximum shift

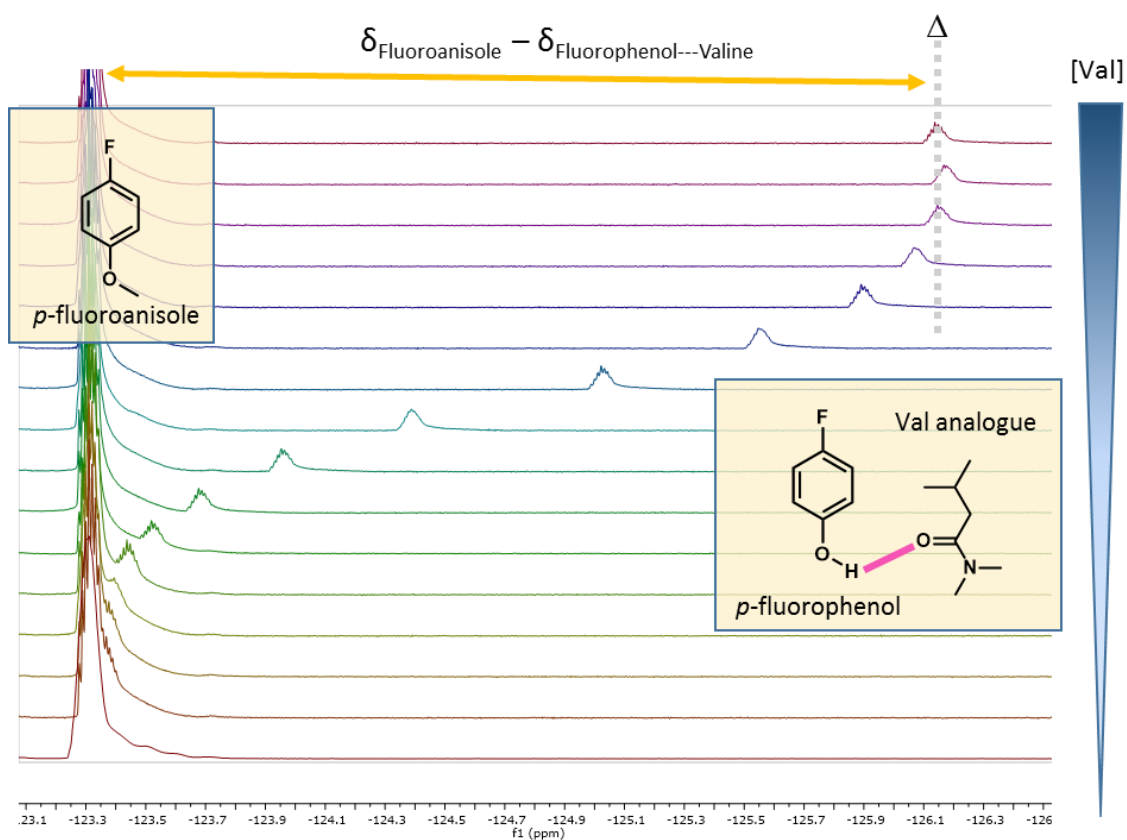


**Figure 9.** Pictured here is a stack of  $^{19}\text{F}$ -NMR spectra over a range of concentrations of  $N,N$ -dimethylvaleramide, an analogue of Val. As  $[\text{Val}]$  increases, more  $p$ -fluorophenol is in a hydrogen bond complex which causes the peak to shift downfield. Eventually this effect levels off, yielding a  $\Delta$  value that along with  $\delta$ , the shift in ppm relative to  $p$ -fluoroanisole, and the concentration of Val analogue can be used to find  $K_f$ .

denoted as  $\Delta$ . A  $K_f$  value can be determined for each point along the rise of the sigmoidal curve using the equation,

$$K_f = \frac{[p\text{-fluorophenol}]_o (\delta/\Delta)}{[p\text{-fluorophenol}]_o(1 - (\delta/\Delta))([\text{acceptor}]_o - [p\text{-fluorophenol}]_o(\delta/\Delta))},$$

where  $[X]_o$  is the concentration of each hydrogen bonding partner and  $(\delta/\Delta)$  is the chemical shift of fluorophenol relative to fluoroanisole at that specific concentration of acceptor divided by the maximum shift observed.

The compounds chosen for this experiment are analogues to the conventional, fluorinated, and  $\alpha$ -hydroxy forms of the amino acids used in the proposed double-mutant cycles (except the F<sub>6</sub>Val analogue, which did not show attenuating ability in the computational studies) and are shown in Figure 8. These analogues were designed to eliminate the amino/hydroxy acid hydrogen bond donor moieties that would complicate any results without changing the electrostatic nature of the carbonyl group. For example, *N,N*-dimethylpropionamide serves as a model compound for alanine as it has a methyl group coming off of the  $\alpha$ -carbon and an amide bond. The  $\alpha$ -hydroxy acids are modeled as esters, and the fluorinated analogues have the appropriate fluorination pattern on the  $\alpha$ -carbon “side chain.” For each compound,  $K_f$  was determined at multiple concentrations and averaged.

A representative set of <sup>19</sup>F-NMR spectra for these experiments is shown in Figure 9 for *N,N*-dimethylisovaleramide (Val), while  $K_f$  results and corresponding  $\Delta G$  values are reported in Table 5. Using these values the overall  $\Delta\Delta G$  of the mutation can be determined using the equation  $\Delta\Delta G_{\text{mutation}} = \Delta G (\text{non-canonical}) - \Delta G (\text{wild-type})$ . Overall, these experiments show that an Ala-Aah mutation causes a 1.48 kcal/mol loss in binding energy,

Ala-F<sub>3</sub>Ala a 1.12 kcal/mol loss, and Val-Vah a 1.20 kcal/mol loss. These results fall in a more reasonable range than the computational study but still follow the same trends overall as shown in Figure 8. They definitively show that

an F<sub>3</sub>Ala substitution is a solid strategy for attenuating the predicted hydrogen bond at the  $\alpha$ 4- $\beta$ 2 nAChR interface. Additionally, the oft-used  $\alpha$ -hydroxy attenuation strategy is further bolstered by these studies.

## 6.5 Double-Mutant Cycle Results

With the proposed fluorination strategy now grounded in theory and experiment, the results from a double mutant cycle analysis utilizing F<sub>3</sub>Ala can be meaningfully interpreted. Thus, dose response experiments were conducted on receptors expressing the following THG73-TQOPS' combinations to make up the mutant cycle: Trp-Ala as the wild-type, NpAla-Ala as the first single-mutant, Trp-F<sub>3</sub>Ala as the second single-mutant, and NpAla-F<sub>3</sub>Ala as the double mutant. Results from this cycle (Table 6) show that F<sub>3</sub>Ala has no effect on EC<sub>50</sub>. The Trp-Ala and Trp-F<sub>3</sub>Ala EC<sub>50</sub> values are both around 2  $\mu$ M, and the NpAla-Ala and NpAla-F<sub>3</sub>Ala EC<sub>50</sub> values are not meaningfully different. The  $\Omega$  value

**Table 5.** Results from Empirical <sup>19</sup>F-NMR Hydrogen Bonding Studies

	$K_f$	$\Delta G_{\text{H-bond}}$	N
<b>EtAc</b>	18.3 ± 0.3	-1.7 ± 0.1	5
<b>Ala</b>	214 ± 6	-3.2 ± 0.7	4
<b>Aah</b>	17.5 ± 0.3	-1.7 ± 0.1	4
<b>F<sub>3</sub>Ala</b>	32.6 ± 0.9	-2.1 ± 0.2	4
<b>Val</b>	113 ± 3	-2.8 ± -0.5	5
<b>Vah</b>	13.9 ± 0.9	-1.6 ± -0.2	5

**Table 6.** Investigating an Interfacial Hydrogen Bond with a F<sub>3</sub>Ala Mutant Cycle

$\alpha$ 4 $\beta$ 2	W149	P120	EC <sub>50</sub> ( $\mu$ M)	n <sub>H</sub>	I <sub>max</sub> ( $\mu$ A)	Fold Shift	N
WT	Trp	Ala	2.18 ± 0.06	1.15 ± 0.03	0.23 - 1.87	1	10
Mut1	NpAla	Ala	0.388 ± 0.008	1.15 ± 0.02	0.35 - 9.92	0.2	14
Mut2	Trp	F <sub>3</sub> Ala	2.0 ± 0.2	0.75 ± 0.03	0.05 - 1.75	0.9	11
Mut1,2	NpAla	F <sub>3</sub> Ala	0.62 ± 0.02	0.8 ± 0.02	0.09 - 0.82	0.3	14
						$\Omega$	1.7
						$\Delta\Delta G$ (kcal/mol)	-0.3

**Table 7.** F<sub>6</sub>Val Double Mutant Cycle Negative Control for Interfacial Hydrogen Bond Studies

<b><math>\alpha 4\beta 2</math></b>	W149	P120	EC <sub>50</sub> ( $\mu$ M)	n <sub>H</sub>	I <sub>max</sub> ( $\mu$ A)	Fold Shift	N	
WT	Trp	Val	2.08 $\pm$ 0.07	1.2 $\pm$ 0.04	0.13 - 5.54	1	15	
Mut1	NpAla	Val	0.65 $\pm$ 0.01	1.16 $\pm$ 0.02	1.25 - 6.36	0.3	13	
Mut2	Trp	F <sub>6</sub> Val	2.1 $\pm$ 0.2	0.78 $\pm$ 0.03	0.07 - 29.91	1.0	13	
Mut1,2	NpAla	F <sub>6</sub> Val	1.22 $\pm$ 0.08	0.77 $\pm$ 0.02	0.11 - 1.96	0.6	11	
							<b><math>\Omega</math></b>	<b>1.9</b>
							<b><math>\Delta\Delta G</math> (kcal/mol)</b>	<b>-0.4</b>

calculated from the F<sub>3</sub>Ala cycle analysis is 1.7, leading to a calculated  $\Delta\Delta G$  of around -0.3 kcal/mol.

A valine-based mutant cycle was then conducted as a negative control, since F<sub>6</sub>Val was predicted computationally to have no effect on hydrogen bonding ability. Results for this cycle (which are reported in Table 7) show a similar effect, with Trp-Val and Trp-F<sub>6</sub>Val having similar EC<sub>50</sub> values about 3- to 2-fold greater than NpAla-Val and NpAla-F<sub>6</sub>Val. These values lead to an  $\Omega$  value of 1.4 and a  $\Delta\Delta G$  of -0.2 kcal/mol, results that are not that different from the alanine cycle.

The results from the alanine cycle alone are not large enough to suggest that a functional indole-backbone carbonyl hydrogen bond exists here. However, the evidence is even stronger when taking into account that the alanine cycle results are not meaningfully different from the negative control valine results. If the valine cycle  $\Delta\Delta G$  value is treated as a baseline, the alanine cycle then has an adjusted  $\Delta\Delta G$  of -0.1 kcal/mol. Remember that weak hydrogen bonds, like those typically found inside a protein, are typically on the order of 0.5 – 1.5 kcal/mol,<sup>20</sup> and that the hydrogen bond between nicotine and a backbone carbonyl on Loop B was determined to be around 2.5 kcal/mol in strength (Chapter 4). Furthermore, the NMR studies presented in this chapter predicted the hit from attenuating the hydrogen bond between an alanine and indole with F<sub>3</sub>Ala to be worth 1.12 kcal/mol.

That the adjusted  $\Delta\Delta G$  from double-mutant cycles is only 0.1 kcal/mol heavily suggests the initial hypothesis that a Loop B-Loop E interfacial hydrogen bond somehow stabilizes the closed state is wrong, and that the gain of function observed with the TrpB to NpAla mutation is due to some other effect.

## 6.6 Studies with 3-Benzothiophene

Though the specific cause remains unclear for the gain of function observed when mutating the TrpB indole ring into a naphthyl ring, it can be said with some certainty that the shift is not due to disrupting a TrpB hydrogen bond with the Leu119 carbonyl on Loop E. It could be quite possible the gain of function has nothing to do with a hydrogen bond at all, that the change in  $EC_{50}$  could be due to another perturbation in the binding pocket caused by NpAla. One way to address this question would be through a 3-benzothiophenyl

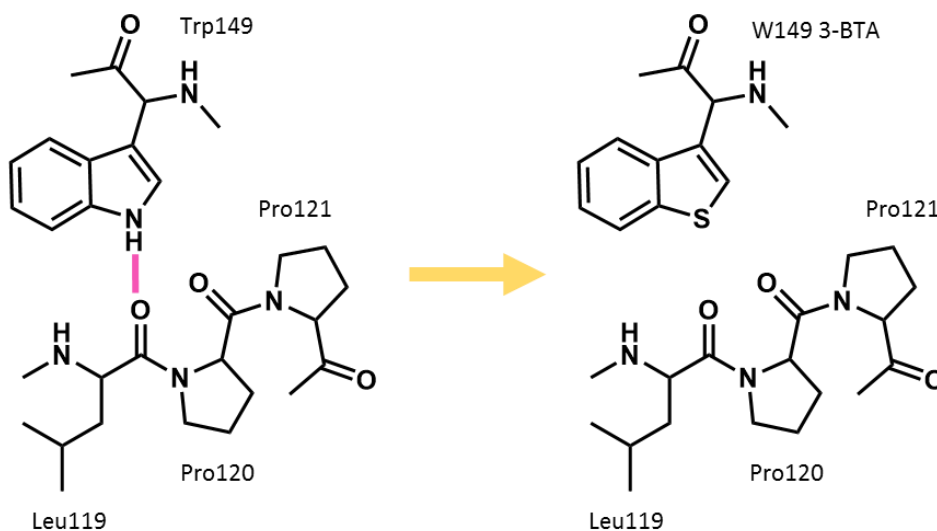


**Figure 10.** A schematic showing the effects of 3-benzothiophene mutation designed to eliminate a potential indole NH hydrogen bond without affecting the geometry of the side chain.

**Table 8.** 3-Benzothiophene Substitution at TrpB to Probe for Interfacial Hydrogen Bond

	$EC_{50}$ ( $\mu M$ )	$n_H$	$I_{max}$ ( $\mu A$ )	Fold Shift	N
Trp	$0.6 \pm 0.01$	$1.19 \pm 0.03$	1.87 - 5.33	1.0	11
3-BTA	$8.0 \pm 0.3$	$1.38 \pm 0.05$	0.99 - 13.37	13	17

**Table 9.** Comparing Experimental EC<sub>50</sub> Values to those Predicted from  $\alpha 4\beta 2$  TrpB Fluorination Plot

	<i>ab initio</i> binding energy	Predicted EC <sub>50</sub>	Empirical EC <sub>50</sub>	Fold-Shift (from prediction)
Trp	32.6	0.52	0.54	1.0
NpAla	28.9	1.21	0.12	0.1
3-BTA	26.9	1.92	8	4.2

*ab initio* values from HF 6-31G\*\* calculations; predicted EC<sub>50</sub> based on published fluorination plot with trend line  $3.24 - 0.10x$ ;  
 Fold-shift = Empirical EC<sub>50</sub> / Predicted EC<sub>50</sub>;

alanine (3-BTA) mutation that essentially substitutes the indole nitrogen with a sulfur atom, thus eliminating any possible hydrogen bond without changing the geometry of the ring system (although sulfur is much larger than nitrogen).

A 3-BTA substitution was conducted using nonsense suppression at TrpB in the  $\alpha 4$  subunit to determine whether the NpAla effect is due to hydrogen bonding, and the mutation actually showed a 13-fold increase in EC<sub>50</sub> (Table 8). This loss of function is in direct contradiction with the NpAla results, which showed a 5-fold decrease in EC<sub>50</sub>. Perhaps then, these changes in function are due to some other reason such as electrostatics. It is important to remember that both the NpAla and 3-BTA mutations bring a change in electrostatics and thus the cation- $\pi$  binding ability of the side chain. Using Hartree-Fock computations in order to remain consistent with other  $\alpha 4\beta 2$  studies, Trp, NpAla, and 3-BTA have *ab initio* Na<sup>+</sup> binding energies of 32.6, 28.9, and 26.9 kcal/mol, respectively. Previously reported fluorination plots can be used to calculate the expected EC<sub>50</sub> values based on these predicted binding energies, reported here in Table 9. Eliminating electrostatics as a factor, NpAla now causes a 10-fold shift in EC<sub>50</sub> less than what is expected, while the 3-BTA shift becomes a more modest 4-fold greater than expected. Therefore, it is unlikely that electrostatics are causing the effect either.

## 6.7 Conclusions

It seems legitimately possible that a combination of all of the above could explain the NpAla gain of function. The only other electrostatics-corrected gain of function reported at TrpB in this thesis occurred in  $\alpha 6\beta 2^{\ddagger}$  with 4-F<sub>1</sub>Trp, which had an EC<sub>50</sub> about 4-fold lower than expected based on electrostatics. This effect was largely ignored as it was the only Trp analogue with a substituent in the 4-position. It is also unclear if this mutation would have the same effect in  $\alpha 4\beta 2$ ; however, assuming that it did, the NpAla mutation adds an ever so slightly greater steric bulk on the same edge of the ring as the 4-position and could be driving a similar effect.

Many more experiments and structure-function studies would be necessary to prove this rather hand-wavy hypothesis, but it is probably worth exploring in the future. While the mystery of what might be causing the NpAla gain of function still lingers, new techniques have been developed in the process. For the first time, two different non-canonical amino acids have been incorporated in a neuronal nAChR, a technique that can likely be applied to other potential interactions and in different neuronal nAChR subtypes. Furthermore, the fluorinated side chain approach to probing hydrogen bonds was proven to be viable through both computational and empirical methods. A positive result would have definitively proven the validity of F<sub>3</sub>Ala as a means of attenuating a carbonyl's hydrogen bond accepting ability, but the end result was negative, so a positive control should be developed to make absolutely certain of its functionality. This could prove quite difficult since the only nAChR carbonyl known to make a functional hydrogen bond is associated with TrpB, which also makes a critical cation- $\pi$  interaction. However, results in Chapter 5 suggest that maybe a secondary amine that forms cation- $\pi$  interactions with

both TrpB and TyrC2 could tolerate a Trp-to-Ala mutation and thus a Trp-to-F<sub>3</sub>Ala mutation. Even without the positive control, a technique has been developed in this chapter that will hopefully prove to be a valuable strategy for probing hydrogen bond interactions both between amino acids and possibly with agonists.

## 6.8 Materials and Methods

### *Molecular Biology*

Rat  $\alpha$ 4L9'A (described as wild-type and/or  $\alpha$ 4 throughout this chapter) and  $\beta$ 2 nAChRs were in the pGEMhe vector, a cDNA plasmid optimized for protein expression in *Xenopus* oocytes. Site-directed mutagenesis was performed by PCR using the Stratagene QuikChange protocol and primers ordered from Integrated DNA Technologies (Coralville, IA). Circular cDNA was linearized with SbfI (New England Biolabs, Ipswich, MA) and then transcribed *in vitro* using T7 mMessage mMachine kit (Life Technologies, Santa Clara, CA), with a purification step after each process (Qiagen, Valencia, CA). Final concentrations were quantified by UV spectroscopy.

### *Ion Channel Expression*

*Xenopus laevis* oocytes (stage V to VI) were sourced from both a Caltech facility and Ecocyte Bio Science (Austin, TX). Oocytes were injected with 50 nL solution containing either 5 or 10 ng mRNA. The  $\alpha$ 4L9'A: $\beta$ 2 mRNA mass ratio was typically 1:3 for wild-type and conventional mutagenesis experiments. Cells were incubated 24-48 hours at 18°C in ND96 solution (96 mM NaCl, 2mM KCl, 1 mM MgCl<sub>2</sub>, and 5mM HEPES, pH 7.5) enriched with theophylline, sodium pyruvate, and gentamycin.

### *Non-canonical Amino Acid Incorporation*

The cyanomethylester form of NVOC-protected tryptophan, leucine, alanine, and valine and their corresponding analogues was coupled to dinucleotide dCA and enzymatically ligated to either UAG-suppressor 74-mer THG73 tRNA<sub>CUA</sub> or UGA-suppressor 74-mer TQOPS'UCA as previously described.<sup>21</sup> The product was verified by MALDI time-of-flight mass spectrometry on a 3-hydroxypicolinic acid matrix. The non-canonical amino acid-coupled tRNA was deprotected by photolysis on a 500 W Hg/Xe arc lamp, filtered with

Schott WG-320 and UG-11 filters, immediately prior to coinjection with mRNA containing the UAG or UGA mutation at the site of interest. mRNA and tRNA were typically injected in a 1:1 or 1:2 volume ratio in a total volume of 50 or 75 nL respectively so that 25 ng of mRNA was injected per cell.

For double mutant experiments  $\alpha 4L9'AW149TAG\beta 2L119TGA$  was injected at a 1:10 mRNA ratio to maintain a  $(\alpha 4)_2(\beta 2)_3$  stoichiometry and confirmed via the Hill coefficient (cases of a shift in stoichiometry resulted in a large increase in this value). In cases where observed agonist-induced currents were low after 48 hour incubation – likely due to low receptor protein expression – a second injection of mRNA and tRNA was performed after 24 hours. The fidelity of non-canonical amino acid incorporation was confirmed at Trp149, Leu119, and Pro120 with the wild-type recovery and 76-mer experiments described above.

### *Whole-Cell Electrophysiological Characterization*

Acetylcholine chloride and lobeline were purchased from Sigma Aldrich (St Louis, MO). Agonist-induced currents were recorded in TEVC mode using the OpusXpress 6000A (Molecular Devices, Sunnyvale, CA) at a holding potential of -60 mV in a running buffer of  $Ca^{2+}$ -free ND96. Agonists were prepared in  $Ca^{2+}$ -free ND96 and delivered to cells via a 1 mL application over 15 sec followed by a 2 min wash. Data from dose-response experiments were normalized, averaged, and fit to the Hill equation using Kaleidagraph (Synergy Software, Reading PA), though data are visualized here with Prism (GraphPad Software, La Jolla, CA). Error bars are presented as standard error of the mean, while  $EC_{50}$  and Hill coefficient errors are reported by Kaleidagraph and represent the sum of the squared error between the data and the calculated fit.

### *Computational Evaluation of Hydrogen Bonding*

All calculations were performed in Spartan '14 (Wavefunction Inc., Irvine, CA) using density functional theory with the M06 functional and the 6-31G(d,p) basis set. Electrostatic potential maps with high resolution were calculated using the Spartan '14 graphical user interface. Electrostatic potential maxima (for indole) and minima (for the acceptors) were determined, and the  $\alpha$ ,  $\beta$ , and  $\Delta\Delta G_{H-bond}$  values were calculated using methods described in section 6.4.1 with values for  $\alpha_s$  and  $\beta_s$  sourced from previously published work.<sup>18</sup>

### *NMR Determination of Hydrogen Bond Acceptor Strength*

All compounds were either purchased from Sigma Aldrich (St Louis, MO) or synthesized using published methods. Solutions of *p*-fluorophenol and *p*-fluoroanisole, both at 0.01 M, and hydrogen bond acceptor in varying concentrations were prepared in purified carbon tetrachloride. <sup>19</sup>F-NMR measurements were taken on a 400 MHz instrument (Varian Associates, Palo Alto, CA).  $K_f$  was calculated as described in section 6.4.2 and  $\Delta G$  was determined using the van't Hoff equation,  $\Delta G = -RT\ln(K_f)$ .

## 6.9 References

1. Brejc, K., *et al.* Crystal structure of an ACh-binding protein reveals the ligand-binding domain of nicotinic receptors. *Nature* **411**, 269–276 (2001).
2. Sauguet, L., Shahsavari, A. & Delarue, M. Crystallographic studies of pharmacological sites in pentameric ligand-gated ion channels. *Biochim. Biophys. Acta BBA - Gen. Subj.* **1850**, 511–523 (2015).
3. Cecchini, M. & Changeux, J.-P. The nicotinic acetylcholine receptor and its prokaryotic homologues: Structure, conformational transitions & allosteric modulation. *Neuropharmacology* **96, Part B**, 137–149 (2015).
4. Hansen, S. B. *et al.* Structures of Aplysia AChBP complexes with nicotinic agonists and antagonists reveal distinctive binding interfaces and conformations. *EMBO J.* **24**, 3635–3646 (2005).
5. Billen, B. *et al.* Molecular actions of smoking cessation drugs at  $\alpha 4\beta 2$  nicotinic receptors defined in crystal structures of a homologous binding protein. *Proc. Natl. Acad. Sci.* **109**, 9173–9178 (2012).
6. Terry Jr., A. V. *et al.* Lobeline and structurally simplified analogs exhibit differential agonist activity and sensitivity to antagonist blockade when compared to nicotine. *Neuropharmacology* **37**, 93–102 (1998).
7. Damaj, M. I., Patrick, G. S., Creasy, K. R. & Martin, B. R. Pharmacology of Lobeline, A Nicotinic Receptor Ligand. *J. Pharmacol. Exp. Ther.* **282**, 410–419 (1997).
8. Zheng, G., Dvoskin, L. P., Deaciuc, A. G., Norrholm, S. D. & Crooks, P. A. Defunctionalized Lobeline Analogues: Structure–Activity of Novel Ligands for the Vesicular Monoamine Transporter. *J. Med. Chem.* **48**, 5551–5560 (2005).
9. Zhong, W. *et al.* From ab initio quantum mechanics to molecular neurobiology: A cation– $\pi$  binding site in the nicotinic receptor. *Proc. Natl. Acad. Sci.* **95**, 12088–12093 (1998).
10. Van Arnam, E. B. & Dougherty, D. A. Functional Probes of Drug–Receptor Interactions Implicated by Structural Studies: Cys-Loop Receptors Provide a Fertile Testing Ground. *J. Med. Chem.* **57**, 6289–6300 (2014).
11. Colquhoun, D. Binding, gating, affinity and efficacy: the interpretation of structure-activity relationships for agonists and of the effects of mutating receptors. *Br. J. Pharmacol.* **125**, 924–947 (1998).
12. Celie, P. H. N. *et al.* Nicotine and carbamylcholine binding to nicotinic acetylcholine receptors as studied in AChBP crystal structures. *Neuron* **41**, 907–914 (2004).

13. Limapichat, W., Lester, H. A. & Dougherty, D. A. Chemical Scale Studies of the Phe-Pro Conserved Motif in the Cys Loop of Cys Loop Receptors. *J. Biol. Chem.* **285**, 8976–8984 (2010).
14. Rodriguez, P. C. *et al.* Fluorescent dopamine tracer resolves individual dopaminergic synapses and their activity in the brain. *Proc. Natl. Acad. Sci.* **110**, 870–875 (2013).
15. Rodriguez, E. A., Lester, H. A. & Dougherty, D. A. Improved amber and opal suppressor tRNAs for incorporation of unnatural amino acids in vivo. Part 1: Minimizing misacylation. *RNA* **13**, 1703–1714 (2007).
16. Rodriguez, E. A., Lester, H. A. & Dougherty, D. A. Improved amber and opal suppressor tRNAs for incorporation of unnatural amino acids in vivo. Part 2: Evaluating suppression efficiency. *RNA* **13**, 1715–1722 (2007).
17. Abraham, M. H. & Platts, J. A. Hydrogen Bond Structural Group Constants. *J. Org. Chem.* **66**, 3484–3491 (2001).
18. Hunter, C. A. Quantifying Intermolecular Interactions: Guidelines for the Molecular Recognition Toolbox. *Angew. Chem. Int. Ed.* **43**, 5310–5324 (2004).
19. Gurka, D. & Taft, R. W. Studies of hydrogen-bonded complex formation with p-fluorophenol. IV. Fluorine nuclear magnetic resonance method. *J. Am. Chem. Soc.* **91**, 4794–4801 (1969).
20. Anslyn, E. V. & Dougherty, D. A. *Modern physical organic chemistry*. (University Science, 2006).
21. Dougherty, D. A. & Van Arnem, E. B. In Vivo Incorporation of Non-canonical Amino Acids by Using the Chemical Aminoacylation Strategy: A Broadly Applicable Mechanistic Tool. *ChemBioChem* **15**, 1710–1720 (2014).

## Appendix A: Investigations of Possible $\alpha 6\beta 2$ -P2X Cross-talk<sup>††</sup>

### A.1 Introduction

In addition to regulating dopamine release in the brain,  $\alpha 6$ -containing nAChRs are also involved in nociception. In a large mouse study, mechanical allodynia, a type of chronic neuropathic pain that results in a sensitized response to innocuous stimuli, was found to correlate with expression levels of the *Chrna6* gene (which codes for  $\alpha 6$ ) in the dorsal root ganglia.<sup>1</sup> This study found that *Chrna6*-knockout mice showed higher levels of allodynia than wild-type mice, an effect that was absent in *Chrna4*-knockouts. Conversely, mice with a *Chrna6* L9'S gain-of-function mutation experienced lower levels of allodynia. These results reveal an anti-allodynic effect of  $\alpha 6$ -containing nAChR activation and suggest a functional interaction between  $\alpha 6$  and a more pain-relevant molecular target in the peripheral nervous system, such as the P2X receptors.

The P2X family consists of ATP-gated ion channels formed by three subunits. Each subunit has two transmembrane helices and intracellular N- and C-terminal domains. There are seven different subunits, labeled P2X1-P2X7, that like nAChRs combine into different subtypes. Dorsal root ganglion neurons express homomeric P2X2, P2X3, and heteromeric P2X2/3 receptor subtypes.<sup>2</sup> Previous work in *Xenopus* oocytes has shown that  $\alpha 6\beta 4$  experiences several forms of functional crosstalk with P2X2, P2X3, and P2X2/3.<sup>3</sup> The P2X2 receptors were found to enter a prolonged desensitized state upon activation by ATP when coexpressed with  $\alpha 6\beta 4$ , resulting in cross-inhibition. That is, when ACh was

---

<sup>††</sup> The dose-response work presented in this appendix is adapted, with permission, from: Wieskopf, J.S. et. al. The nicotinic  $\alpha 6$  subunit gene determines variability in chronic pain sensitivity via cross-inhibition of P2X2/3 receptors. *Science Translational Medicine* **7:287** 287ra72 (2015). doi:10.1126/scitranslmed.3009986

applied to the receptors following a dose of ATP, there was an observed decrease in current. Additionally, when ACh and ATP were applied simultaneously, the induced current was less the sum of the currents invoked from individual application of each agonist. When  $\alpha 6\beta 4$  was coexpressed with P2X3, cross-talk was seen through dose response experiments. The ATP dose response curve was shifted to the right, with a roughly 3-fold increase in  $EC_{50}$  both in the presence and absence of ACh.

With the development of the  $\alpha 6\beta 2^{\ddagger}$  heterologous expression system, these experiments could be repeated with  $\alpha 6\beta 2$  to determine whether there is a similar cross-interaction with P2X receptors. The data presented in this appendix suggest that there is an effect with P2X2, though results for P2X3 raise perhaps more questions than they could answer.

**Table 1.** Investigating  $\alpha 6\beta 2$ -P2X2 and  $\alpha 6\beta 2$ -P2X3 Interactions through Dose-Response Effects

Receptor	Dose-Response Agonist	Additional Agonist	$EC_{50}$ ( $\mu M$ )	$n_H$	$I_{max}$ ( $\mu A$ )	N
P2X2*	ATP		$24 \pm 1$	$1.5 \pm 0.1$		
P2X3*	ATP		$38 \pm 6$	$0.9 \pm 0.1$		
$\alpha 6\beta 2^{\ddagger}$	ACh		$0.121 \pm 0.006$	$1.12 \pm 0.05$	1.32 - 14.09	15
$\alpha 6\beta 2^{\ddagger}$	ACh	100 $\mu M$ ATP	$0.121 \pm 0.003$	$1.33 \pm 0.05$	2.38 - 19.67	14
$\alpha 6\beta 2^{\ddagger}$ -P2X2	ACh		$0.15 \pm 0.01$	$1.17 \pm 0.08$	0.79 - 4.93	11
$\alpha 6\beta 2^{\ddagger}$ -P2X2	ACh	100 $\mu M$ ATP	$0.3 \pm 0.06$	$1.3 \pm 0.3$	0.75 - 2.42	11
$\alpha 6\beta 2^{\ddagger}$ -P2X2	ATP		$26 \pm 2$	$1.6 \pm 0.2$	0.18 - 13.42	14
$\alpha 6\beta 2^{\ddagger}$ -P2X2	ATP	10 $\mu M$ ACh	$29 \pm 2$	$1.9 \pm 0.2$	0.12 - 6.52	12
$\alpha 6\beta 2^{\ddagger}$ -P2X3	ACh		$0.127 \pm 0.006$	$1.19 \pm 0.05$	0.2 - 9.22	11
$\alpha 6\beta 2^{\ddagger}$ -P2X3	ATP		$44 \pm 7$	$0.9 \pm 0.1$	0.17 - 3.5	13

\*P2X data previously reported in Limapichat et al

## A.2 $\alpha 6\beta 2$ -P2X2 Cross-talk Experiments

To investigate whether functional cross-talk exists between  $\alpha 6\beta 2$  and P2X2, dose response experiments were conducted with ACh and ATP at  $\alpha 6\beta 2^{\ddagger}$ , P2X2, and coexpressed  $\alpha 6\beta 2^{\ddagger}$ -P2X2. Then, dose response curves were generated for ACh in the presence of ATP as well as ATP in the presence of ACh. Results from these experiments are shown in Table 1 and reveal that the presence of P2X2 has no meaningful effect on either the ATP- or the ACh-generated dose response curves.

Instead, functional cross-talk between  $\alpha 6\beta 2$  and P2X2 is observed in cross-inhibition Delta tests. In these experiments, ACh and ATP are applied in independent doses followed by a dose of both ACh and ATP. The current evoked from the ACh+ATP dose is then compared to the current level predicted from the sum of each independent current amplitude. Nonadditivity of these two currents would suggest functional cross-inhibition of the two receptors. For  $\alpha 6\beta 2$  and P2X2, the dual agonist-invoked current is 19% percent smaller than expected (represented by Delta, Figure 1), supporting the idea that these two receptors are involved in cross-inhibition.

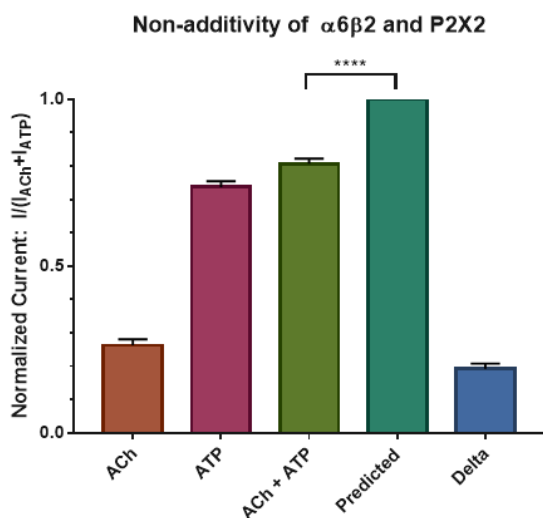


**Figure 1.** Results from a Delta test to determine whether  $\alpha 6\beta 2$  and P2X2 functionally interact with each other. In this test, ACh and ATP are applied to cells expressing both receptors in independent doses with a washout step in between. The currents generated from these doses are added and normalized to create the predicted current column, assuming perfect additivity. Then, a combined ACh and ATP dose is applied to the same cells. The difference in this current and the predicted current result in the Delta value. A paired t-test was used to determine whether there was a statistical difference between the combined dose current and the predicted current ( $P < 0.0001$ ,  $N = 12$ ).

### A.3 $\alpha 6\beta 2$ -P2X3 Cross-talk Experiments

To test whether  $\alpha 6\beta 2$  and P2X3 engage in cross-talk, dose response curves were generated for each subtype individually and while coexpressed (Table 1). From these experiments there is little evidence of  $\alpha 6\beta 2$ -P2X3 cross-talk as there are no meaningful shifts in  $EC_{50}$  observed. It is important to note that P2X3 is a quickly desensitizing receptor subtype, and studying the effects of dual agonist applications is challenging. To do this,

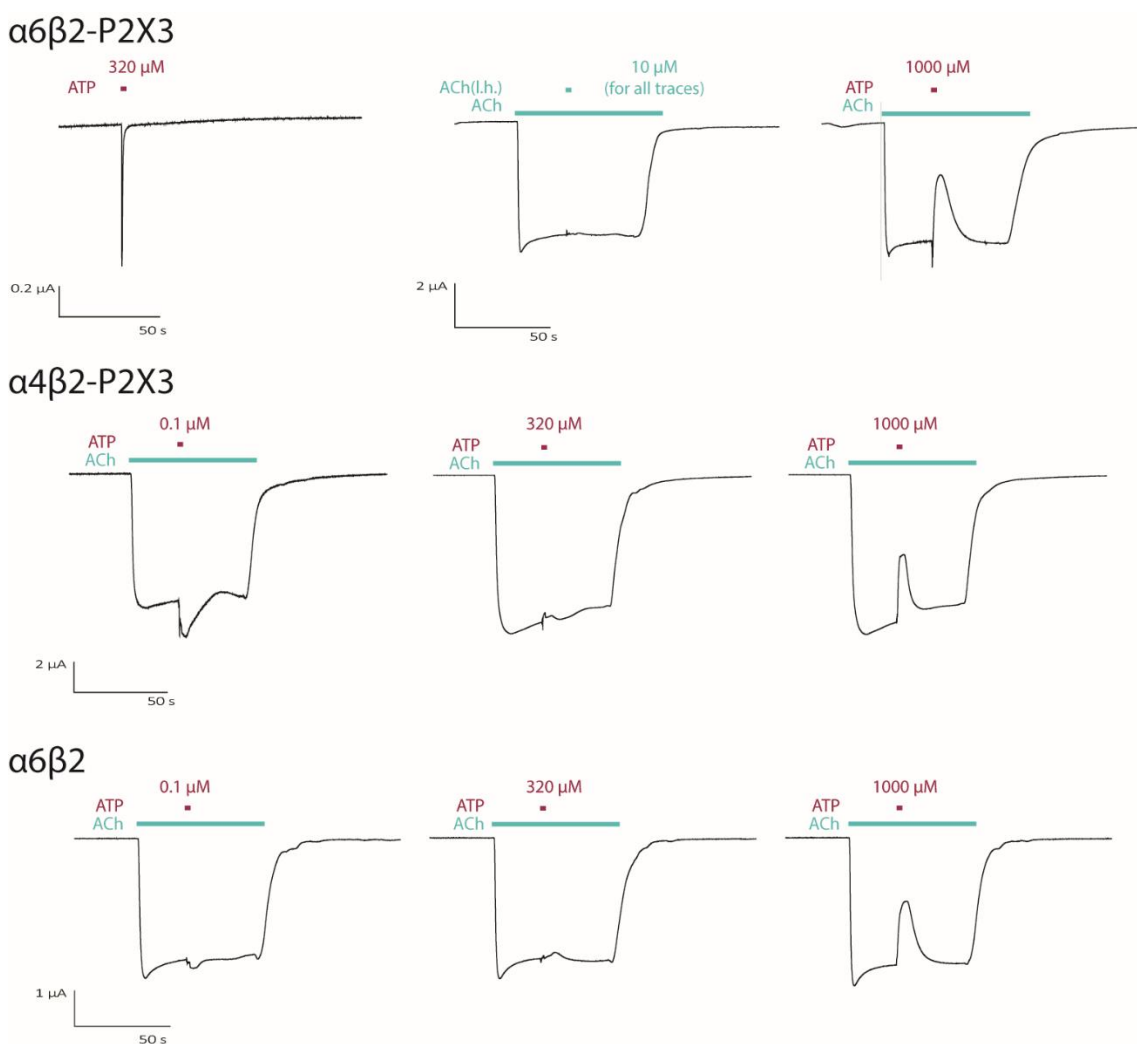


**Figure 2.** The top left trace is representative of P2X3 activation by ATP. In each of the other current traces, ACh is added to the cells by perfusion over one minute and a dose of ATP (or ACh in the fluidics control on the top center) is added by the liquid handler over 2 sec. As shown here, a concentrated dose of ATP causes a large inhibitory spike at  $\alpha 6\beta 2$ -P2X3,  $\alpha 4\beta 2$ -P2X3, and  $\alpha 6\beta 2$  alone. With fluidics effects ruled out, this suggest ATP is able to channel block  $\beta 2$ -containing nAChRs.

ACh is delivered to cells by the buffer perfusion system and a mixture of ATP and ACh is applied by the liquid handler as is typical, followed by perfusion with only ACh, and then a wash-out with buffer (this protocol was followed for most traces shown in Figure 2). This is the identical experimental set up used for the  $\alpha 6\beta 4$  experiments; however, a strange inhibition-like peak is observed in the current trace at high concentrations of ATP when  $\alpha 6\beta 2^\ddagger$  and P2X3 are coexpressed, that disappears as ATP is washed out with ACh. At first this was thought to be a fluidics issue; however, the same phenomenon is absent when an ACh-only dose is applied via the liquid handler. The next most-rational explanation is that activation of P2X3 by ATP causes an immediate but temporary deactivation of  $\alpha 6\beta 2$ . This could be due a direct interaction with  $\beta 2$ , as the same effect is seen in  $\alpha 4\beta 2$ -P2X3 expressing cells as well. Yet, a control experiment where only  $\alpha 6\beta 2^\ddagger$  is expressed also has the same result. This then suggests that ATP acts as a channel blocker for  $\beta 2$ -containing nAChR subtypes. More work must be done to fully resolve the cause of this unexpected result. If ATP does indeed channel block certain subtypes of nAChRs, it would have interesting consequences for the understanding of neurotransmission.

## A.4 Materials and Methods

### *Ion Channel Expression*

Rat  $\alpha 4L9'A$  (described as  $\alpha 4$  throughout),  $\beta 2$ ,  $\alpha 6L9'S$  and  $\beta 2L9'S_{LFM/AAQA}$  nAChRs were in the pGEMhe vector, a plasmid optimized for protein expression in *Xenopus* oocytes. P2X2 and P2X3K65A (referred to as P2X3 throughout the appendix) were in the pcDNA3 vector. *Xenopus laevis* oocytes (stage V to VI) were sourced from both a Caltech facility and Ecocyte Bio Science (Austin, TX). Oocytes were injected with 50 nL solution containing 5 ng mRNA in a 10:10:1 ratio for  $\alpha 6\beta 2$ -P2X2 and a 1:1:1 ratio for  $\alpha 6\beta 2$ -P2X3. Cells were incubated 24-48 hours at 18°C in ND96 solution (96 mM NaCl, 2mM KCl, 1

mM MgCl<sub>2</sub>, and 5mM HEPES, pH 7.5) enriched with theophylline, sodium pyruvate, and gentamycine.

### *Whole-Cell Electrophysiological Characterization*

Acetylcholine chloride, and ATP disodium salt hydrate were purchased from Sigma Aldrich (St Louis, MO). Agonist-induced currents were recorded in TEVC mode using the OpusXpress 6000A (Molecular Devices, Sunnyvale, CA) at a holding potential of -60 mV in a running buffer of Ca<sup>2+</sup>-free ND96. Agonists were prepared in Ca<sup>2+</sup>-free ND96; ACh was either delivered to cells via a 1 mL application over 15 sec or through the buffer perfusion system; ATP was delivered via a 1 mL application over 15 sec for P2X2 or a 0.5 mL dose over 5 sec for P2X3. Data from dose-response experiments were normalized, averaged, and fit to the Hill equation using Kaleidagraph (Synergy Software, Reading PA), though data is visualized here with Prism (GraphPad Software, La Jolla, CA). Data from delta experiments were normalized to the predicted current and averaged. A pair-wise t-test was used to determine significance between ATP+ACh and predicted currents. Error bars are presented as standard error of the mean, while EC<sub>50</sub> and Hill coefficient errors are reported by Kaleidagraph and represent the sum of the squared error between the data and the calculated fit.

## **A.5 References**

1. Wieskopf, J. S. *et al.* The nicotinic  $\alpha 6$  subunit gene determines variability in chronic pain sensitivity via cross-inhibition of P2X2/3 receptors. *Sci. Transl. Med.* **7**, 287ra72–287ra72 (2015).
2. Cockayne, D. A. *et al.* P2X2 knockout mice and P2X2/P2X3 double knockout mice reveal a role for the P2X2 receptor subunit in mediating multiple sensory effects of ATP. *J. Physiol.* **567**, 621–639 (2005).
3. Limapichat, W., Dougherty, D. A. & Lester, H. A. Subtype-Specific Mechanisms for Functional Interaction between  $\alpha 6\beta 4^*$  Nicotinic Acetylcholine Receptors and P2X Receptors. *Mol. Pharmacol.* **86**, 263–274 (2014).

## Appendix B: Initial Studies of Alcohol- $\alpha 6\beta 2$ Interactions

### B.1 Introduction

For a long time, it was believed that ethanol acts as an unspecific pharmacological agent. The last few decades have definitively proven otherwise, with several ligand-gated ion channel targets identified, including NMDAR glutamate receptors, GABA<sub>A</sub> receptors, glycine receptors, and nAChRs.<sup>1</sup> In nAChRs, ethanol typically has a concentration-dependent potentiating effect, i.e. it acts as a positive allosteric modulator. This is true for concentrations less than 100 mM<sup>††</sup> with  $\alpha 2\beta 4$ ,  $\alpha 4\beta 4$ ,  $\alpha 2\beta 2$ , and  $\alpha 4\beta 2$ , and all of the subtypes studied (though  $\alpha 6\beta 2$  is notably absent from these surveys) for concentrations greater than 100 mM.<sup>2</sup>

This observation is actually a result of a more comprehensive chain length effect: as the chain length of the alcohol increases, the effect of the alcohol shifts from potentiating to inhibitory, with each subtype having a unique transitional chain length wherein the effect actually changes as the concentration increases.<sup>3</sup> In  $\alpha 4\beta 2$ , the total amount of potentiation or inhibition was plotted against chain length, and a corresponding  $\Delta\Delta G$  was calculated to be 0.4 kcal/mol/CH<sub>2</sub> for potentiation and 0.8 kcal/mol/CH<sub>2</sub> for inhibition.<sup>4</sup> That there were two distinct  $\Delta\Delta G$  values suggests there are two definitive binding sites depending on the molar volume of the alcohol. The effects of ethanol on  $\alpha 4\beta 2$  have also been studied using single channel analysis. These experiments showed a shift in  $P_{\text{open}}$  from 0.023 to 0.029 in the presence of ethanol.<sup>5</sup>

---

<sup>††</sup> For reference, a 0.08 blood alcohol concentration (the legal limit for driving drunk) is the equivalent of 17.4 mM. A value of 0.50, the lower end of the BAC spectrum that leads to death from alcohol poisoning, is equivalent to a concentration of 108.7 mM.

Most of the research conducted on nAChRs and alcohols date back to the 1990s and early 2000s. Recently, however, studies are emerging revealing the role  $\alpha 6$ -containing receptors have on the behavioral effects of ethanol. A 2012 knockout study showed that  $\alpha 6$  modulates ethanol's sedative effects, and a 2013 study showed L9'S mutant mice show a higher preference for alcohol in behavioral studies.<sup>6,7</sup> In 2015, a paper showed that co-application of nicotine and ethanol was enough to elicit response from AMPA receptors even when the nicotine concentration would typically lie below the threshold required to cause such a response. However, this effect was blocked by  $\alpha 6$ -selective MII conotoxin antagonist.<sup>8</sup> Reports have also been published beginning to hypothesize the location of discreet binding sites in pLGIC receptors. The M2 helix 15' position in GABA<sub>A</sub> and GlyR have shown some sensitivity to the effects of alcohol as have the 16' and 17' positions in nAChRs. In GLIC, structural data suggests a phenylalanine at the 14' position is a possible ethanol binding site.<sup>9</sup>

With mounting evidence that  $\alpha 6\beta 2$  plays a substantial role in how the brain processes ethanol, new clues leading toward a possible specific binding site, and a well-optimized heterologous expression system discussed in Chapter 2, the pieces are in place

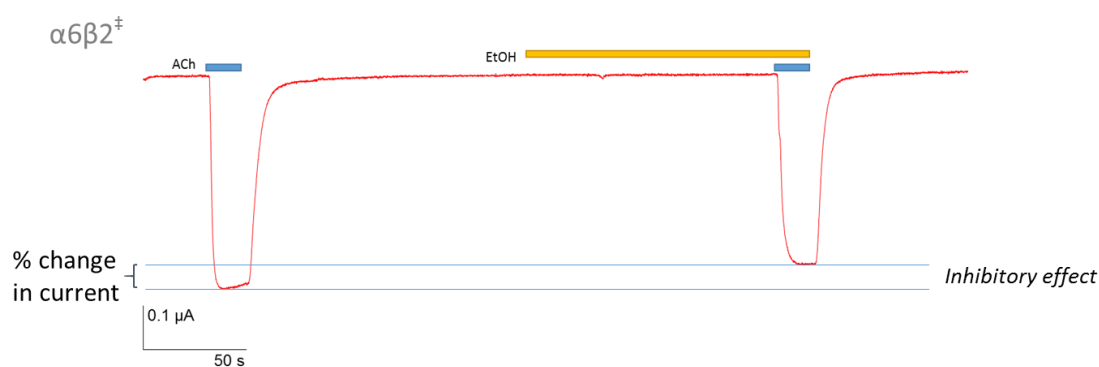


**Figure 1.** A typical current trace from tests used to determine the allosteric effect of an alcohol on  $\alpha 6\beta 2$ . An initial dose of ACh is followed by an incubation period of just alcohol. A second dose of ACh plus alcohol is applied, and the percent difference in current is determined.

to both characterize the effects that ethanol and other alcohols have on  $\alpha 6\beta 2$ . Using  $\alpha 6\beta 2^{\ddagger}$ , the effects of various alcohols can be catalogued, and structure-function studies using non-canonical amino acid mutagenesis could be conducted to fully characterize ethanol binding. This appendix details initial experiments done in that vein and possible experiments to conduct going forward.

## B.2 Determining the Allosteric Effects of EtOH at $\alpha 6\beta 2$

Because the  $\alpha 6\beta 2$  subtype was absent from previously published work, it was unclear where on the chain-length spectrum the potentiation-inhibition transition point might occur. Thus, methanol, ethanol, and isopropanol were studied at  $\alpha 6\beta 2^{\ddagger}$ . In this experiment, an application of ACh is applied after which the cell is incubated in the alcohol

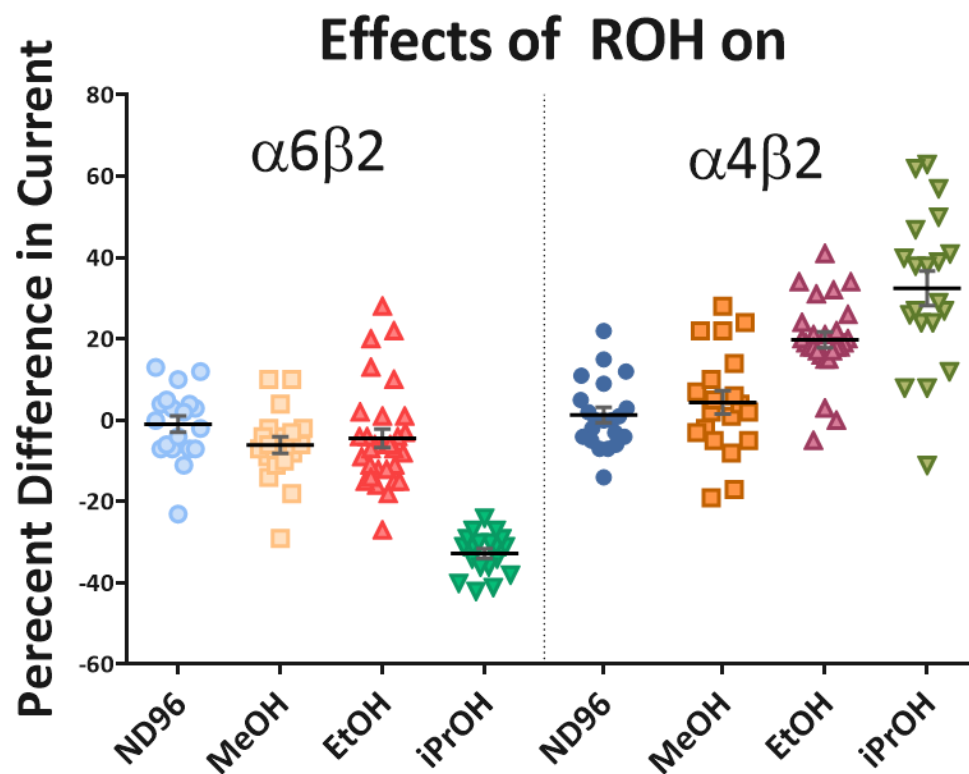


**Figure 2.** A scatter plot depicting the effect various alcohols have on  $\alpha 6\beta 2$  and  $\alpha 4\beta 2$ . The horizontal line shows the mean, with error bars representing the standard error of the mean. Note that only isopropanol has a meaningful effect at  $\alpha 6\beta 2$ . The trends seen in  $\alpha 4\beta 2$  data agree with previously published results.

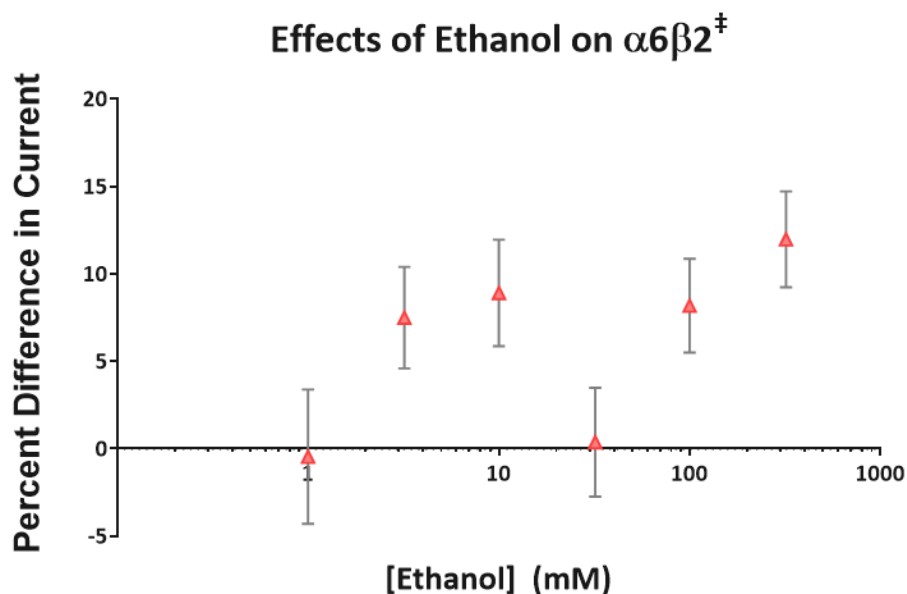


**Figure 3.** Results from a dose response experiment (N=16) for ethanol at  $\alpha 6\beta 2^{\ddagger}$ . The percent difference in current between a control dose of ACh and an ACh+EtOH dose after two minutes of incubation is plotted against the corresponding concentration of ethanol. While there are no obvious trends or correlations here, there is a general though modest potentiating effect seen here that was not in the previous chart (Figure 2).

of interest for two minutes. This period is followed by an application of both the alcohol and ACh and finally a washout step (Figure 1). The percent difference in current amplitude between the ACh and ACh+ROH peaks is then determined. If that number is positive the alcohol has a potentiation effect, whereas a negative percent difference in current amplitudes means the alcohol is inhibitory. Results were collected at  $\alpha 4L9'A\beta 2$  to verify the method, and the general trends are consistent with what is published (though differences in effect magnitude are likely due to the presence of the L9'A mutation which was not present in the original study). The results from  $\alpha 6\beta 2^{\ddagger}$  show that only isopropanol has any meaningful effect on current level, a  $33\pm 1\%$  decrease in current (Figure 2).

That no effects were seen with ethanol or methanol suggests the so-called transition point could be near these chain lengths. It is also possible that the concentrations used for these tests were outside the effective range. Thus, a dose response experiment was

conducted with ethanol at  $\alpha 6\beta 2^{\ddagger}$  using the same protocol described above, but with increasing concentrations of ethanol. The resulting plot of percent difference in current against concentration of ethanol shows no apparent trends, other than modest potentiation at certain concentrations (Figure 3).

This lack of effect is incongruous with the previously published neurological and pharmacological studies discussed above. It could be due to a number of factors, though additional work is required to fully understand these results. Dose response curves should be generated for other alcohols of varying chain lengths in order to determine this subtype's transitional chain-length. Because these effects are likely causing changes in gating, single-channel analysis would also be useful to determine what effect each alcohol has on  $\Theta$ ,  $P_{\text{open}}$ , and the general kinetics of the receptor.

If a trend is eventually observed, non-canonical amino acid mutagenesis could be used to determine the specific binding site of these alcohols. There is a Phe in the M2 helix at position 14' in both  $\alpha 6$  and  $\alpha 4$  that, based on studies in GLIC and GABA<sub>A</sub>R, could be a likely target. If so, ethoxyphenylalanine might prove to be an effective analogue to mimic ethanol-bound receptor. TEVC experiments could determine the potentiation effects while single channel analysis could determine the  $P_{\text{open}}$  for the mutant, wild-type, and wild-type in the presence of ethanol. If F14' is indeed responsible for ethanol binding, a fluorination series could then be conducted to determine if the binding interaction is a polar- $\pi$  interaction between the hydroxyl and the aromatic side chain.

Based on the literature, studying alcohol effects at  $\alpha 6\beta 2$  should be fertile ground for new experiments and important findings. However, it is clear that further optimization

of the protocols and a better understanding of ethanol's basic effects on the receptor are necessary before comprehensive studies can be performed.

### **B.3 Materials and Methods**

#### *Ion Channel Expression*

Rat  $\alpha 4L9'A$  (described as  $\alpha 4$  throughout),  $\beta 2$ ,  $\alpha 6L9'S$  and  $\beta 2L9'S_{LFM/AAQA}$  nAChRs were in the pGEMhe vector, a plasmid optimized for protein expression in *Xenopus* oocytes. *Xenopus laevis* oocytes (stage V to VI) were sourced from both a Caltech facility and Ecocyte Bio Science (Austin, TX). Oocytes were injected with 50 nL solution containing 5 ng mRNA in a 10: 1 ratio. Cells were incubated 24-48 hours at 18°C in ND96 solution (96 mM NaCl, 2mM KCl, 1 mM MgCl<sub>2</sub>, and 5mM HEPES, pH 7.5) enriched with theophylline, sodium pyruvate, and gentamycine.

#### *Whole-Cell Electrophysiological Characterization*

Acetylcholine chloride, methanol, and isopropanol were purchased from Sigma Aldrich (St Louis, MO). Koptec 200 proof ethanol (Decon Labs, King of Prussia, PA) was used to make ethanol solutions. Agonist-induced currents were recorded in TEVC mode using the OpusXpress 6000A (Molecular Devices, Sunnyvale, CA) at a holding potential of -60 mV in a running buffer of Ca<sup>2+</sup>-free ND96. Agonists and alcohols were prepared in Ca<sup>2+</sup>-free ND96 and applied according to protocols discussed above. Data from dose-response experiments were normalized, averaged, and fit to the Hill equation using Kaleidagraph (Synergy Software, Reading PA), though data is visualized here with Prism (GraphPad Software, La Jolla, CA). Error bars are presented as standard error of the mean.

## B.4 References

1. Spanagel, R. Alcoholism: A Systems Approach From Molecular Physiology to Addictive Behavior. *Physiol. Rev.* **89**, 649–705 (2009).
2. Aistrup, G. L., Marszalec, W. & Narahashi, T. Ethanol modulation of nicotinic acetylcholine receptor currents in cultured cortical neurons. *Mol. Pharmacol.* **55**, 39–49 (1999).
3. Zuo, Y., Kuryatov, A., Lindstrom, J. M., Yeh, J. Z. & Narahashi, T. Alcohol Modulation of Neuronal Nicotinic Acetylcholine Receptors Is  $\alpha$  Subunit Dependent. *Alcohol. Clin. Exp. Res.* **26**, 779–784 (2002).
4. Zuo, Y. *et al.* Dual Action of n-Alcohols on Neuronal Nicotinic Acetylcholine Receptors. *Mol. Pharmacol.* **60**, 700–711 (2001).
5. Zuo, Y., Nagata, K., Yeh, J. Z. & Narahashi, T. Single-Channel Analyses of Ethanol Modulation of Neuronal Nicotinic Acetylcholine Receptors. *Alcohol. Clin. Exp. Res.* **28**, 688–696 (2004).
6. Powers, M. S., Broderick, H. J., Drenan, R. M. & Chester, J. A. Nicotinic acetylcholine receptors containing  $\alpha 6$  subunits contribute to alcohol reward-related behaviours. *Genes Brain Behav.* **12**, 543–553 (2013).
7. Kamens, H. M., Hoft, N. R., Cox, R. J., Miyamoto, J. H. & Ehringer, M. A. The  $\alpha 6$  nicotinic acetylcholine receptor subunit influences ethanol-induced sedation. *Alcohol* **46**, 463–471 (2012).
8. Engle, S. E., McIntosh, J. M. & Drenan, R. M. Nicotine and ethanol cooperate to enhance ventral tegmental area AMPA receptor function via  $\alpha 6$ -containing nicotinic receptors. *Neuropharmacology* **91**, 13–22 (2015).
9. Howard, R. J. *et al.* Structural basis for alcohol modulation of a pentameric ligand-gated ion channel. *Proc. Natl. Acad. Sci.* **108**, 12149–12154 (2011).